## *The spatial characteristics of low energy muons in cosmic ray showers*

A. I. Gibson

# THE SPATIAL CHARACTERISTICS OF LOW ENERGY MUONS IN COSMIC RAY SHOWERS

by

A.I. Gibson, B.Sc., M.Sc.

A Thesis submitted to the University of Durham in accordance with the Regulations for Admittance to the Degree of Doctor of Philosophy

Department of Physics,
University of Durham.

December 1981

# The Spatial Characteristics of Low Energy Muons in Cosmic Ray Showers

A.I. Gibson B.Sc., M.Sc.

## Abstract

Previous work on the muon component of extensive air showers is described and reviewed with particular reference to the muon heights of origin with respect to the main cascade. The mechanical and operating details of a specialist experiment to determine the heights of origin of muons are described together with the results from detailed computer simulations which are tailored to resemble the characteristics of the equipment. The raw experimental data are examined in detail as a precursor to interpreting the data from the equipment. The final results from the experiment are given in detail and their relevance to air shower cascade development discussed. Suggestions are made for future work in this and related fields.

# Contents

# Chapter One

# Introduction

## 1-1 The Cosmic Rays at the Highest Energies.

The presence of a universal ionizing radiation was first noticed in 1900 when C.T.R. Wilson (the inventor of the Wilson Cloud Chamber) observed that a thoroughly insulated gold leaf electroscope slowly lost its charge. This phenomenon was originally ascribed to ionizing radiations emanating from rocks in the earth's crust. When the experiments were repeated at sea no change in the rate of charge loss was observed which led to suggestions that the radiation was extra-terrestrial in origin. This was confirmed in 1912 when Hess and colleagues made several balloon ascents and found a steady increase in the radiation with altitude [Hess (1912)]. The cosmic radiation as it became known has been responsible for many important and exciting discoveries in both Nuclear Physics and Astronomy.

Over sixty years research work at the earth's surface and above the atmosphere has shown the existence of a wide range of radiations in the primary beam varying from soft X rays to atomic nuclei. At present the upper energy limit for this radiation is in excess of $10^{20}$eV. The study of the primary spectra of both mass and energy have important implications to both astrophysics and cosmology and accordingly a great deal of time, effort and money has and is being expended on these two points.

At low energies ($<10^{14}$eV) the primary flux is sufficient for direct measurements to take place at very high altitudes from either balloon or orbital spacecraft. At such energies it is possible to calibrate detector systems directly by means of particle accelerators

and hence the data can be interpreted with a reasonable degree of certainty. With increasing energies the primary beam weakens and direct observation becomes difficult which is unfortunate as the most energetic of these particles ($>10^{18}$eV) are possibly of extragalactic origin. It is the mass spectrum and acceleration mechanisms of these particles that is currently of great interest to astrophysicists. Fortunately there exist techniques by which these highly energetic particles can be indirectly studied with a reasonably worthwhile yield of data.

## 1-2 The Extensive Air Shower.

When a highly energetic cosmic ray particle impinges upon the earth's atmosphere it is presented with approximately 1030gcm$^{-2}$ of material to traverse before reaching sea level. Laboratory studies have shown the proton to have an interaction length of approximately 80gcm$^{-2}$ in air (the mean free path for a heavy nucleus is correspondingly shorter). Thus, in passing through the atmosphere a primary is likely to interact inelastically with an air nucleus producing a shower of secondary cosmic rays. Accelerator and other experimental data indicate that the secondaries are pions, strange particles and heavy mesons. With a sufficiently energetic primary the secondaries carry off sufficient energy to initiate further interactions with air nuclei. This atmospheric cascade is repeated until the secondaries decay and are no longer energetic enough to initiate further interactions with air nuclei or the ground is reached. The transverse momentum of the secondaries plus Coulomb scattering in the atmosphere causes a laterally-developing extensive shower of particles covering many square kilometres at ground level.

Due to relativistic time dilation effects the charged pions are more likely to collide with the nucleus of an oxygen or nitrogen atom than decay in the early stages of a shower. As the energy of the pions is reduced in further interactions the relativistic effects are reduced and more decay (to muons and neutrinos) before they have the opportunity to interact. The transverse momentum of the parent pions is transferred to the daughter muons causing the shower to spread laterally and the muons to dominate the outer regions.

Due to their small interaction cross section and long life, many of the muons survive to sea level. Scattering due to Coulomb effects and interactions with the geomagnetic field is modest and well understood; thus study of the muon component yields much information about shower development. In the past work has been mainly concerned with the definitive measurement of the average momentum spectrum, arrival times etc., but current trends are tending towards a study of the muon component's origin and development in individual showers.

Neutral pions (which are highly unstable) decay almost instantaneously giving rise to pairs of photons. These photons naturally lead to pair production and the electron-positron pairs so produced then radiate bremsstrahlung photons leading to more pair production and a self perpetuating cascade of electrons, positrons and photons. Early experimental investigation of the electron photon cascade quickly showed that the size of the electron shower was directly related to the primary energy. Difficulties arose in that accurate measurement of shower size is difficult due to the low particle densities at the greater distances from the core giving rise to the necessity for large detector areas. Recently this problem has been overcome by measuring a ground parameter in showers which is

principally dependent on primary energy, shows small fluctuations and may be well measured [see e.g. Hillas et al (1971)].

## 1-3. The Detection of Extensive Air Showers.

In 1938 Auger and colleagues working in Paris with a very small array of Geiger tubes of extent a few tens of metres recorded many simultaneous discharges over the array. They concluded that the cause of these discharges came from the air above and were in fact showers of fast particles covering large areas (several hundred square metres) and as a consequence were named Extensive Air Showers. This pioneering work showed the way for other workers and the next big step, to measure the showers individually and investigate their characteristics instead of merely recording their existence, was made in 1948 by Williams at the Massachusetts Institute of Technology.

He used ionization chambers on a 12 metre triangular array recording their response photographically (from oscilloscope traces) every time coincidences were registered. Knowing the response characteristics of his detectors, he was able to locate the impact point of the shower and estimate the number of particles therein.

Five years later the basis of 'modern air shower detection' was laid down by Bassi, Clark and Rossi at M.I.T. using widely spaced (30m) scintillation detectors with fast recording equipment. With this experiment they were able to make basic investigations into shower front structure and also estimate shower arrival directions from studying the time differences between the response of the detectors in the array.

By 1956 Rossi and collaborators had set up an array of 15 large scintillation counters covering a square kilometre at Agassiz near

Boston and were able to further refine the techniques until the number of particles in a shower (and hence the energy of the primary particle) could be estimated to better than 20% and the directional parameters to within a few degrees. As the arrays got bigger so did their ability to detect larger air showers and in 1957 the Agassiz Array recorded an event with an energy of approximately $10^{18}$eV to the great excitement of the astrophysical world.

The laterally extensive nature of the air showers means that sufficient data for their analysis can be obtained by sampling over a large area with many detectors and the larger the array the greater its collection efficiency. The next quantum jump in air shower studies occurred in 1959 when Linsley and Scarsi commissioned their giant array at Volcano Ranch in New Mexico, increasing the sensitive area over the Agassiz Array by a factor of fifty. Since then more giant arrays have been commissioned at Haverah Park in Great Britain. Sydney in Australia and Yakutsk in the Soviet Union. All these experiments are similar, sampling and making timing measurements over large inter-detector distances. With the exception of the Haverah Park Array which employs Čerenkov radiation in large area water tanks, scintillators are still used as the detection medium.

Over the years the large arrays have spawned many parasitic experiments studying specialized aspects of air showers. The largest range of such experiments have been made at Haverah Park. Some have used the existing detectors; e.g. relating pulse profiles to shower development, whilst the remainder (like the subject of this thesis) require a separate apparatus to be constructed within an existing array. One of the latter category of experiments (Night Sky Optical Čerenkov emission) has now been developed to the extent that it can

Figure 1-1 The Integral Primary Energy Spectrum, from Pickersgill (1973).

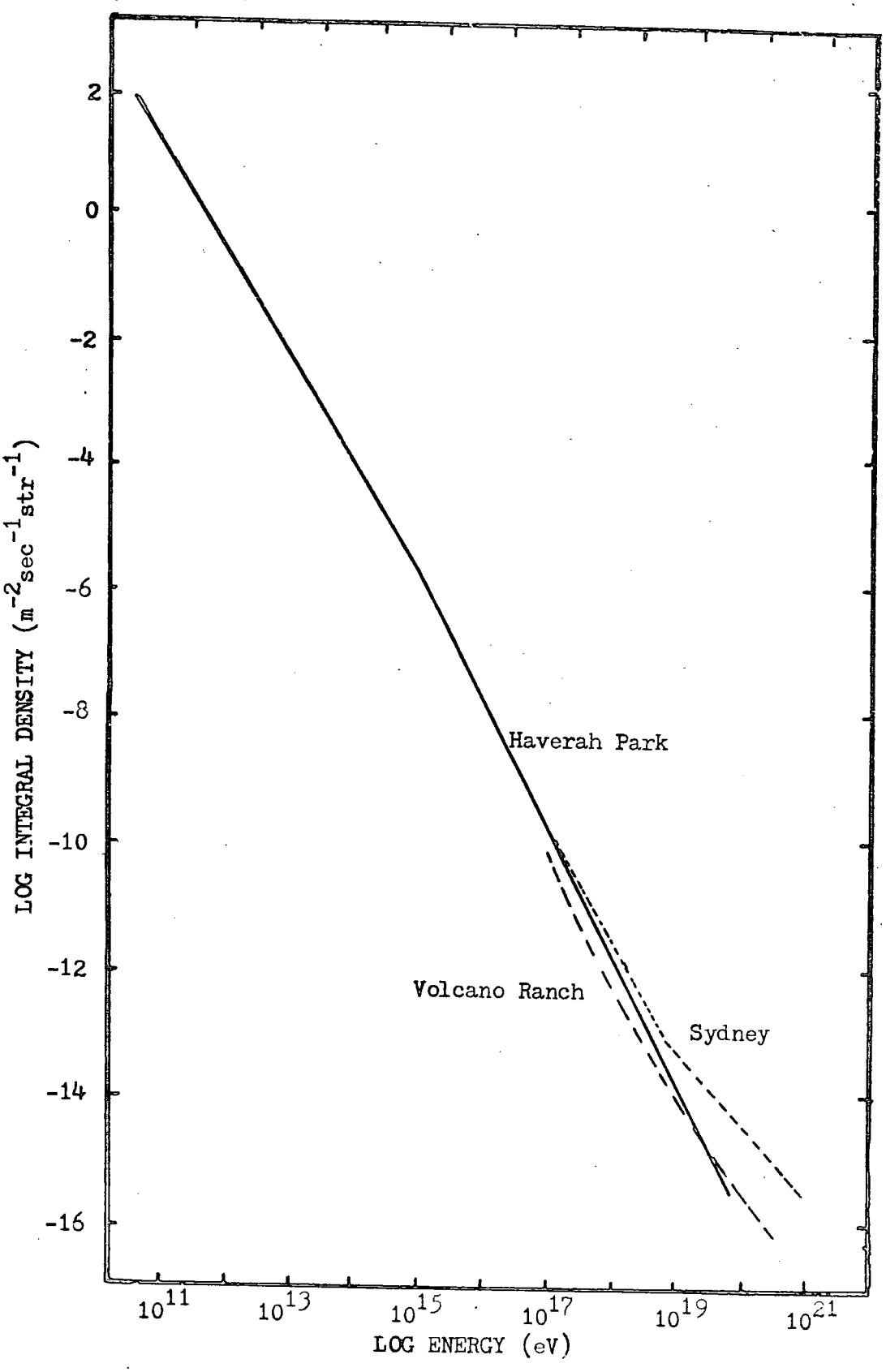
2
0
-2
-4
-6
-8
-10
-12
-14
-16
LOG INTEGRAL DENSITY ($m^{-2}sec^{-1}str^{-1}$)
Haverah Park
Volcano Ranch
Sydney
$10^{11}$
$10^{13}$
$10^{15}$
$10^{17}$
$10^{19}$
$10^{21}$
LOG ENERGY (eV)

stand alone as an air shower array.

The modern night sky Čerenkov experiments stem from the work of Galbraith and Jelley (1953) which was further refined and developed at Haverah Park and Yakutsk in the early 1970s. Unfortunately such work is dependent upon good clear dark sky conditions which are not particularly prevalent at the locations of many of the existing arrays. Fortunately light detector arrays, although necessarily complex, are very compact and thus easily transported to a region of good sky clarity and favourable weather. As a development of the Haverah Park work [described by Wellby (1977)] a totally independent Čerenkov Detector Array has been operating in the Utah Desert, U.S.A. for the period 1977 - 1980. It is now almost certain that, as a result of this work, the previous problems and doubts arising from the technique due to a small data sample will be overcome and the publication of the final results is eagerly awaited.

The final and possibly definitive new experimental technique relies on detecting the fluorescent light produced by the passage of a shower through the atmosphere. Unlike Čerenkov light, fluorescence is emitted isotropically upon de-excitation of nitrogen molecules and thus, even though its intensity is considerably reduced, it should be possible to detect it at a distance of many kilometres. As a result the technique is currently under development in Japan and the U.S.A. In the latter case a device (named 'Fly's Eye') capable of observing the entire night sky at once is under construction in the Utah desert. The detector should be capable of reconstructing the track of an event in all three spatial dimensions which will give directly the energy and arrival direction of the primary particle. Due to its all-sky capability and ability to respond to showers at enormous distances

it is expected that the device will accumulate data on the very highest energy events some ten times faster than the rest of the arrays combined, despite being constrained to the same observing conditions as a Čerenkov detector array.

## 1-4 The Primary Composition and Energy Spectrum of the Cosmic Radiation

At energies where direct observation is possible the primary mass spectrum has been investigated by emulsion stacks flown in balloons and from orbital satellites. Up to about $10^{13}$eV it has been possible to identify the primaries confirming the presence of protons and heavier nuclei although the relative abundances remain undetermined at the highest energies.

In the air shower region of the energy spectrum the chemical composition of the primaries is still largely unknown and the identification of the mass spectrum in these regions is one of the major quests of current research. In the forseeable future it is unlikely that much direct or detailed data will become available on the primary composition but it may well be possible to determine e.g. the ratio of protons to heavy nuclei at these energies. A review of the available data in the energy range $10^{10}$ - $10^{19}$eV has been made by Sreekantan (1972) which demonstrates the (present) inconclusive position.

The shape of the primary energy spectrum has posed a problem over many regions and current data indicates a slope equivalent to an exponent of 2·2 in the integral energy spectrum for energies between $10^{16}$ and $10^{19}$eV. In contradiction to earlier indications a flattening in the spectrum is again suggested at higher energies. Greisen (1966) suggested the existence of a cut off at the highest energies ($10^{19}$eV)

arising from the interaction between high energy protons and the low energy photons of the $3^{\circ}K$ background radiation. Extragalactic protons with a path length greater than the characteristic distance for the $p-\gamma$ interaction should be removed from the primary flux. Investigations to date have been hampered by the scarcity of such high energy primaries although no evidence for a cut-off has yet been observed.

## 1-5 Outline of this Thesis.

This thesis describes a new experiment built at the Haverah Park Air Shower array to measure the spatial angles of muons in large extensive air showers. Large-scale computer simulations of the muon component are described and related where possible to the experimental results. Several other phenomena are investigated, particularly the lateral distribution of muons at two energy thresholds. The mean characteristics of recorded data are established and discussed. Investigations into fluctuations in discrete showers have been made and are described and discussed.

# Chapter Two

## Muons - A Summary to Date

### 2-1 Introduction.

In the early investigation of air showers it was soon recognised that the muon component was of great importance. The very weak interaction of muons with atmospheric nuclei and relatively long lifetimes compared to their parent pions ensured the survival to sea level of a large proportion, bringing with them direct information from their source in the shower cascade. To exploit this, many experiments have studied the muon component and a great deal of information is now available, giving much help in the interpretation and understanding of air shower cascades.

In this chapter some of the past work on the muon component both experimental and theoretical will be reviewed with particular reference to the experimental work with which this thesis is concerned. As an introduction to the subject matter of this thesis previous work on spatial characteristics of muons in extensive air showers is described in some detail giving an insight into the design philosophy of the new experiment.

### 2-2 Lateral Distribution Measurements.

The lateral distribution of air shower particles is one of the easiest parameters to measure (and consequently one of the earliest phenomena investigated) and as a consequence they are well understood. The addition of a substantial amount of shielding material to a 'standard' air shower array detector filters out the soft component leaving a relatively pure muon sample. As lateral distributions are so

Figure 2-1 The muon lateral distribution in large EAS as measured by Strutt (1976) and Armitage (1973) at Haverah Park, ($\theta < 25^{\circ}$) (From Strutt (1976)).

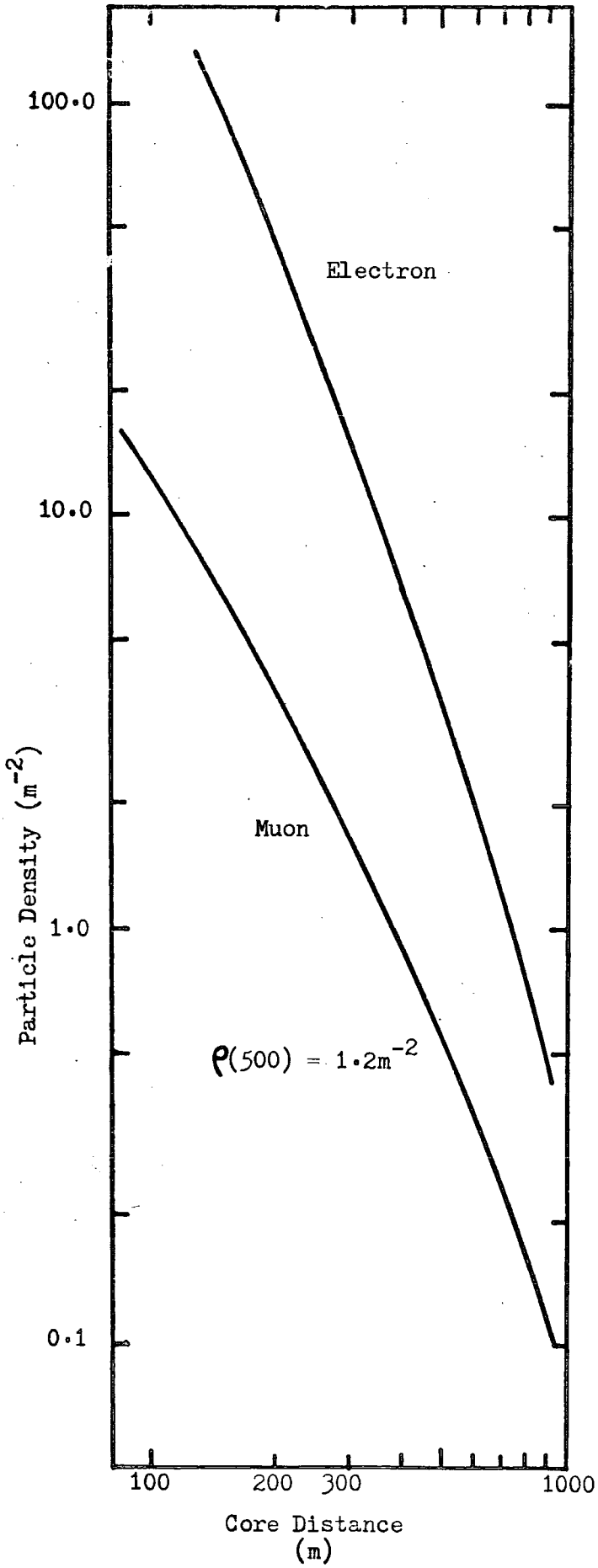
100·0
10·0
1·0
0·1
Electron
Muon
ρ(500) = 1·2m⁻²
Particle Density (m⁻²)
100
200
300
1000
Core Distance
(m)

easy to measure, they can also serve as a useful check on the performance of, and be used as a means of calibrating a new detector or experiment. The consistency of the lateral distribution of muons (due to their very weak interactions with the atmospheric nuclei and the geomagnetic field) makes it an ideal measure for the cross calibration of different air shower arrays. As muon physics is comparatively well understood lateral distributions are easily derived from simulations and thus are a good measure for the comparison of simulations with observations.

An up to date composite lateral distribution for both muons and soft component ($\theta < 25^{o}$) is given in figure 2-1 and is derived from the scintillator data of Strutt (1976) and Armitage (1973); all the measurements being made by the University of Nottingham group at Haverah Park, with a shower size normalized to $\rho_{500} = 1{\cdot}2m^{-2}$. It will be seen that at larger core distances the muons dominate and this led Hillas (1971) to develop the Haverah Park primary energy estimator, $\rho_{500}$ which was later refined to Pd(500) by Lapikens (1977).

Independently, Strutt found a muon structure function exponent of $2{\cdot}9 \pm 0{\cdot}1$ compared to Armitage's value of $2{\cdot}8 \pm 0{\cdot}06$, the difference being ascribed to the underestimation of muon densities by flash tubes, particularly at smaller core distances. This phenomenon is discussed in more detail in Chapter 4.

The lateral distribution has been clearly shown to be dependent on zenith angle (figure 2-2), broadening with increasing zenith angle, indicating a receding of the shower maximum into the atmosphere. Hillas (1969) has observed that at large zenith angles, particularly with showers from the North, geomagnetic effects become significant splitting the particles into two subshowers of positive and negative

Figure 2-2 The zenith angle dependence (Sec $\theta$) of the exponent of lateral distributions from Strutt (1976) and Armitage (1973).

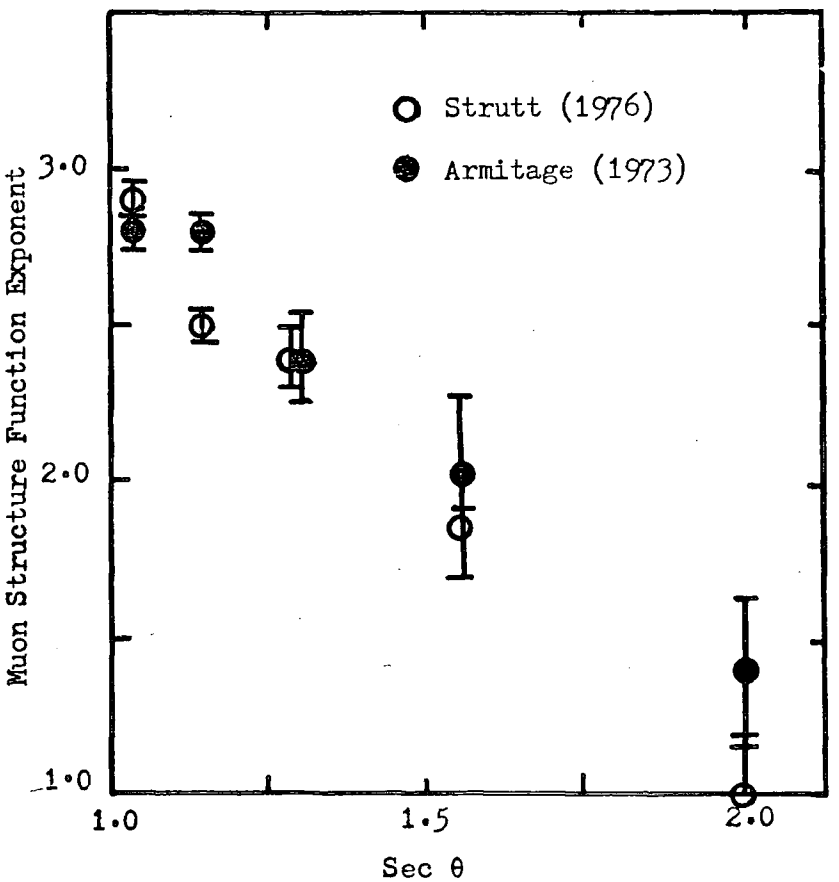
Strutt (1976)
Armitage (1973)
Muon Structure Function Exponent
3·0
2·0
1·0
1.0
1.5
2.0
Sec θ

Figure 2-3 The muon/deep water Čerenkov signal ratio measured at Haverah Park by Strutt (1976) and Armitage (1973).

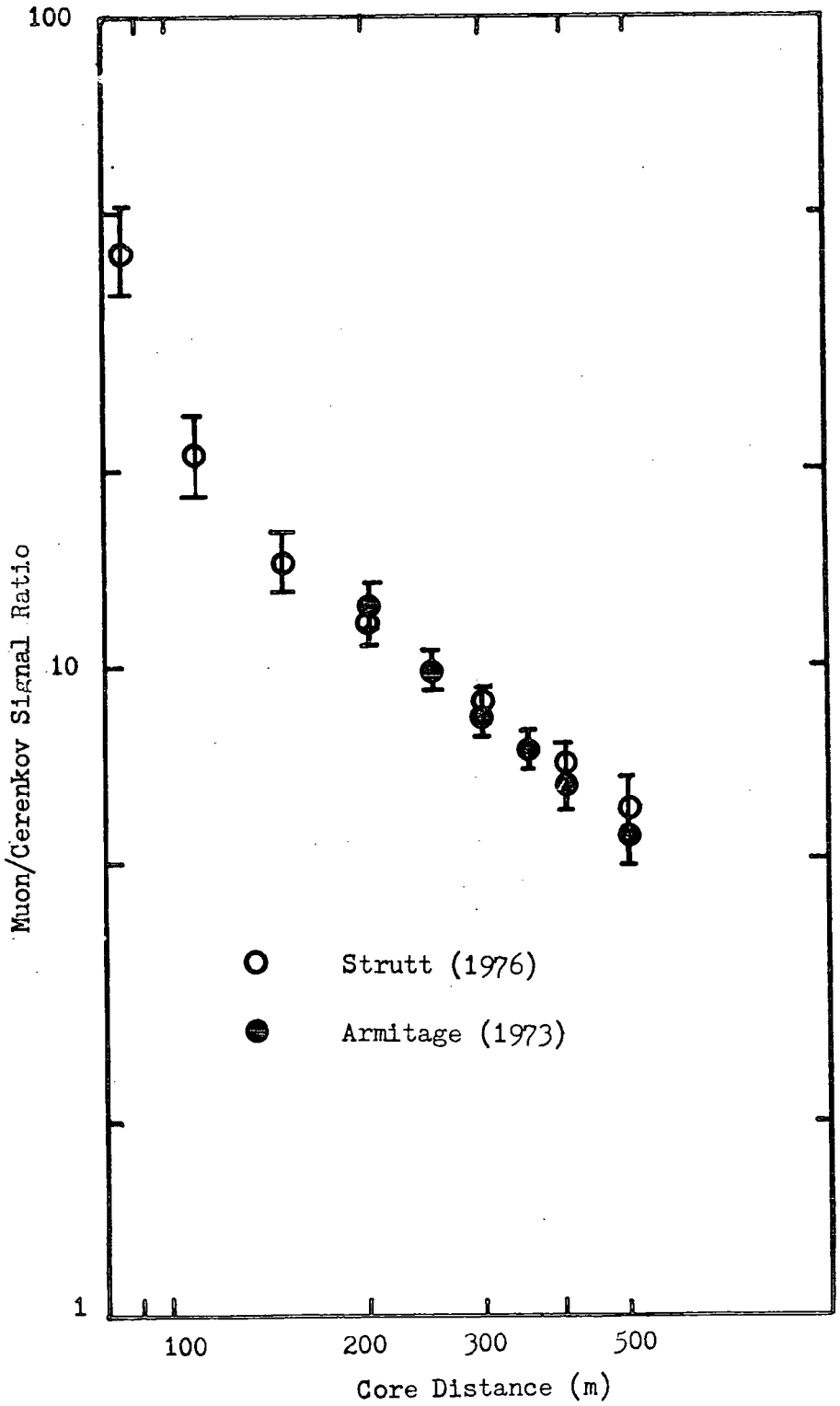
100
10
1
Muon/Cerenkov Signal Ratio
Strutt (1976)
Armitage (1973)
100
200
300
500
Core Distance (m)

Figure 2-4 The differential muon momentum spectrum in large air showers as measured by Dixon et al (1974) at Haverah Park.

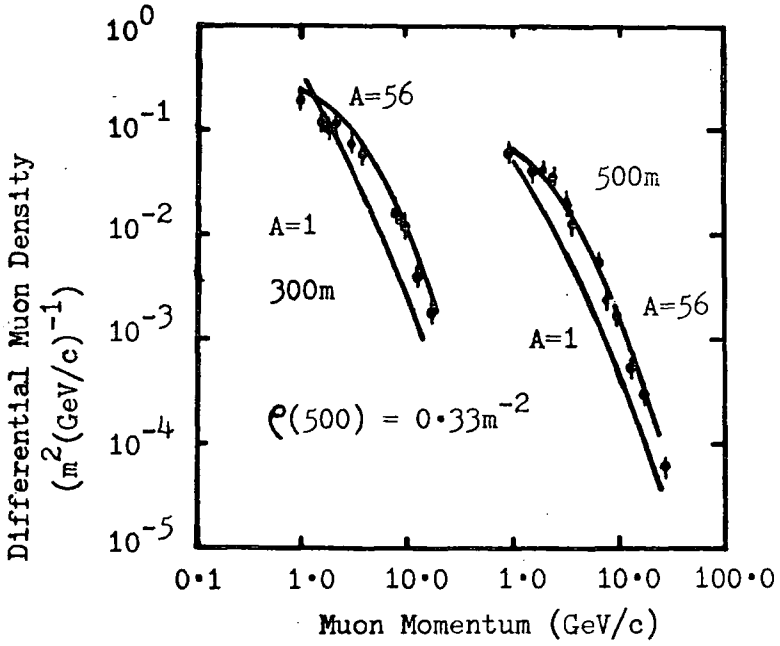


• Dixon et al (1974)

— Simulation, Landau $E_p^{\frac{1}{4}}$ model

muon. This may cause confusion with the interpretation of some sets of data under certain circumstances, particularly with direction sensitive equipment such as that described in this thesis. This geomagnetic splitting of the muon component was used by Earnshaw et al (1973) in an investigation of muon heights of origin - see section 2-4.

If a muon detector is located adjacent to one of the main detectors in an air shower array a further useful parameter can be obtained, viz the muon/total charged particle ratio (in the case of Haverah Park the muon/deep water Čerenkov detector signal ratio). Simulations have shown the ratio to be related to shower development and studies of average features and fluctuations in individual showers have recently yielded useful information on the longitudinal cascade [McComb and Turver (1981 Private communication)].

## 2-3 Muon Momentum and Energy Spectra.

Although the majority of the muons occur in the outer regions at a comparatively low density, when integrated over the whole shower their total number is large (some $10^6$ muons in a shower of energy $10^{17}$ - $10^{18}$eV). Furthermore, their average energy is much greater (≈1GeV) than that of the shower electrons (10 's MeV) Thus the muons in a typical shower at sea level carry much more total energy than the electron-photon component.

It is clear that at large core distances (>500m) the spectrum is as soft as that for the ever-present natural muon background. Of the muons in and around the shower core (<10m) several per cent are sufficiently energetic to penetrate far into the ground and have been followed by Barratt et al (1952) and later workers to a depth of 1600m

water equivalent.

The differential muon momentum spectrum in large air showers has been well measured at Haverah Park and reported by Dixon et al (1974). Figure 2-4 shows their measured momentum spectrum at core distances of 300 and 500 metres for showers within $30^{\circ}$ of the zenith and normalized to a $\rho_{(500)}$ of $0{\cdot}33 m^{-2}$ (primary energy $\approx 10^{17}$eV). Also shown are the simulations of Gaisser et al (1978) using the Landau model with iron and proton primaries in vertical showers. Good agreement is seen for showers arising from heavy primaries but is less evident for proton simulations particularly at a core distance of 300m where a steeper spectrum is predicted than is measured.

## 2-4 The Heights of Origin of Muons.

The relatively long lifetimes of the muons together with their weak interactions ensures that a substantial proportion survive to sea level carrying with them data from all parts of the shower cascade. Accordingly, if the development of the muon component itself is investigated in detail it can be expected to mirror the main cascade from initiation to ground level. To achieve these ends several experiments have been performed together with computer simulations. Some of the latter were with a view to designing a new experiment - the subject of this thesis - and these will be summarised in this section.

It will be appreciated that, although weak, the geomagnetic field will under certain conditions have an appreciable effect on the charged particle component of an air shower, splitting it into two lobes of oppositely charged particles.

If it is assumed that:-

Figure 2-5 The distortion in muon charge ratio as measured by Earnshaw et al (1973) using the Haverah Park Spectrograph. The effect of the geomagnetic field separating the muon component into two oppositely charged lobes is clearly visible.

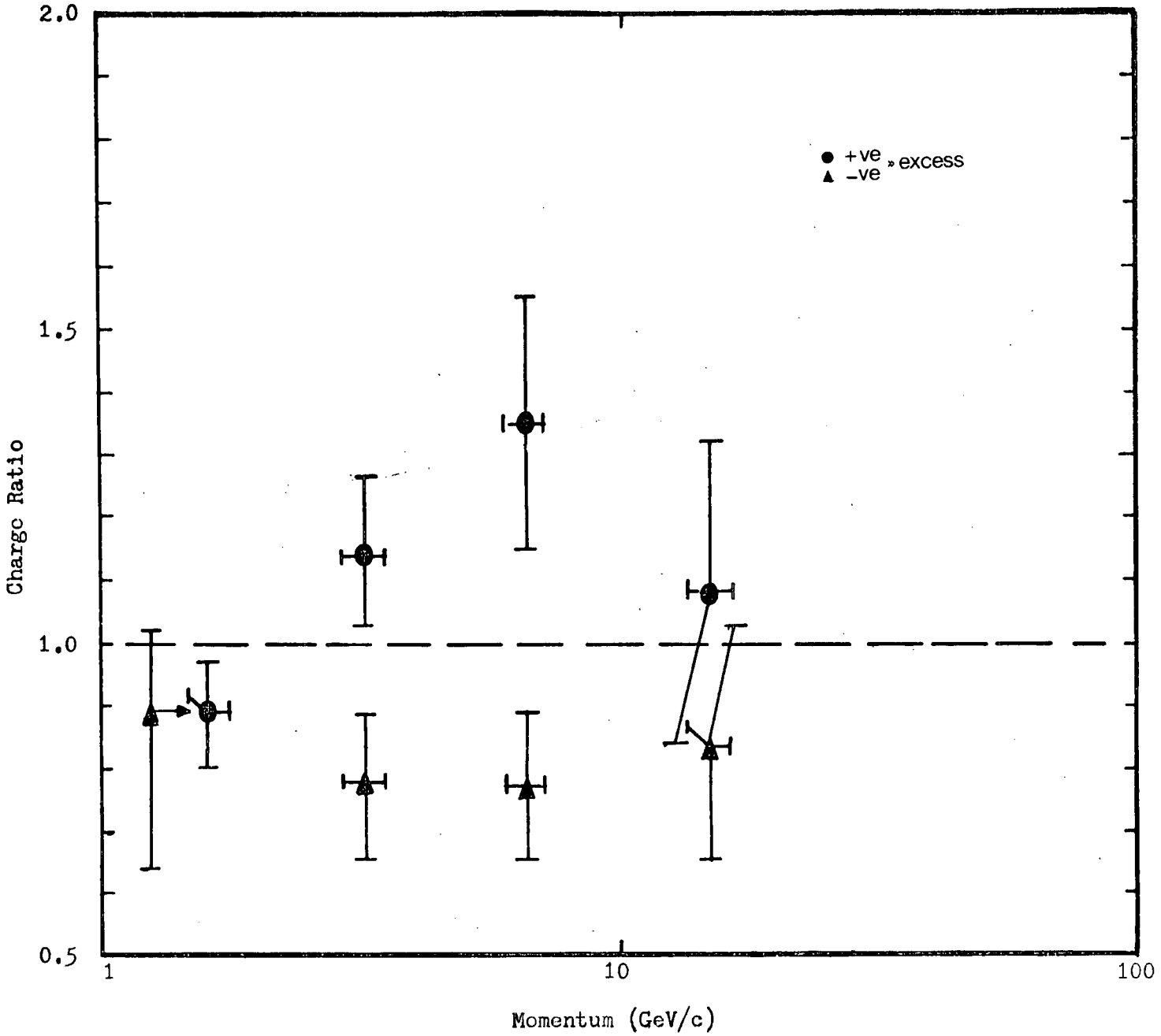
2.0
1.5
1.0
0.5
Charge Ratio
+ve
-ve
excess
1
10
100
Momentum (GeV/c)

(1) the lateral distributions and momentum distributions of oppositely charged particles are identical, and

(2) all geomagnetic effects on positively and negatively charged muons are equal and opposite

then, at a given core distance the ratio of the ordinates of the two measured lateral distributions indicates the expected charge ratio. It is obvious that the distortions which are seen in the charge ratio due to geomagnetic interactions can therefore be directly related to the heights of origin. This direction of research was first followed by Earnshaw et al (1971-3) at Haverah Park whilst they were engaged on making measurements on the muon momentum spectrum with the solid iron magnet spectrograph. The results from this study are given in figure 2-5 for two categories of showers, one where the shower had overflown the spectrograph (ratio less than unity with a negative charge excess) and the other for those showers falling short (ratio greater than unity with a positive charge excess). From this it was possible to estimate the muon heights of origin and these are shown in figure 2-6. It should be noted that the data are based on samples of single muons averaged over many showers.

A similar type of experiment was performed by Burger et al (1975) giving results which are comparable with Earnshaw et al in a limited range of core distances ($r < 100m$). As well as charge ratio distortion they also attempted to use measurements of the energy spectrum, adapting the production height distribution of pions by Hasegawa et al (1975). At a mean core distance of 30m and with muons of energy of 15GeV a mean production height of $0{\cdot}92 \pm 0{\cdot}15$ Km for near vertical showers was reported.

A more straightforward and direct approach was developed by

Figure 2-6 Muon heights of origin from distortions of the charge ratio, from Earnshaw et al (1973).

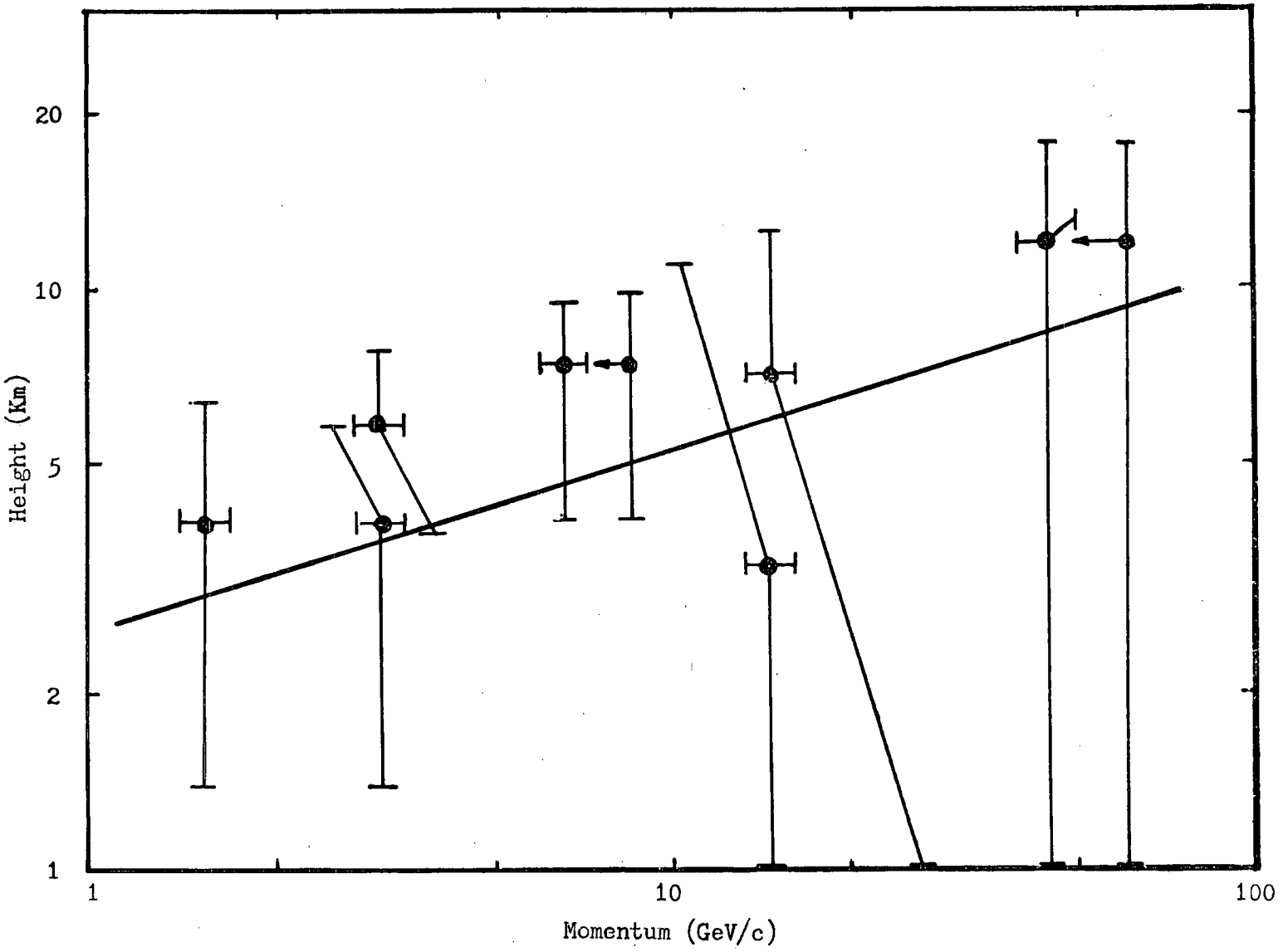
20
10
5
2
1
Height (Km)
1
10
100
Momentum (GeV/c)

Earnshaw et al after their geomagnetic work and used a simple trigonometric technique, details of which are given in Appendix One. Measurements were made of the angle subtended to the zenith by single low energy muons ($E_\mu > 1{\cdot}0$ GeV) in the upper flash tube trays of the MkII Haverah Park Spectrograph. Transforming these angles to the shower core and knowing the core distance then gives a direct indication of the muon's origin with respect to the shower's core. Summing over a large number of such events enabled the average characteristics to be determined and these are shown in figure 2-7. A monotonic relation between muon-core angle and core distance is observed. From these results a relation was derived for the height of origin of a muon [H(P,r)] given a known momentum (P GeV/c) and core distance (r m) [Earnshaw et al (1973)].

$$H(P,r) = H_0 + \alpha \log_{10} P + r/\beta$$

where $H_0 = 1{\cdot}68 \pm 0{\cdot}15$ km

$\alpha = 1{\cdot}78 \pm 0{\cdot}2$ km

$\beta = 0{\cdot}263 \pm 0{\cdot}033$

From these and other unpublished results Gaisser et al (1978) have compiled a summary of the mean muon heights of origin (figure 2-8) and compared it with recent simulations. Reasonable agreement is observed for simulated showers with the cascade development expected from iron nucleus primaries using the scaling model (other masses/models provide equally acceptable predictions).

The data produced by Earnshaw et al was limited in scope, being restricted to confirming the validity of the technique; nevertheless it provided valuable information together with simulations for the design of a purpose-built experiment. Full details were given

Figure 2-7 Muon-core angle as a function of core distance from Machin, Stephenson and Turver (1973) (unpublished).

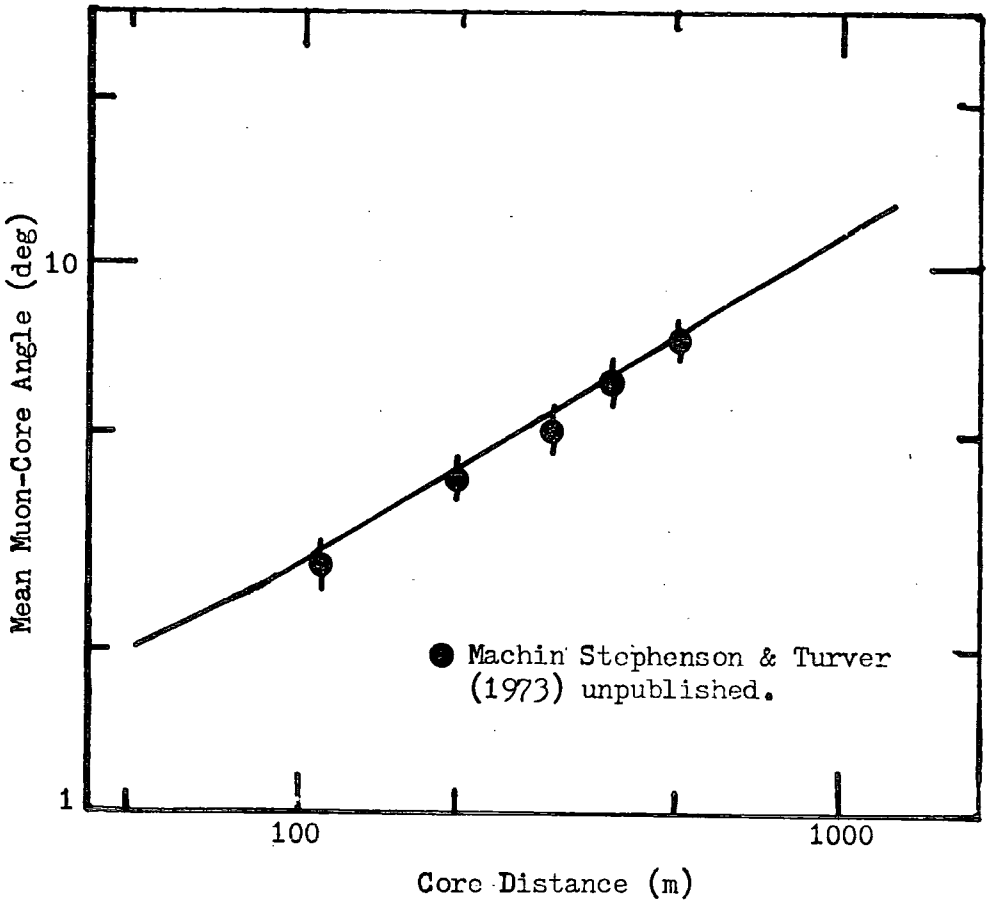
Mean Muon-Core Angle (deg)
10
1
100
1000
Core Distance (m)
Machin Stephenson & Turver
(1973) unpublished.

Figure 2-8 The heights of origin of muons as measured by several experiments. Also shown are data for iron primaries using a scaling model. (From Gaisser et al (1978)).

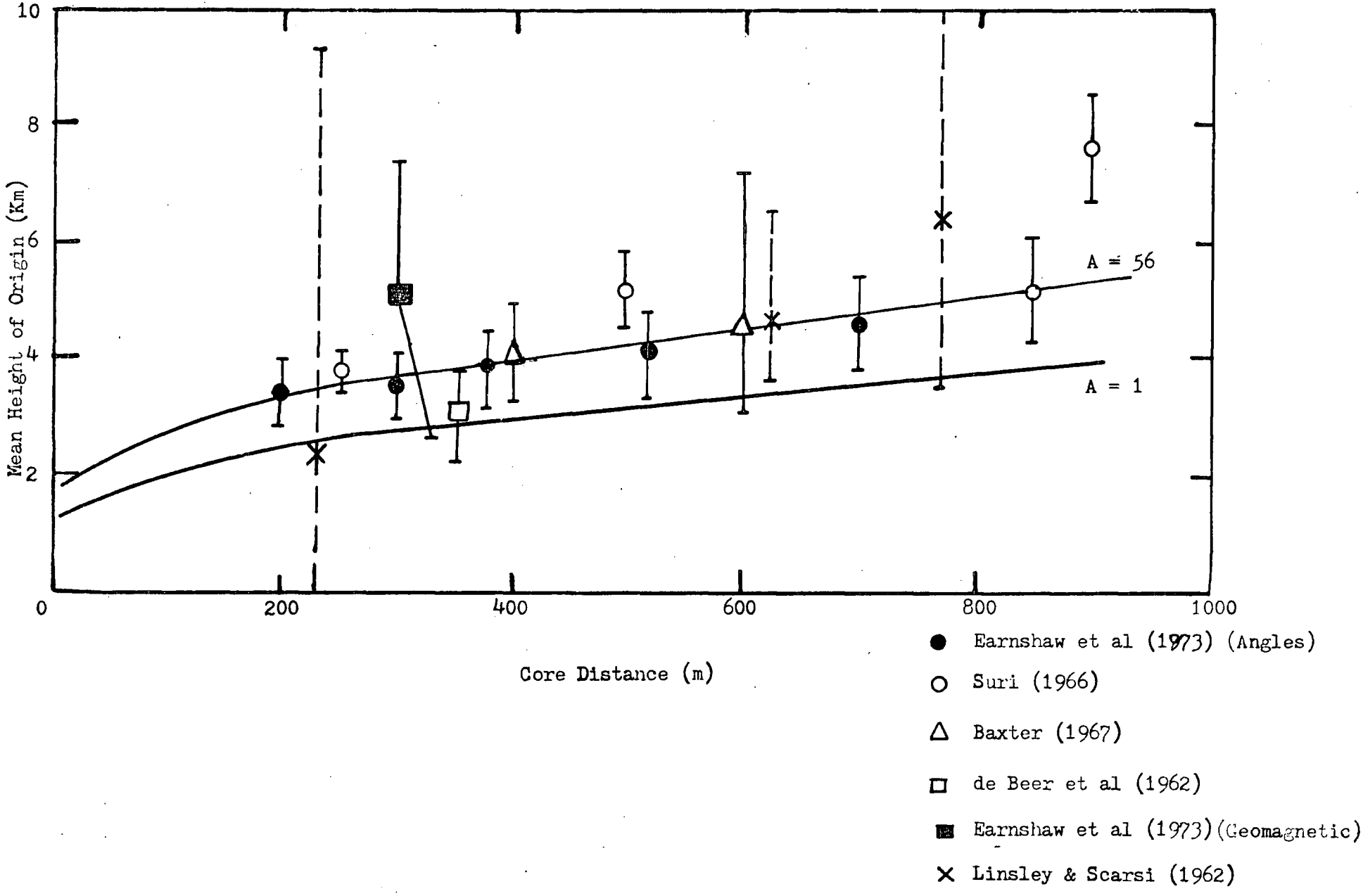
10
8
6
4
2
0
200
400
600
800
1000
Mean Height of Origin (Km)
Core Distance (m)
A = 56
A = 1
Earnshaw et al (1973) (Angles)
Suri (1966)
Baxter (1967)
de Beer et al (1962)
Earnshaw et al (1973) (Geomagnetic)
Linsley & Scarsi (1962)

by Turver (1975) and Gibson (1976).

The original simulations used the then universally popular CKP model for the shower cascade and included both the spatial and temporal characteristics of the muon component in vertical $10^{18}$eV showers. The simulations followed the muons produced in a small azimuthal segment which contained hypothetical detectors at various core distances and of various areas. To simulate a 'real' detector the muons were passed through various thicknesses of shielding (lead) and then unspecified track delineating devices of high accuracy. The output data available for each muon were:- arrival time, height of origin, energy and spatial angle. In addition external perturbations, for example Coulomb and geomagnetic scattering plus scattering in the detector shielding, were considered.

The results were considered in three ways whilst designing a new experiment:-

a) By assuming that the only data available on particle directions are those from muon detectors. Such data are presented in figure 2-9a from a single simulation of a typical shower.

b) By assuming that data from other sources (fast timing, particle density etc.) exist enabling the shower's axial direction and impact point to be determined. In this case the data in (a) above may be considered as angles with respect to the shower core direction.

c) Finally, to consider the muon angular data in one detector and compare it with that recorded by another similar detector at a different core distance. Such data are shown in figure 2-9b, again for a single typical shower.

As the existing data were obtained from the Haverah Park Spectrograph and any future experiment would, in all probability, also

Figure 2-9a Individual core angles in a single simulated shower recorded in an ideal detector, [from Turver (1975) unpublished].

Figure 2-9b A different simulated event recorded in two widely spaced ideal detectors, [from Turver (1975) unpublished].

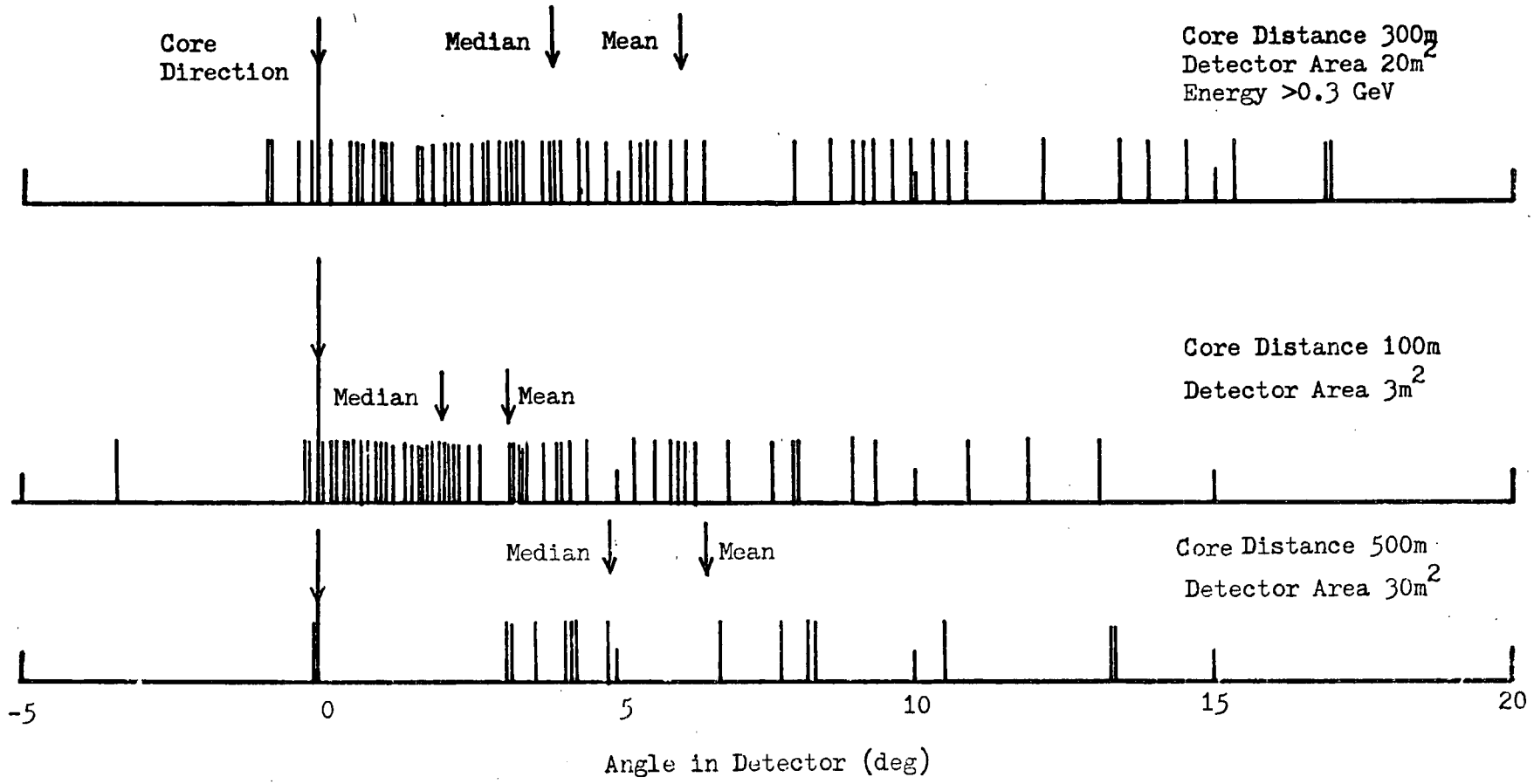
Core
Direction
Median
Mean
Core Distance 300m
Detector Area 20m2
Energy >0.3 GeV
Median
Mean
Core Distance 100m
Detector Area 3m2
Median
Mean
Core Distance 500m
Detector Area 30m2
-5
0
5
10
15
20
Angle in Detector (deg)

be located at Haverah Park items (b) and (c) would be much closer to reality than (a).

Having now performed a preliminary experiment and feasibility study, it only remained to design, construct and operate some specialist equipment.

# Chapter Three

# The Experiment

## 3-1 Introduction

The work of Earnshaw et al described in the previous chapter plus the encouraging predictions of simulations indicated that the heights of origin of the muon component in air showers could be estimated from the ground with obvious important consequences for the study of the cascade development. In their work, using data from the Haverah Park muon spectrograph, Earnshaw et al investigated the charge ratio distortion caused by geomagnetic effects plus the lateral and angular scatter of muons with respect to the shower core. Due to the small sensitive area of the spectrograph it was necessary for the results to be averaged over many similar events.

Subsequent simulations confirmed that the height of origin of the muon component was directly related to the cascade development. The simulations also indicated a sensitivity to the mass of the primary particle in that showers which show fluctuations in their development which are to be expected if, and only if, there exist primary protons should also show fluctuations in the height of origin of muons. In view of the encouraging nature of this work it was decided to go ahead with the construction of a detector system at Haverah Park with the capability of studying the heights of origin in individual large showers ($E_p > 10^{18}$eV).

The termination of the MkII Spectrograph programme and simultaneously the Durham Nuclear Active Particle Spectrograph made available some 18,000 neon flash tubes of various sizes and it was decided to re-deploy the flash tubes and existing hardware to build

two new large area detectors.

The two detectors (a detailed description of which follows) have been designed on the basis of further simulation results and are of sufficient area to enable 15 - 30 muons to be studied in a shower of primary energy $>10^{17}$eV. The core direction resolution available from the main array, the trade off between the detector sensitive area and particle track resolution dictated a designed maximum measurement error of $0{\cdot}5^{o}$ in the individual muon directions.

The larger of the two new detectors is located on the site of the magnet spectrograph in the centre of the air shower array and the other approximately 250m away in a newly commissioned experimental area. This latter site also accommodates a muon timing detector (operated by the University of Nottingham group). These two detectors are fully integrated and use the same shielding material.

Previous experience of the use of neon flash tubes in air shower measurements suggested a photographic recording system which, once commissioned, would require a minimum of maintenance ensuring reliability over long recording periods.

A detailed description of the equipment is given in Gibson (1976) and only a short resumé and report of subsequent modifications developed under operational conditions are presented here.

## 3-2 The Haverah Park Experimental Array.

The Haverah Park Air Shower Array is described in detail by Tennent (1967) and Andrews (1970) so only a brief description will be presented here. The array is located at a latitude of $53^{o}58{\cdot}2'$N longitude $1^{o}38{\cdot}1'$W and at a mean altitude of 220m equivalent to an atmospheric depth of 1016 gm $cm^{-2}$. A plan of the array is presented

Figure 3-1 The Haverah Park EAS Array.
(N.B. The 'Infilling Array' is omitted for clarity).

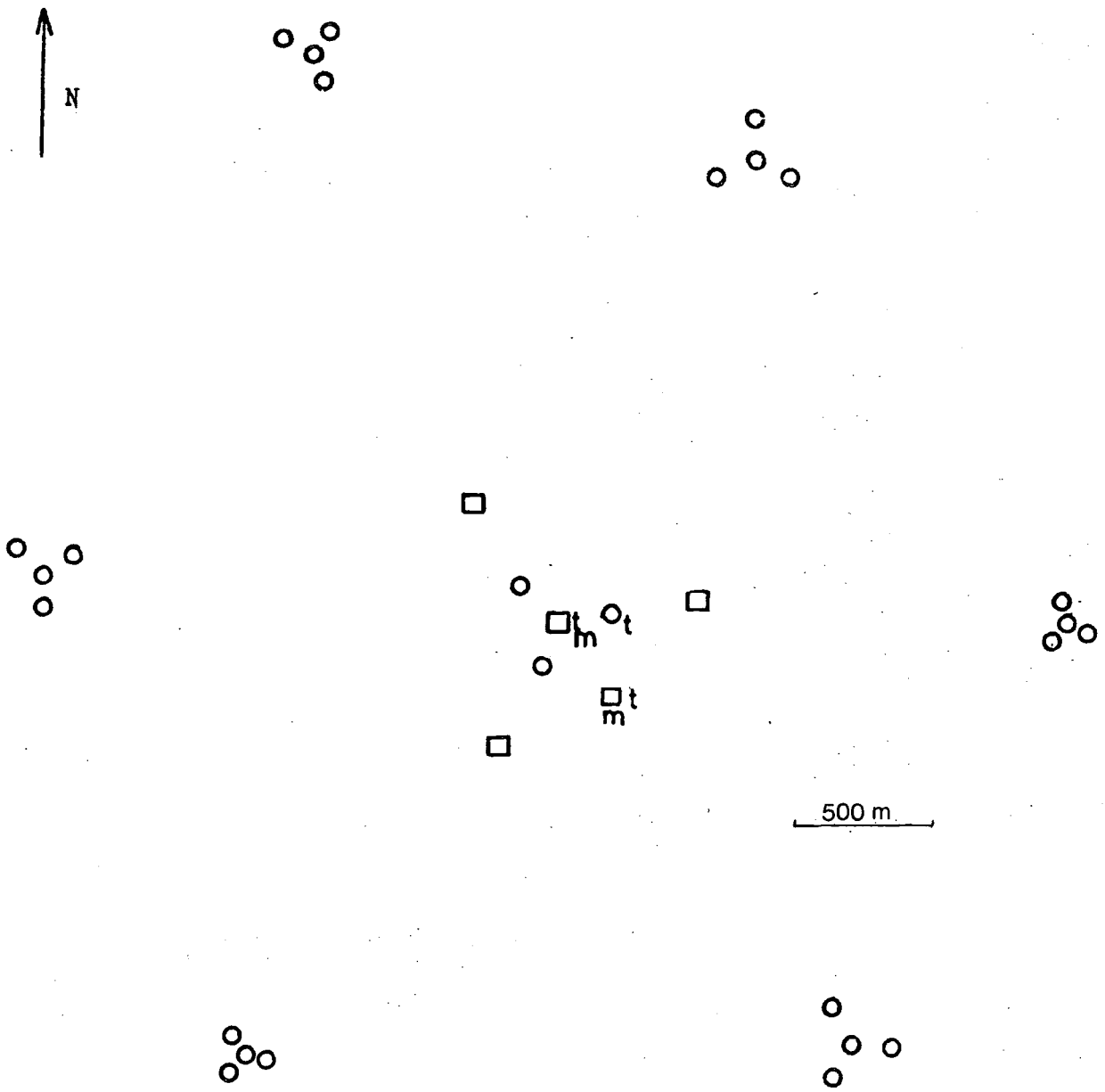
N
500 m
2Km Array
500m Array
Central Detector
150m Array
m Muon Spatial Angle Detectors
t Muon Timing Detectors

in figure 3-1.

The detection technique employed (Čerenkov radiation produced in deep water tanks) is quite unique in air shower work and has the great advantage of providing very large area detectors ($34m^2$) cheaply and easily. Detailed descriptions of the water tanks and their performance can be found in Turver (1963). In addition to the main detectors the 500m array contains another array of small ($1{\cdot}25m^2$) closely spaced water detectors to study the regions close to the shower cores [see Craig et al (1979)]. The large area detectors (out to distances of 500m) are linked to the centre for all recording, an air shower being recorded whenever the "ten particle level" in the centre detector and two of the 500m detectors is exceeded simultaneously. In addition to the main and infilled arrays, the Nottingham University group operate three muon timing detectors which use shielded liquid scintillators.

## 3-3 The Muon Angle Detectors.

### 3-3.1 The neon flash tube.

The neon flash tube particle detector was introduced by Conversi and Gozzini (1955) and has since been used in one form or another in many cosmic ray experiments. Flash tubes are ideally suited to the current experiment where a large sensitive area and good particle track delineation is required.

The flash tubes used in this case consist of flat-ended sealed glass tubes filled with neon at slightly below atmospheric pressure. In use a layer of tubes is placed between sheet metal electrodes and, when an external trigger detector records the passage of a charged particle a high voltage pulse is applied across the plates. The tubes

Figure 3-2 Muon Detector A.

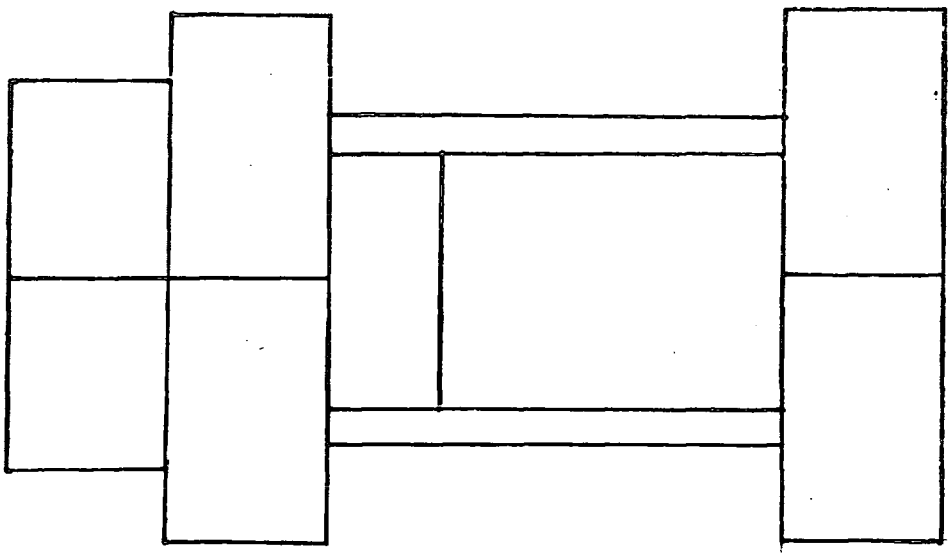

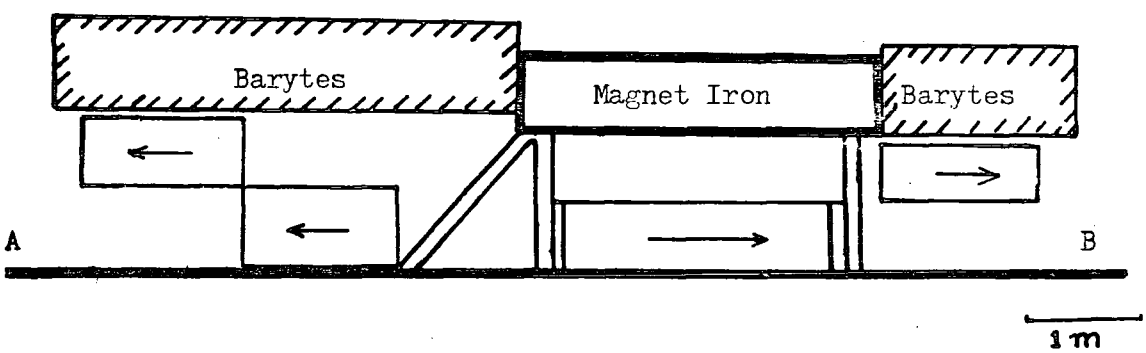
Barytes
Magnet Iron
Barytes
A
B
1 m

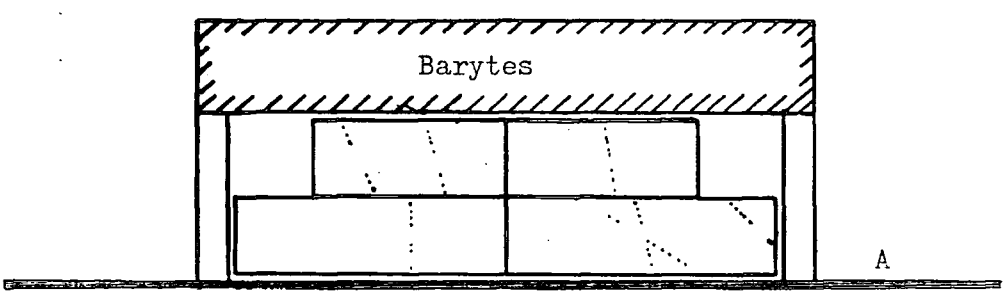
Barytes
A

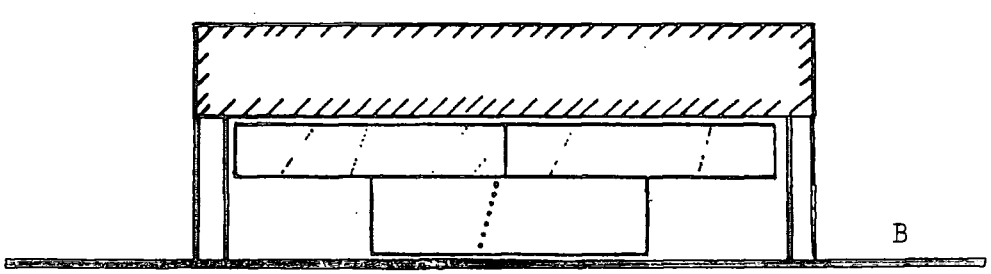
B

through which the particle passed give a flash of light which can be recorded photographically or electronically.

3-3.2 The Detectors.

a) Basic mechanical details.

Simulations by Bull et al (1962) showed that the relative positions of flash tubes in a detector had little or no bearing on the accurate resolution of particle tracks. Thus a simple half-pitch stagger in the horiziontal plane and a constant vertical pitch was adopted for both detectors.

Previous experience with both the MkI and MkII spectrographs at Haverah Park led to a simple, cheap, accurate and reliable system for supporting flash tubes. Dural bars (durals) are milled with a series of constant and parallel pitch slots across their length [exact details can be found in Pickersgill (1973)]. The durals are then mounted at the front and rear of each flash tube tray and carefully aligned to ensure that the front and rear slots correspond.

As may be expected the weight of the glass tubes causes considerable distortion along the length of the durals. This problem was overcome by mounting vertical 6mm perspex strips along the front and rear of the tray at frequent intervals. The durals are then bolted to the perspex and, as the operation was performed under controlled workshop conditions, exact dural alignment was ensured.

b) Detector A.

The larger of the two detectors is located at the approximate centre of the main particle array on the site originally occupied by the solid iron magnet spectrograph [described by Machin (1973) and Pickersgill (1973)]. Of the spectrograph only the magnet iron remains, and this has been degaussed and the hole for the windings

Figure 3-3 Muon Detector B.

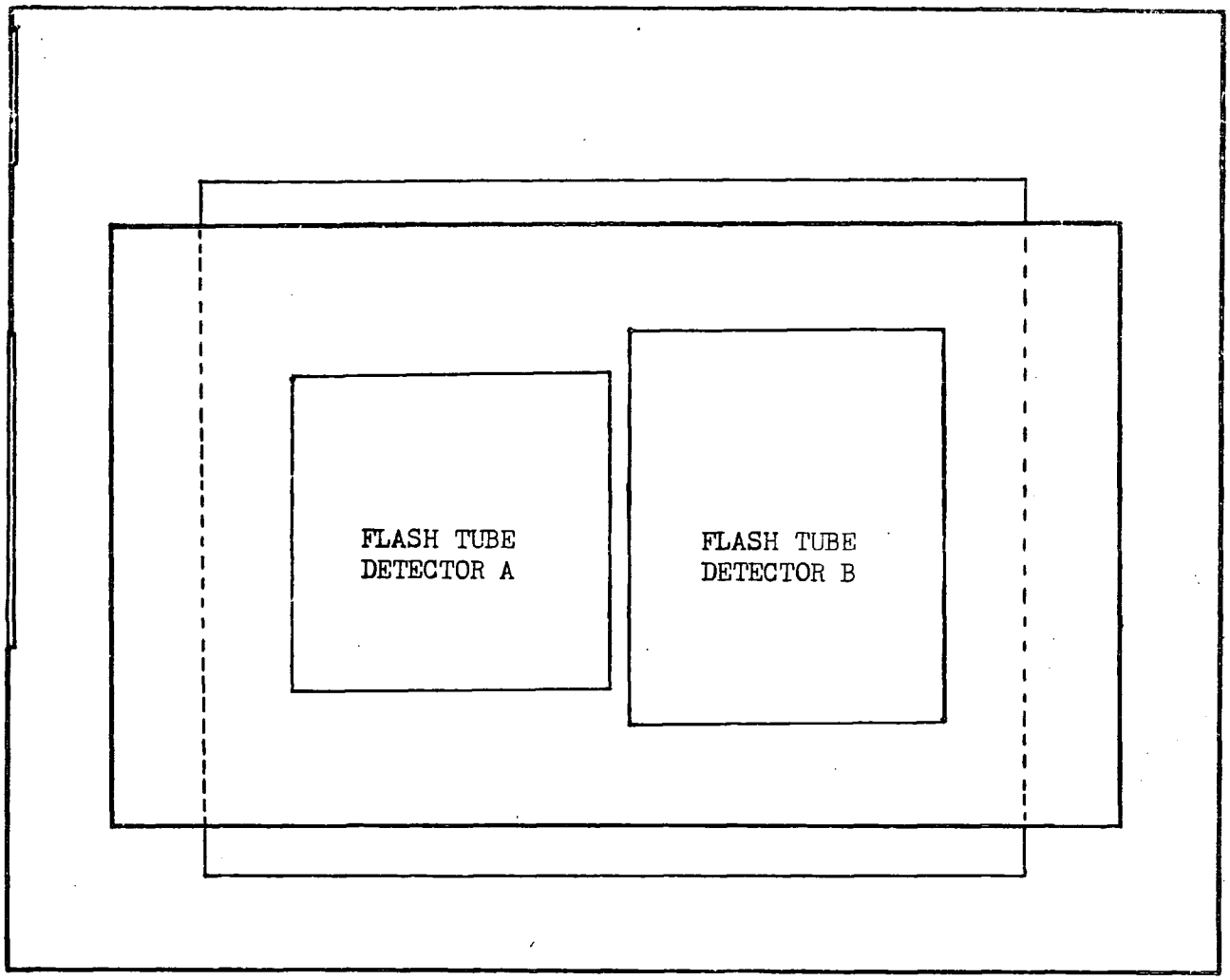
FLASH TUBE
DETECTOR A
FLASH TUBE
DETECTOR B

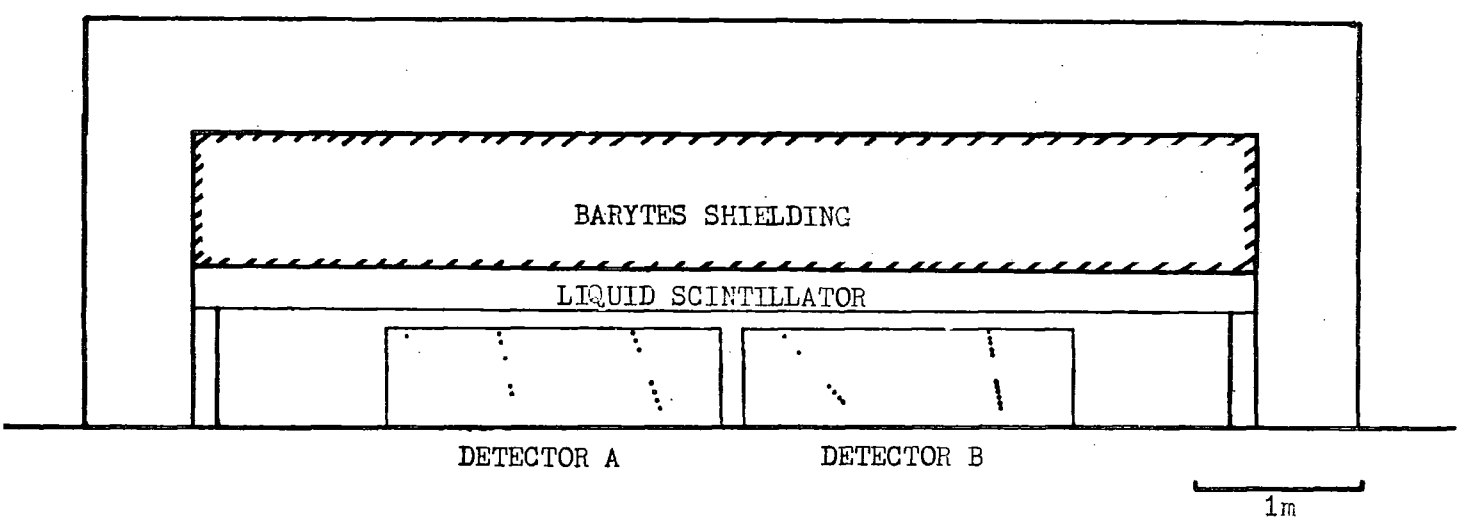
BARYTES SHIELDING
LIQUID SCINTILLATOR
DETECTOR A
DETECTOR B
1m

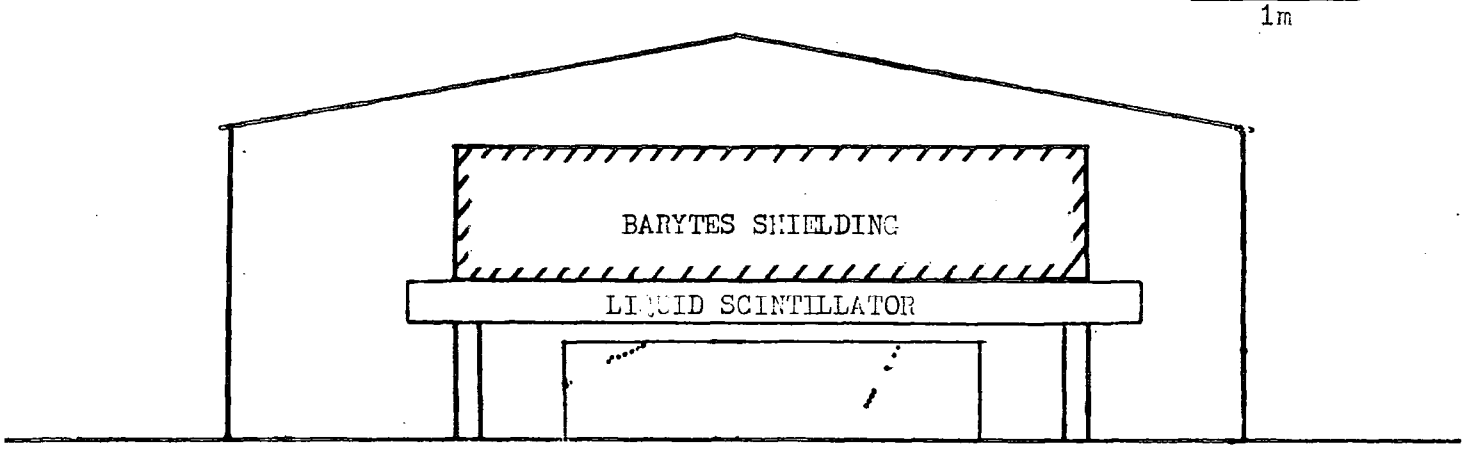
BARYTES SHIELDING
LIQUID SCINTILLATOR

filled with sufficient lead to give the same approximate thickness ($500gcm^{-2}$) and thus energy threshold (1·0GeV). It now shields two of the original flash tube trays which have been re-located with their axes perpendicular to each other.

The remainder of the original flash tubes have been re-deployed in six trays each of area slightly less than $2·4m^2$ shielded by 0·53m of new barytes concrete. These six trays are of similar mechanical design with variations where appropriate to allow for different tube diameters. Each tray is divided into two banks of tubes spaced by an air gap to give the designed (± 0·5 degrees) angular resolution of particle tracks. For convenience in track reconstruction this gap is adjusted to correspond to an exact number of tubes (7 on trays containing 1·7cm diameter tubes; 13 on 0·7cm tube trays). A flash tube bank consists of five layers of durals with one layer of flash tubes per dural. To prevent inter-tube contamination by photo-ionisation the large tubes are either painted black or enclosed in polythene sleeves; the small tubes are alternately painted black and white and the electrodes covered by a non reflective black paint.

The large diameter tubes are all located at one end of the detector in four trays of two different sizes. The smaller trays are mounted in front of and above the other two (see Figure 3-2). The two trays containing 0·7cm diameter tubes are also mounted above the ground to enable the lower sub-magnet tray to be photographed. In the early stages of commissioning the experiment it was discovered that excessive radiative pick up generated by the pulsing system together with faint images on film rendered the 0·7cm diameter tubes non viable and they were therefore disconnected.

c) Detector B.

This smaller detector is located 250m from and 7·86m above the array centre in a south easterly direction beneath an array of liquid scintillation counters operated by the University of Nottingham group. Both detectors are shielded by 0·76m of barytes concrete (see figure 3-3).

The thickness of the shielding material, the space requirements of the optical recording system and the limited headroom of the enclosing hut caused a compromise to be made between keeping the height of the flash tube array as small as possible whilst spacing the flash tubes to enable the desired 0·5 degree angular resolution to be achieved. With these constraints the following design evolved.

The detector consists of two floor standing trays giving a total sensitive area of $9m^2$ involving 6400 black or sleeved 1·7cm diameter flash tubes (the flash tube lengths are either 2.0 or 2·5m). To compensate for the modest area of the detector it was decided to have the capability of viewing the muon tracks in perpendicular planes, thus increasing the azimuthal acceptance.

Each viewing plane has a depth of twelve tubes which are split into two banks of six with a centre separation of 30cm. Three layers of tubes in each bank are mounted on durals as previously described and the other three layers rest on top of these in the gaps between tubes.

## 3-4 The Electronics and Recording Systems.

a) Electronic Systems.

Both detectors are controlled by a simple circuit (see figure 3-4) which is responsible for the correct sequencing of the equipment.

Figure 3-4 The Electronics System

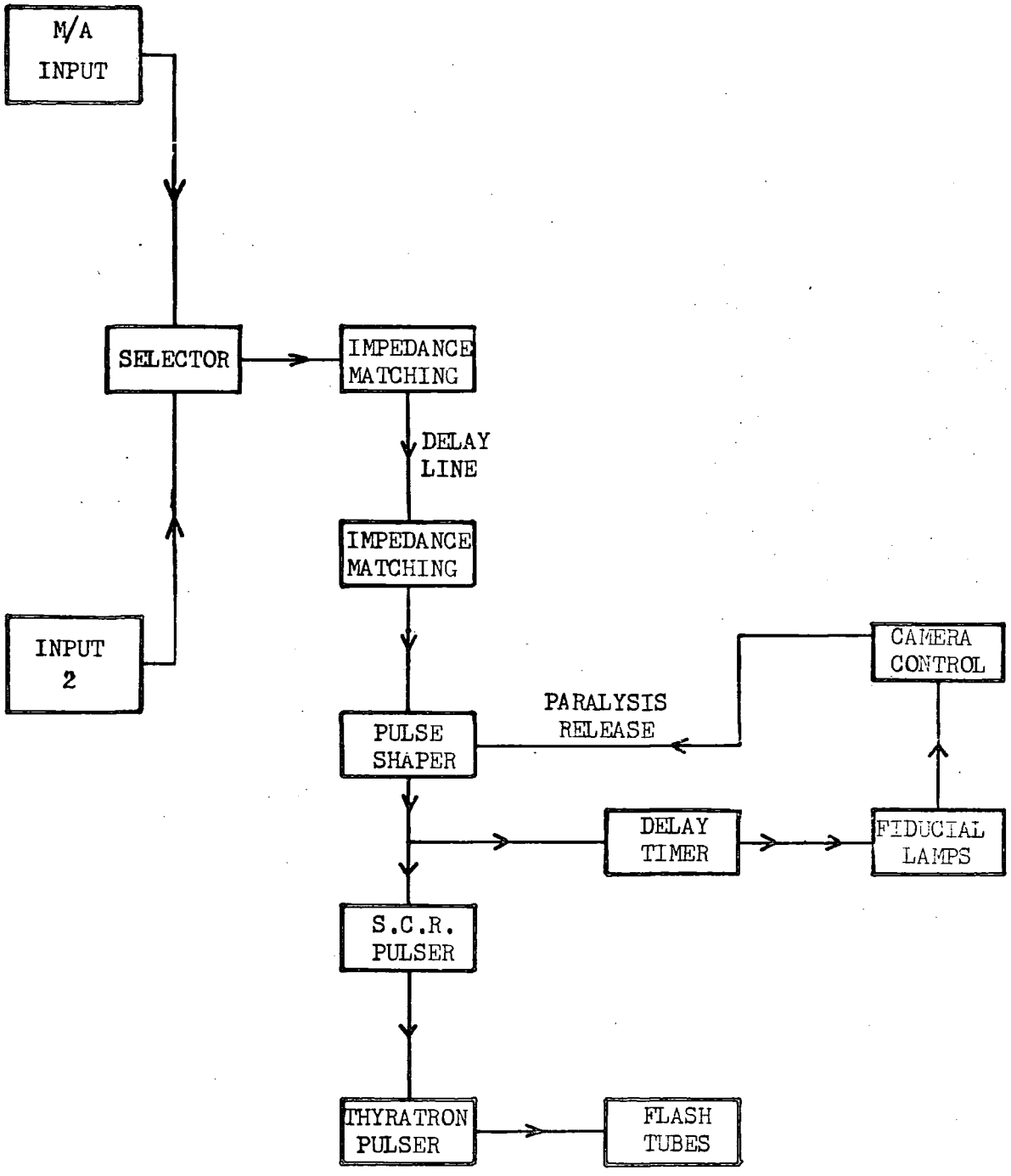
M/A
INPUT
SELECTOR
IMPEDANCE
MATCHING
DELAY
LINE
IMPEDANCE
MATCHING
INPUT
2
CAMERA
CONTROL
PARALYSIS
RELEASE
PULSE
SHAPER
DELAY
TIMER
FIDUCIAL
LAMPS
S.C.R.
PULSER
THYRATRON
PULSER
FLASH
TUBES

On receipt of a trigger signal from the main array a delay of approximately 12 $\mu$s occurs (to prevent electronic interference in other transient recording equipment in the vicinity). A 20 $\mu$s long high voltage pulse is then applied to the flash tube electrodes via thyratons. Subsequently, fiducial and event identifying markers are illuminated and the cameras advanced, resetting the detectors for the next event.

b) Optical Systems.

To utilise existing materials and ease construction time the flash tube signals are recorded photographically with two Shackman 35mm recording cameras in each detector. The enclosing huts are completely darkened and as a consequence no shutters are required in the cameras. As the detectors cover large areas and large numbers of flash tubes have to be recorded by each camera a complicated system of mirrors was devised to compress the tube images on to the films and give sufficient path length to eliminate inefficiencies due to polar angle effects from flashed tubes at the extremities of the field of view. As might be expected when supporting large areas of glass at large angles from the vertical considerable sagging of the mirrors and hence distortion of the film images occurs. This, however, is of no consequence and is easily removed in the data extraction stages (see chapter 4).

## 3-5 Operation and Reliability of the System.

From the outset it was realised that the manpower available for the project would be limited and once full time operation commenced the majority of effort would have to be devoted to analysis and interpretation of the data. Accordingly strong consideration was given

to minimise the amount of time spent on routine and other maintenance and by and large this objective has been obtained. Routine maintenance (performed on an approximately weekly basis) consisted of changing and developing the films, at the same time checking for malfunctions. To speed the identification of system faults all film output (which of course provides the most reliable indication of the equipment's health) was processed and subjected to a preliminary scan at Haverah Park to check for faults which could be rectified immediately.

Specific failures causing loss of data generally fall into two categories. The most common were camera faults, specifically loading errors and jammed films together with electrical and mechanical failure due to the advanced age of parts of the equipment. The other main source of failure has been due to the fairly short ( $\gtrsim$ 6 months) life of the thyratron valves. A valve failure was usually preceded by electronic interference in nearby equipment and hence the tube could be changed before total failure occurred.

# Chapter Four

## Raw Data Extraction and Processing.

### 4-1 Introduction

The majority of the experimental results presented in this thesis are based on the data gathered from Detector A during the period November 1977 to April 1979. Detector B became operational during the latter part of this period but in the first instance the analysis effort was concentrated on Detector A as more data were available and it would be easier to extract and interpret than those for the second detector.

For a preliminary investigation to verify that the instrument fulfilled the design criteria and to test the proposed data extraction and analysis techniques a sample of some 100 showers of all energies, core distances, zenith angle and impact positions was taken. A brief investigation of the lateral distribution was encouraging. The angle data required careful consideration and involved strictly restricting the azimuthal and core impact requirements of showers to be studied. A further improvement was obtained by systematically correcting the arrival directions from the University of Leeds Data Analysis to take account of a non-planar shower front.

This chapter describes in detail the selection and analysis procedure and is illustrated with data from typical events. Together with an examination of the basic data this gives an understanding of the detector response for comparison with simulations in Chapter 5.

### 4-2 Event Selection and Classification.

From the results of the study of the initial sample it was

Figure 4-1 Event Classification Diagram showing the ground impact parameters for events analyzed.

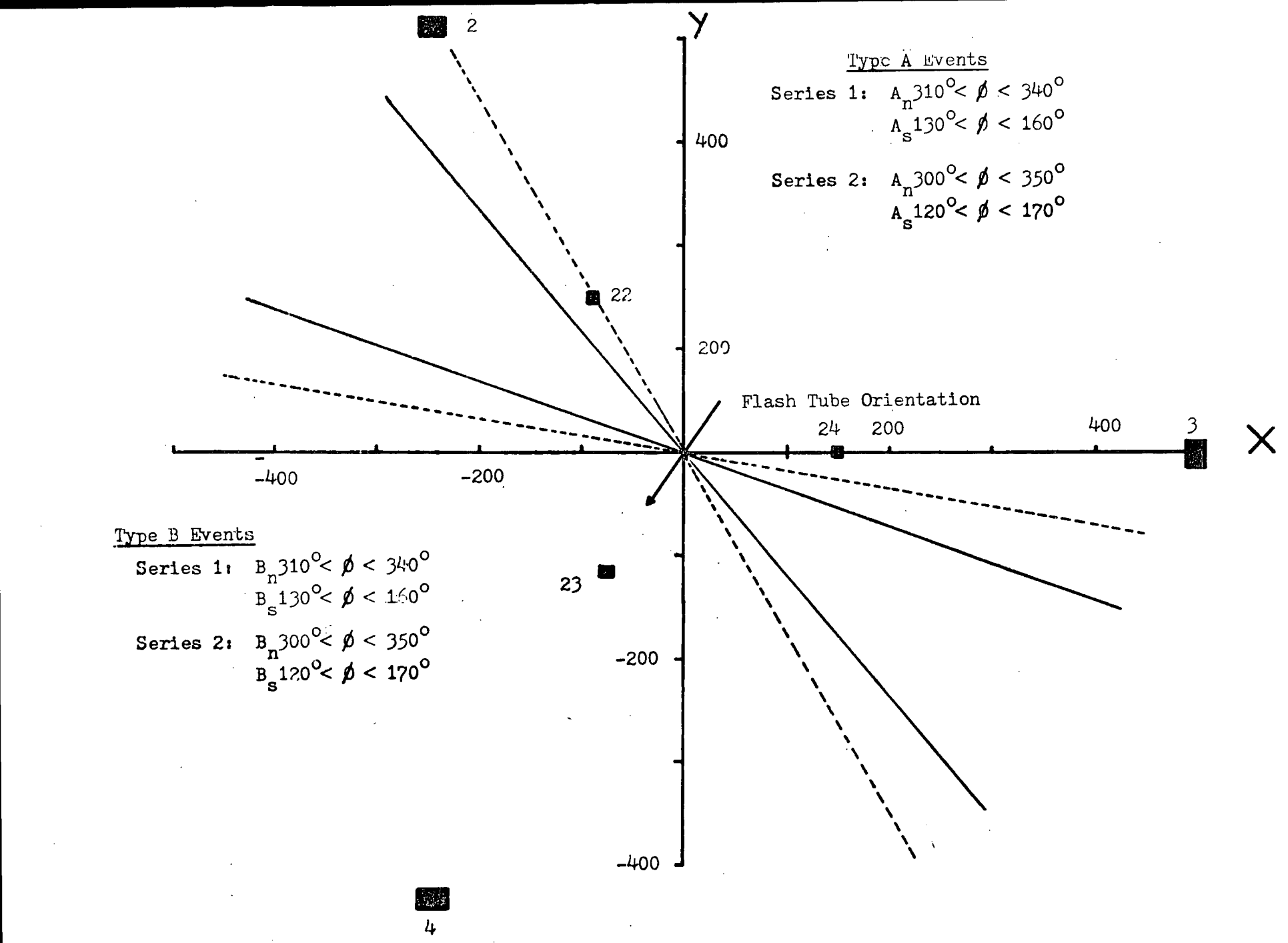


Type A Events

Series 1: $A_n 310^\circ < \phi < 340^\circ$

$A_s 130^\circ < \phi < 160^\circ$

Series 2: $A_n 300^\circ < \phi < 350^\circ$

$A_s 120^\circ < \phi < 170^\circ$

Type B Events

Series 1: $B_n 310^\circ < \phi < 340^\circ$

$B_s 130^\circ < \phi < 160^\circ$

Series 2: $B_n 300^\circ < \phi < 350^\circ$

$B_s 120^\circ < \phi < 170^\circ$

Figure 4-2 Definition of over and undershot events.

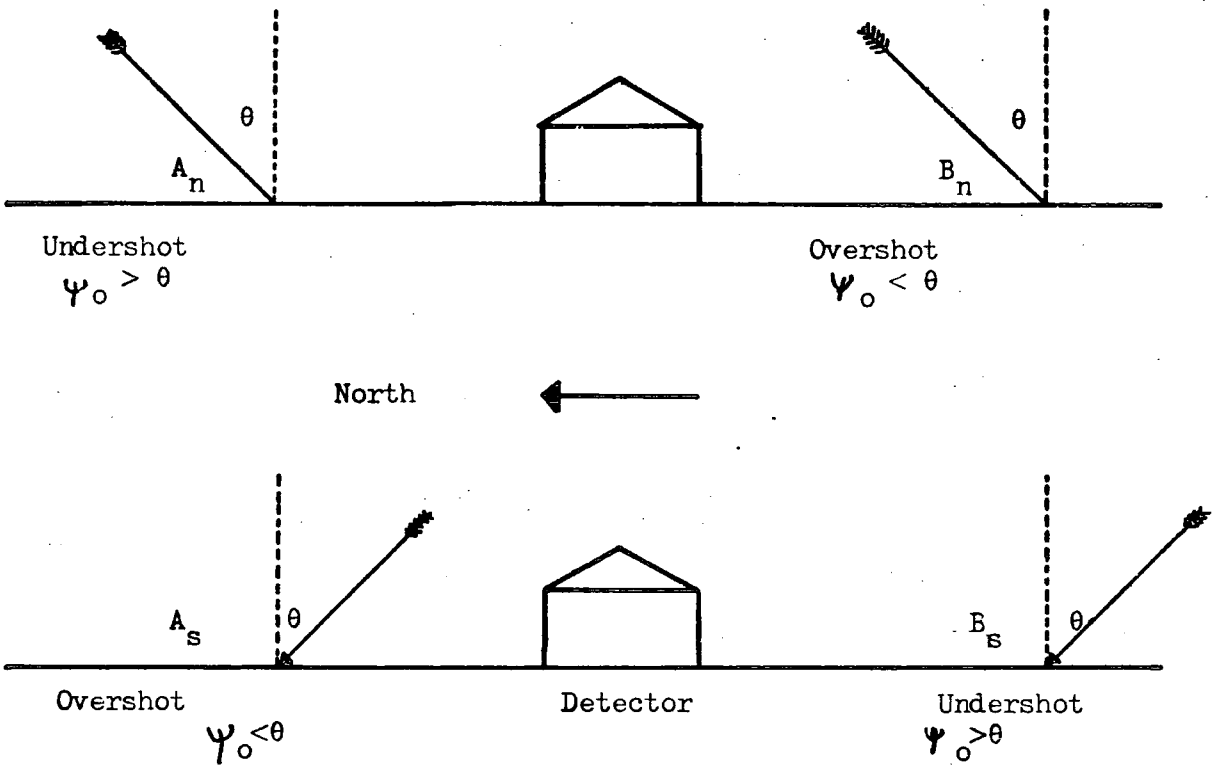
θ
$A_n$
θ
$B_n$
Undershot
$\psi_o > \theta$
Overshot
$\psi_o < \theta$
North
$A_s$
θ
$B_s$
θ
Overshot
$\psi_o < \theta$
Detector
Undershot
$\psi_o > \theta$

obvious that great care was necessary to obtain a clean, meaningful data sample. It will be appreciated that the angles to the zenith ($\psi$) recorded in the viewing plane of the detector will need correcting to the plane of the shower before they make any sense (as described in Appendix I). As the angle between the measuring plane ($\eta$) and the azimuthal angle ($\phi$) increases the precision with which $\psi$ can be measured decreases (due to the muons passing more obliquely through the flashed tubes). Thus it is necessary to restrict the selected showers to narrow azimuth and impact position bands perpendicular to the recording plane of the instrument. Two bands have been utilized. The first (series 1 events) is $30^{\circ}$ wide and gives a small but very high precision set of measurements. The second (series 2 events) is $50^{\circ}$ wide, slightly less precise than series 1 but contains a much larger data sample (see figure 4-1).

It is necessary to subdivide the initial classifications still further into events, the cores of which have fallen short of (class A) and those which have overflown the detector (class B). Due to the above azimuthal requirements with showers arriving from either north or south a further reclassification is possible. However, as will be seen from figure 4-2 events of class $A_n$ and $B_s$ are directly equivalent to each other as are $A_s$ and $B_n$.

Due to the array geometry and the orientation of the muon detectors it is also necessary, where possible, to refine the basic shower parameters. In the basic shower analysis $\theta$ and $\phi$ for each shower are defined by a plane front fitted through three of the 500m detectors. A correction was devised by Dennis (1962) and has been used here although employing the more recent measurements of the shower front curvature made by Barratt (1976). Without these selection

criteria and corrections the muon angle measurement gets totally masked in the experimental noise.

The evolved event selection procedure is as follows. The analyzed shower information (supplied by the University of Leeds as a computer listing) is scanned by eye for events satisfying the selection criteria. The appropriate muon films are then scanned for the event and if a significant number of muon tracks are visible (>5) the event is marked for measurement. Once an event has been selected the relevant photographs are printed on to a large format paper (30.5 x 40.6cm) and allowed to dry thoroughly for several days to eliminate any measurement error due to paper shrinkage.

## 4-3 Data Extraction and Analysis.

The data recorded on the muon films consist of a series of dots representing the end windows of flashed tubes. As the position of each tube is accurately known in relation to its fellows, a two dimensional picture of the tracks of muons through the detectors can be obtained with a track being defined by a minimum of five flashed tubes. When selecting tracks in a tray particular attention was paid to the identification and elimination of particles emanating from bursts in the shielding material. This is straightforward as bursts are easily identified by their much greater localised densities.

The tracks are enumerated from the prints by means of carefully prepared transparent overlays which were themselves prepared from carefully exposed 'daylight' prints, thereby incorporating the effects of distortions due to the mirror systems. The flashed tube coordinates so obtained are then computer processed firstly to translate the measured coordinates to 'real space' and then the particle track is

calculated by means of a least squares optimization technique. The output from this is printed by the machine as a facsimile of the tray of the detector in question together with the fitted track. Errors in track selection and those produced by misread tubes are thus easily seen and corrected.

## 4-4 Data Samples.

The data used in this thesis has been rigorously selected and refined to give as reliable a sample as possible so that well established average characteristics can be derived. These will enable fluctuations to be investigated at a later date when the nature of the data is fully understood and a larger sample is available.

The angle data from several typical events are displayed in figure 4-3. Indicated on the diagrams are the mean muon-core angle ($\bar{A}$) and standard deviation ($\sigma$). Early in the investigation of the data it was discovered that $\sigma$ was strongly influenced by the leading and trailing components of the angle distribution which contain the lower energy and hence more scattered (by the local absorber) particles. A potentially more meaningful measure was found to be the standard deviation of the middle quartiles in the distribution ($S_{25}^{75}$). If the muon signal is considered as a pulse in angle (see figure 4-4) similar to that observed in time by a scintillator for example, $S_{25}^{75}$ is analagous to measuring the full width half maximum. A further measurement can be extracted from such considerations, namely the peak value of the 'pulse' or the median angle in the distribution ($A_m$).

A complication in the angle measurements is what has been termed a 'crossed track'. These appear as completely decorrelated particle tracks varying from the mean direction by some $90^{\circ}$. Fortunately they

are quite rare and usually occur singly with extremely rare pairs. There are several possible explanations for crossed tracks.

(1) Totally unconnected particles. As flash tubes have a long 'event memory' it is possible for a sporadic particle from the cosmic ray background which passed through the detector many micro seconds before or actually during an event to be recorded. Tests performed by random pulsing of the central detector showed that such random particles are recorded in 2% of all events.

(2) Severely scattered low energy shower particles which have been deviated by very large angles in the atmosphere and shielding material. These cannot be eliminated but may be allowed for in rigorous simulations.

(3) 'Knock on' and particles resulting from interactions in the shielding material.

It is interesting to note that the incidence of cross track events is approximately halved under the iron shielding indicating that half of the particles responsible have energies between 0·3 and 1·0GeV. Naturally, for every crossed track there will be a corresponding percentage of tracks 'lost' in the main beam and these have to be treated as noise on the true signal. Where spurious tracks of type (1) can be detected they are excluded from any further analysis.

As well as recording angle data the equipment is capable of making lateral distribution measurements simply by counting the number of visible tracks (obtainable straight from the film record) and amending the area presented by the detector to the effects of varying zenith angles. The very rigorous selection of showers described above is not necessary for lateral distribution measurements which can be made with showers landing at all points in the array. The

Figure 4-3 Sample events at a selection of core distance, zenith angles and primary energies. Each vertical bar represents a measured muon.

Note These are "clean events" (no crossed tracks)

Figure 4-4 Muon Angle Profiles for the events in Figure 4-3.

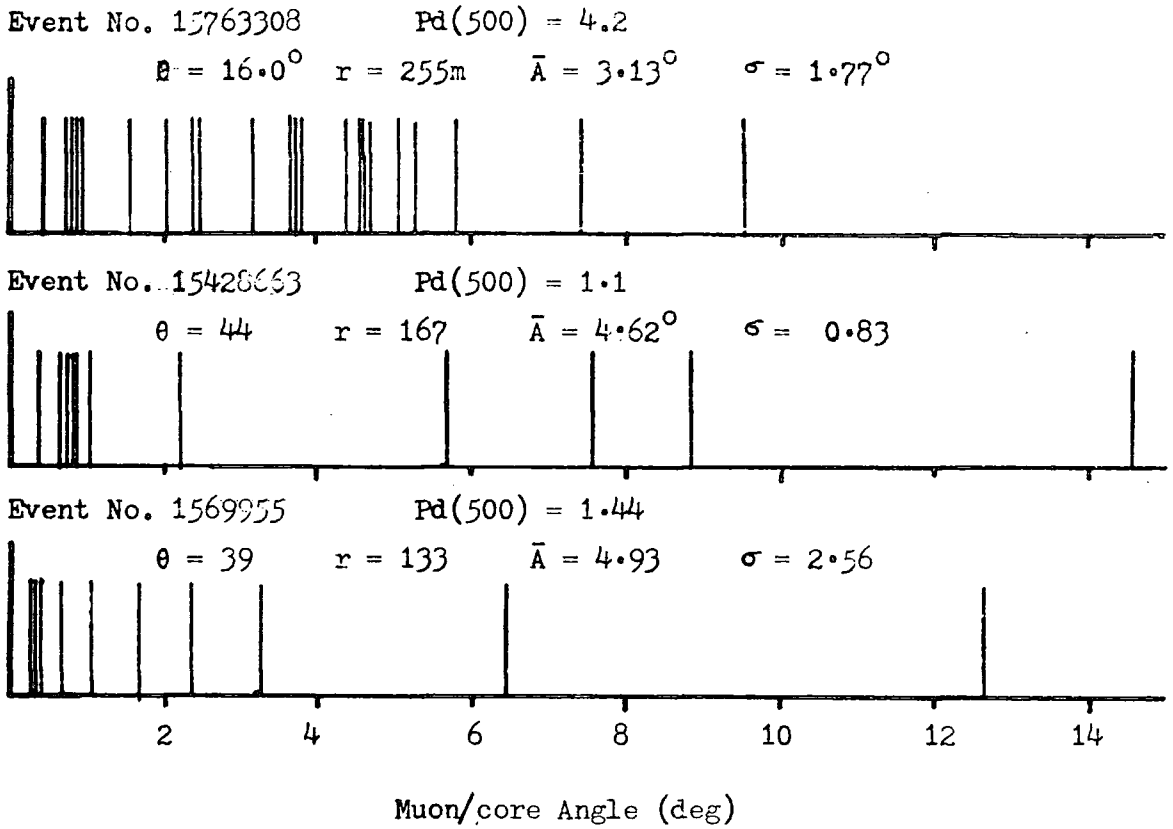
Event No. 15763308 Pd(500) = 4.2
θ = 16.0° r = 255m Ā = 3.13° σ = 1.77°
Event No. 15428663 Pd(500) = 1.1
θ = 44 r = 167 Ā = 4.62° σ = 0.83
Event No. 1569955 Pd(500) = 1.44
θ = 39 r = 133 Ā = 4.93 σ = 2.56
2 4 6 8 10 12 14
Muon/core Angle (deg)

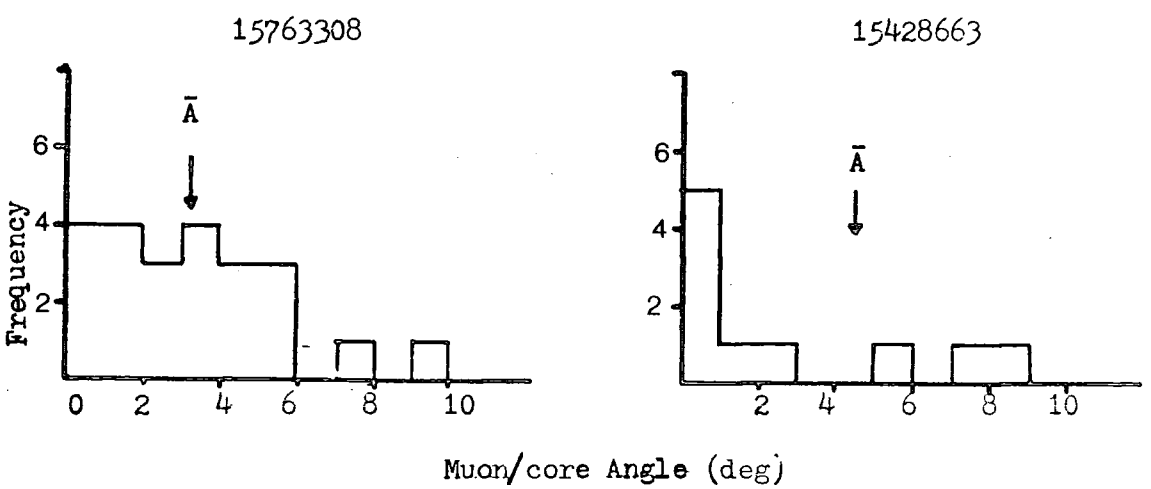
15763308
15428663
Ā
Frequency
0 2 4 6 8 10
Muon/core Angle (deg)

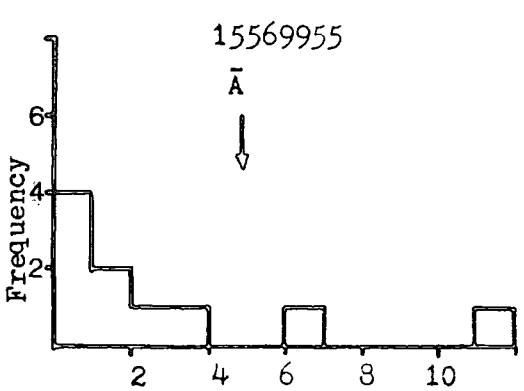
15569955
Ā
Frequency
2 4 6 8 10

results of simulation (Chapter 5) had predicted a new cascade sensitive measure obtainable from such measurements in the central detector, the ratio of densities beneath the barytes absorber (0·3GeV) and that under the steel absorber (0·8GeV) ($\Delta_S/\Delta_B$).

## 4-5 Introduction to the Experimental Results.

The remainder of this chapter considers the raw experimental data. Comparisons will be made, where possible, with existing data in an attempt to understand the workings and performance of the equipment before attempting any major physical interpretation of the results.

The measurement capabilities and shortcomings are assessed so that the data eventually used for air shower interpretation are as free as possible from any effects arising from the equipment itself. All the parameters the experiment was designed to measure are considered in detail.

## 4-6 The Lateral Distribution of Muons.

The experiment is ideally suited to lateral distribution measurements and the centre detector, with its two different thicknesses of shielding, can also give a two point energy spectrum for low energy muons.

The muon density measurements are made on some 2000 consecutive showers spanning the middle of the operational period considered for this thesis. As angle information is not required the instruments can record in an omnidirectional mode increasing the data acquisition rate manyfold. To be consistent with other Haverah Park data the results were binned in bands of zenith angle ($\theta$) and the shower

energies were normalised to $Pd(500) = 1 \cdot 0m^{-2}$ (corresponding to an energy of approximately $10^{18}$eV). To arrive at the measured lateral distributions several corrections to the raw data were required. As these add up to some 40% a brief summary and description is in order.

Blake et al (1971) described a technique for coping with the finite track resolving power of visual detectors. This is particularly relevant to flash tube detector arrays because of the relatively large area ($\approx$ 1% with this experiment) of each flash tube compared to the total area of the detector exposed to incident particles. Two particle tracks passing through adjacent or the same tubes are easily counted as one particularly as the internal efficiency of the tubes is of the order of 80% and not every tube crossed by each track will have flashed. The other major correction factor required is due to the fact that the individual flash tube trays are thick (unlike the scintillator) and a track has to appear in both upper and lower parts to be recorded. This is dependent on the zenith angle of the recorded shower and dramatically affects readings for zenith angles greater than $40^{\circ}$.

The minor effects which influence the measured densities include human errors in measurement (a factor which will probably be neutralized with a large enough data sample), the internal efficiency of flash tubes in responding to the passage of a particle and fluctuations in the film development conditions resulting in some flashed tubes becoming faint and difficult to see by eye. Finally there is a distinct dependence of core distance range upon the primary energy of showers recorded because of the main detector array geometry and the recording instruments. At small core distances smaller showers predominate (the flash tubes saturating in large showers) and at large

Figure 4-5 The relation between core distance and/$^{\text{mean}}$primary energy for the showers in the data sample used for the lateral distribution measurements.

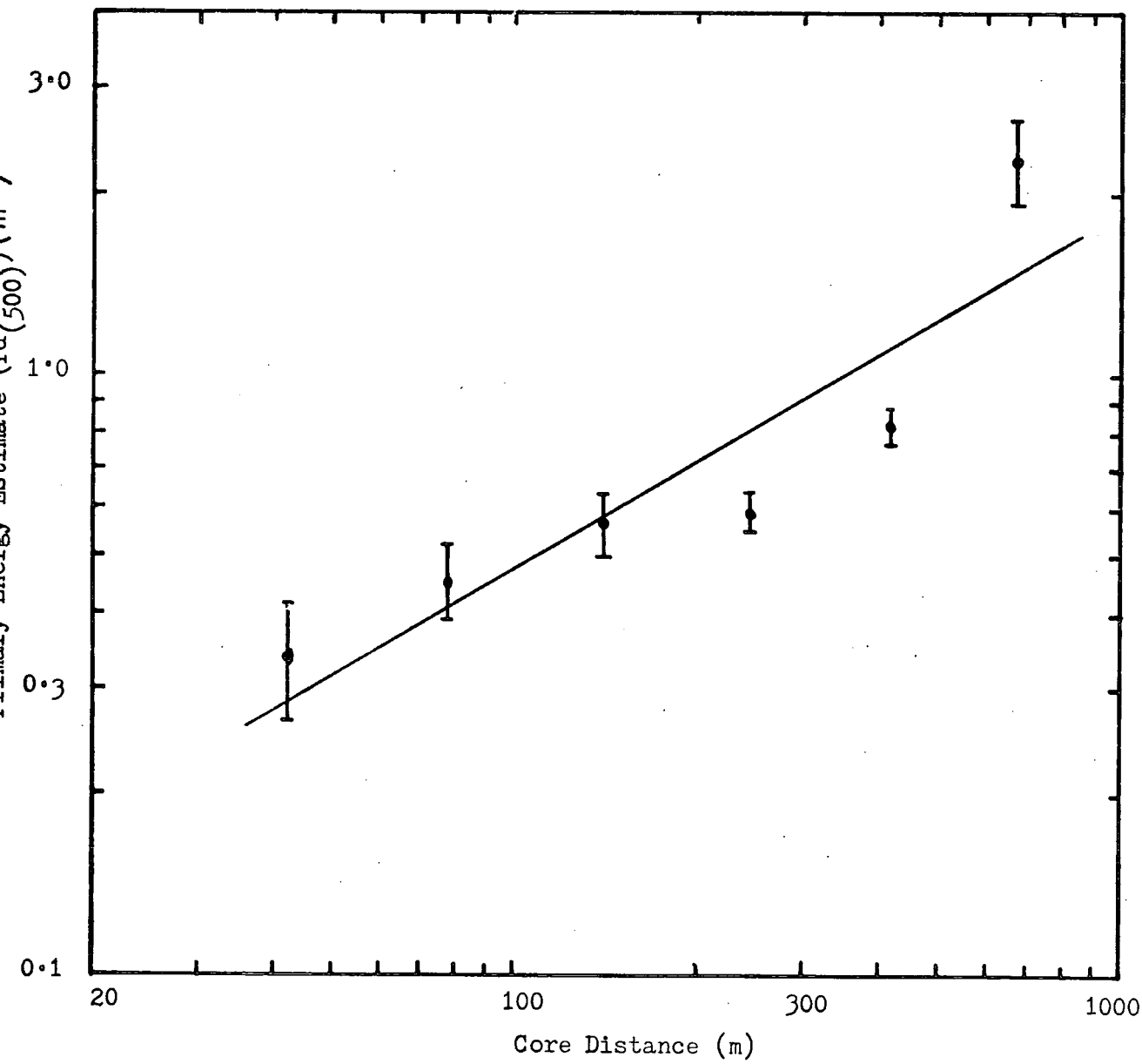
3·0
1·0
0·3
0·1
20
100
300
1000
Core Distance (m)

core distances small showers are not detected by the main array (figure 4-5).

Figure 4-6 shows a fully normalised lateral distribution for muons in vertical showers beneath both barytes and steel. Also shown is the lateral distribution measured by Strutt (1976) using scintillator detector data. Reasonable agreement is seen for core distances above 200m but at core distances below this our recent measurements indicate a flatter structure function. This effect has been remarked upon before [Strutt (1976)] and is clear evidence of the flash tubes beginning to saturate. Similar effects are evident for measurements at larger zenith angles and are shown in figures 4-7 and 4-8. As expected, the densities beneath the barytes are greater than those under steel and the possibility of some high energy electron contamination should not be discounted. Good agreement with both the simulations and the results of Strutt is seen. The slight differences in density compared to Strutt's work are easily accounted for by differences in thickness of shielding and hence thresholds in the two experiments.

Electron contamination is clearly visible when the $\Delta_S/\Delta_B$ ratio (the relative response of detectors covered by steel or barytes) is considered - see figure 4-9. Here the ratio is plotted for 3 zenith angle bins and also shown are the results of a simulation for a $10^{17}$ eV vertical iron primary initiated shower. It is noticeable that there is good agreement with vertical showers at the larger core distances ($\geq$300m). Below this distance a large discrepancy develops when compared to the simulation data for muons alone. If it is assumed that the particles observed beneath the iron contain an extremely small number of electrons - born out by the MkI and MkII Spectrograph

results - the observed discrepancy must arise from the sub-barytes measurements. The results are compatible with the presence of many electrons at the smaller core distances.

If near vertical showers are considered (see figure 4-10) and binned by energy, the contamination is again evident as a turning point in the curve and, as would be expected, the critical distance recedes with increasing energy.

The presence of this contamination does not, however, negate the usefulness of any of the lateral distribution measurements provided that it is allowed for in the interpretation and also in any simulations.

The Muon/Čerenkov Ratio

As the central muon detector is adjacent to the central deep water detector another common parameter (the muon/Čerenkov signal ratio) could be easily measured. Armitage (1973) has shown it to be independent of primary energy over a wide range. As a consequence it provides another possible way of intercalibrating different arrays, besides being a serviceable parameter for testing simulation models and equipment. The muon/Čerenkov ratio has been investigated in depth by the University of Nottingham group at Haverah Park [Strutt (1976)] and as its only purpose here would be another test of the muon angle equipment it will not be discussed further.

## 4-7 Angle Measurements:- Introduction.

In an experiment such as the one under consideration it is important to know the uncertainties and major sources thereof in the basic air shower data. The accuracy with which they can be determined is dependant upon three factors:-

Figure 4-6 A fully normalized lateral distribution for muons in vertical showers normalized to $\rho_{VE}(500) = 1 \cdot 0 m^{-2}$ with $\theta \leq 30^{\circ}$. Also shown are the results of measurements by Strutt (1976) and computer simulations using a Landau type model.

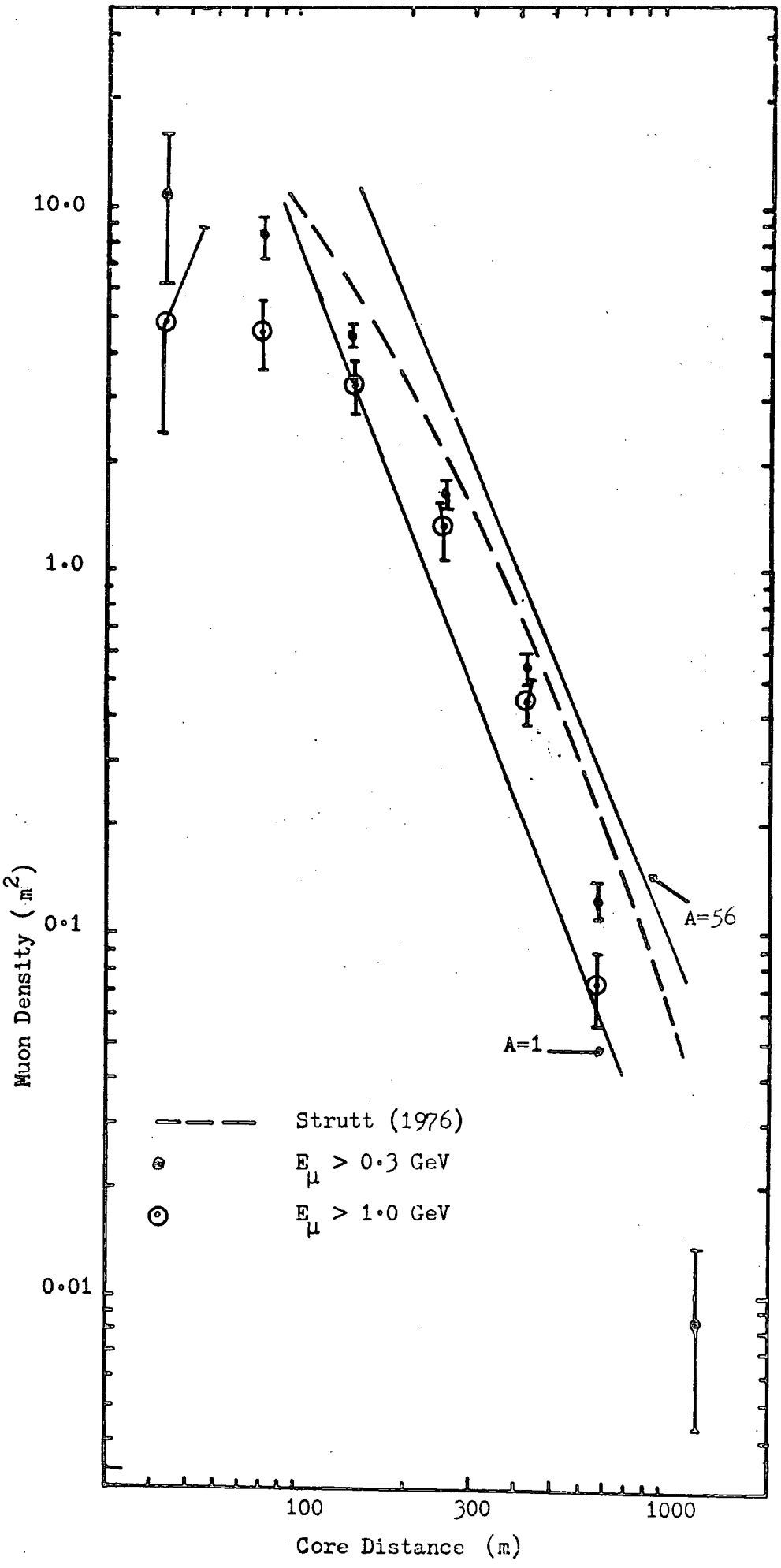
10·0
1·0
0·1
0·01
Muon Density ( m$^{-2}$)
A=56
A=1
Strutt (1976)
$E_\mu$ > 0·3 GeV
$E_\mu$ > 1·0 GeV
100
300
1000
Core Distance (m)

Figure 4-7 As for figure 4-6 but with $30^{\circ} < \theta < 40^{\circ}$

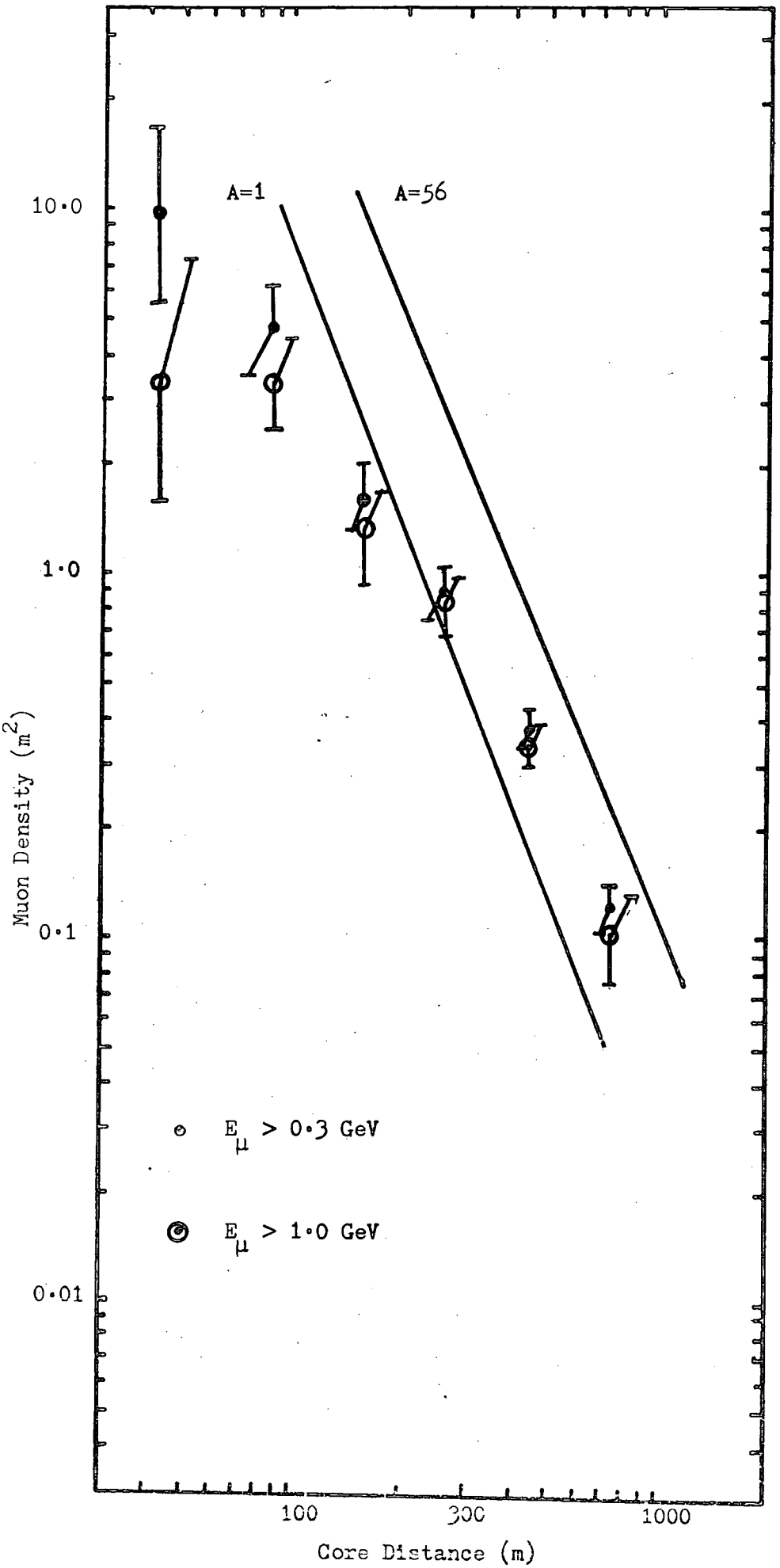
A=1
A=56
10·0
1·0
0·1
0·01
Muon Density (m$^2$)
$E_\mu$ > 0·3 GeV
$E_\mu$ > 1·0 GeV
100
300
1000
Core Distance (m)

Figure 4-8 As for figure 4-6 but with $40^{\circ} < \theta < 50^{\circ}$

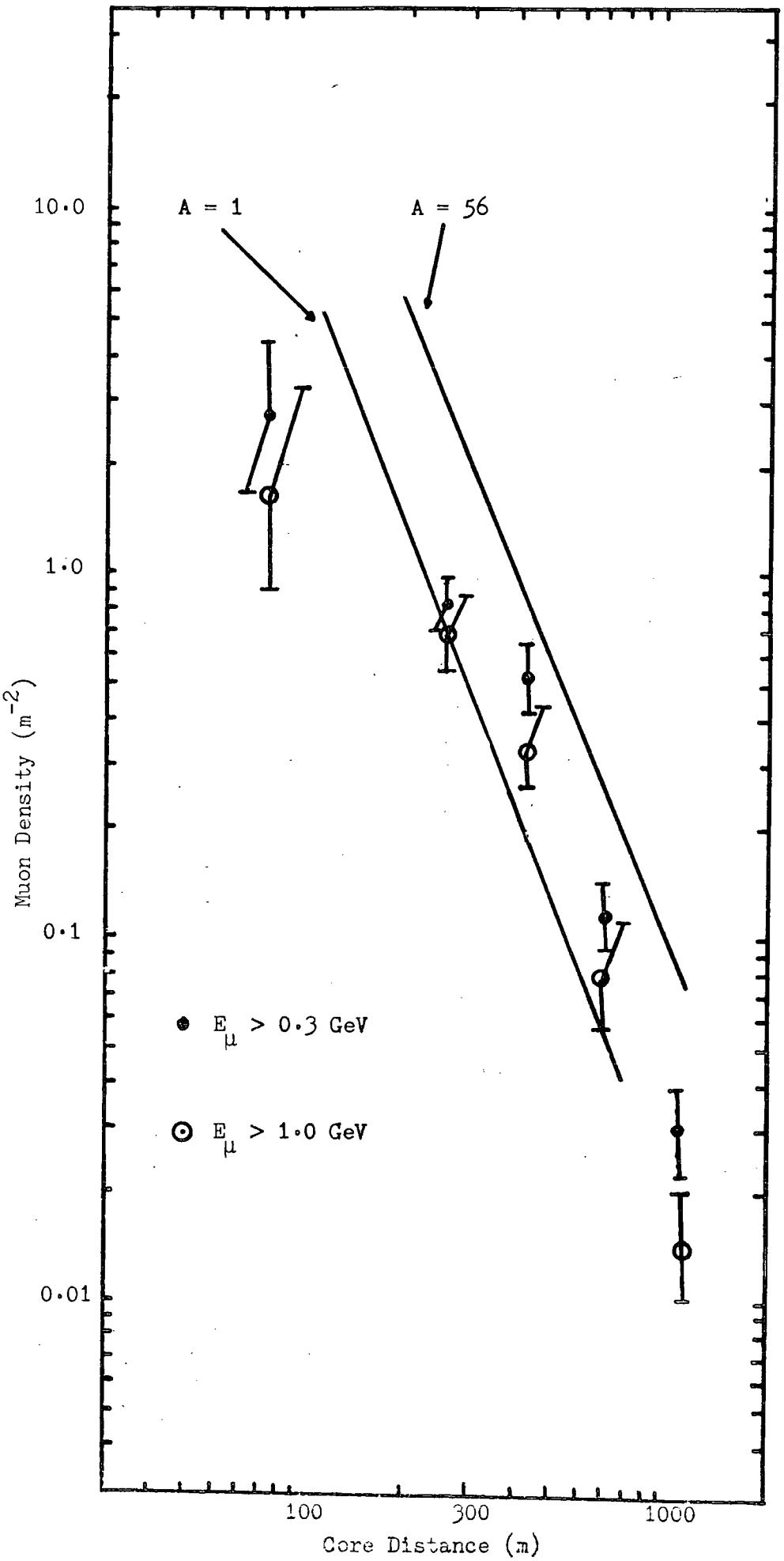
A = 1
A = 56
10·0
1·0
0·1
0·01
Muon Density ($m^{-2}$)
$E_\mu$ > 0·3 GeV
$E_\mu$ > 1·0 GeV
100
300
1000
Core Distance (m)

Figure 4-9 The ratio of measurements made under steel and barytes absorber($\Delta_S/\Delta_B$)binned by zenith angle. Also shown are the predictions from a $10^{17}$eV iron primary initiated simulated shower.

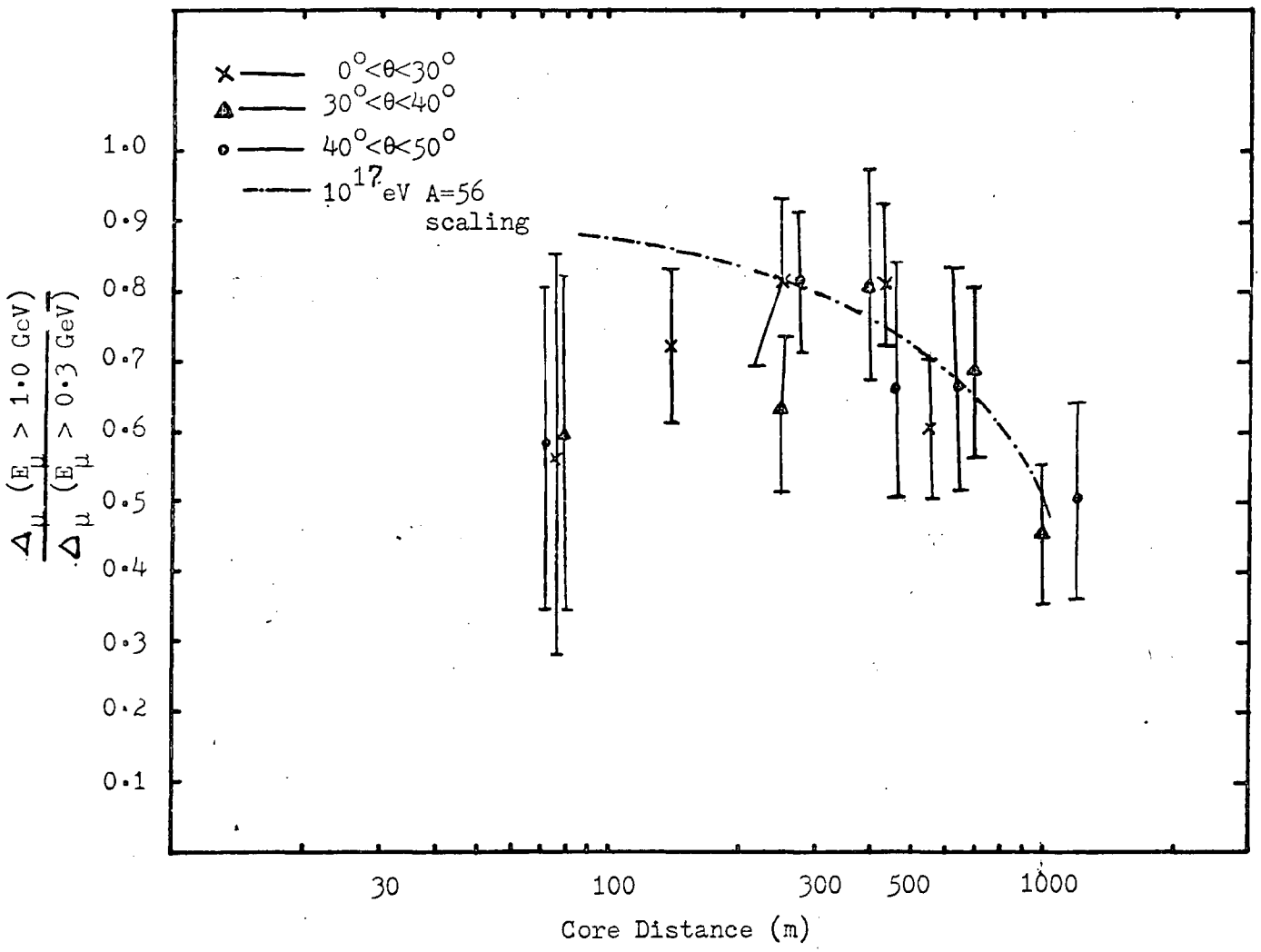
0°<θ<30°
30°<θ<40°
40°<θ<50°
10^17 eV A=56
scaling
1.0
0.9
0.8
0.7
0.6
0.5
0.4
0.3
0.2
0.1
30
100
300
500
1000
Core Distance (m)
Δμ (Eμ > 1.0 GeV) / Δμ (Eμ > 0.3 GeV)

Figure 4-10 $\Delta_S/\Delta_B$ as a function of core distance binned by primary energy compared with a simulated $10^{17}$ eV iron primary initiated shower.

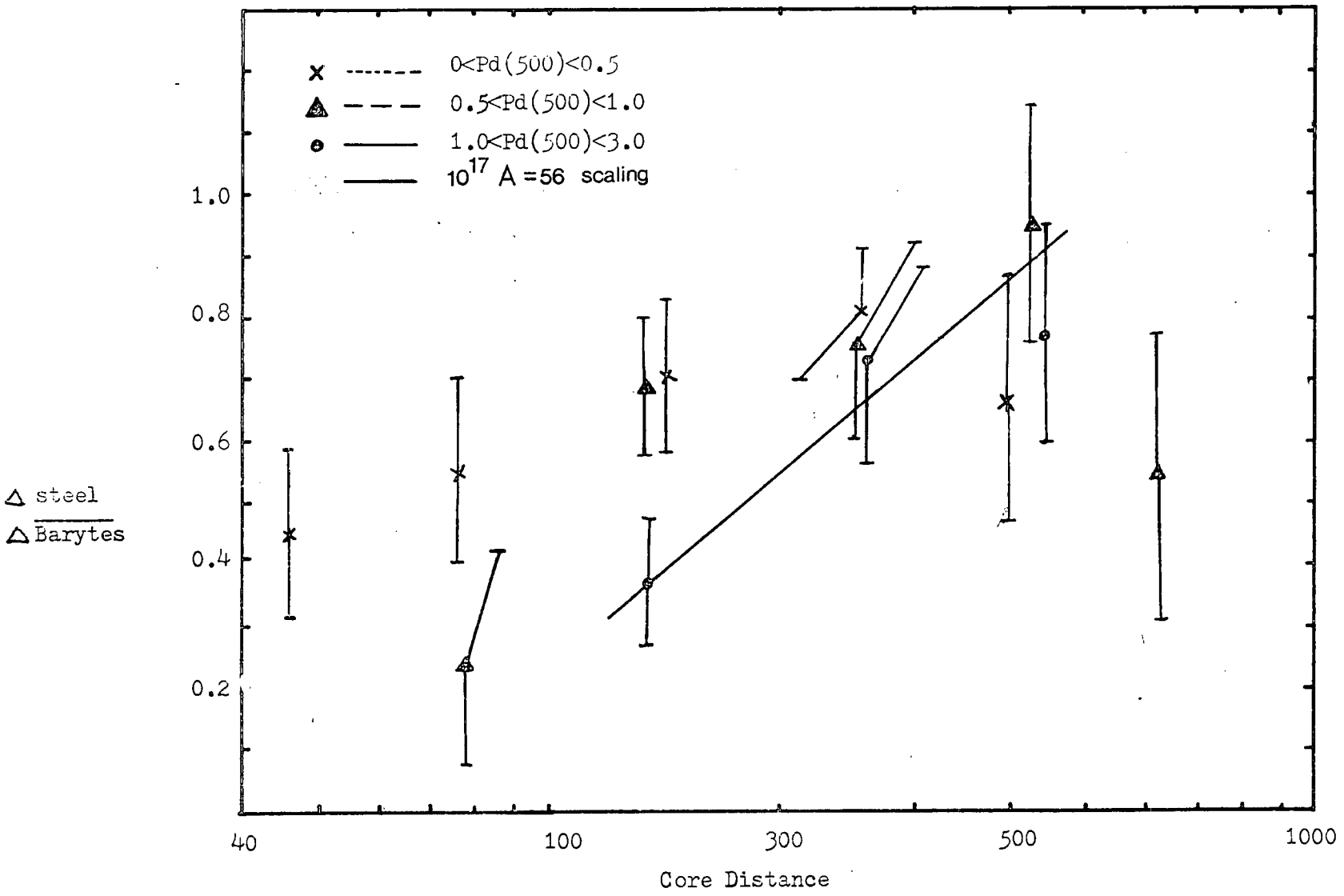
0<Pd(500)<0.5
0.5<Pd(500)<1.0
1.0<Pd(500)<3.0
$10^{17}$ A =56 scaling
1.0
0.8
0.6
0.4
0.2
40
100
300
500
1000
Core Distance
△ steel
△ Barytes

(1) The design and geometry of the main shower detector array.

(2) Uncertainties in the lateral distribution and the consequent effects upon the analysis of showers.

(3) Timing and density measurement fluctuations occurring during the sampling of a shower by widely spaced detectors.

The effects of these uncertainties have been investigated by Evans (1971). In a series of simulations he randomly bombarded the array imposing fluctuation effects upon the detector responses. Re-analysis of the shower using the new densities gave an indication of the errors that may be present. It was discovered that the cores of 85% of the events were likely to be located within 20m of the correct core position. The determined core position is sensitive to the shape of the distribution function; in practice this is known to be better than 10% so that systematic changes are probably of the order of 5-10m, which really only becomes important for measurements made close to the core (<100m).

The parameters used to estimate the primary energy are determined simultaneously with the core position and so the uncertainties in both are inter-related. Andrews (1970) has shown that for R<500m the errors in $\rho_{500}$ decrease with increasing shower size. This is confirmed by McComb (private communication) who finds showers with $Pd(500) > 0{\cdot}6m^{-2}$ to be well measured.

At large zenith angles the showers become more muon rich and the overall densities are smaller; the sampling fluctuations therefore increase, leading to correspondingly poorer determinations of core positions and primary energy.

For the present experiment uncertainties in the arrival

Figure 4-11a The relationship of the mean muon-core angles ($\bar{A}$) in the two halves of detector A.

Figure 4-11b The standard deviations of muon-core angles in the two halves of detector A.

Note The results in these figures cover all core distances, zenith angles and energies.

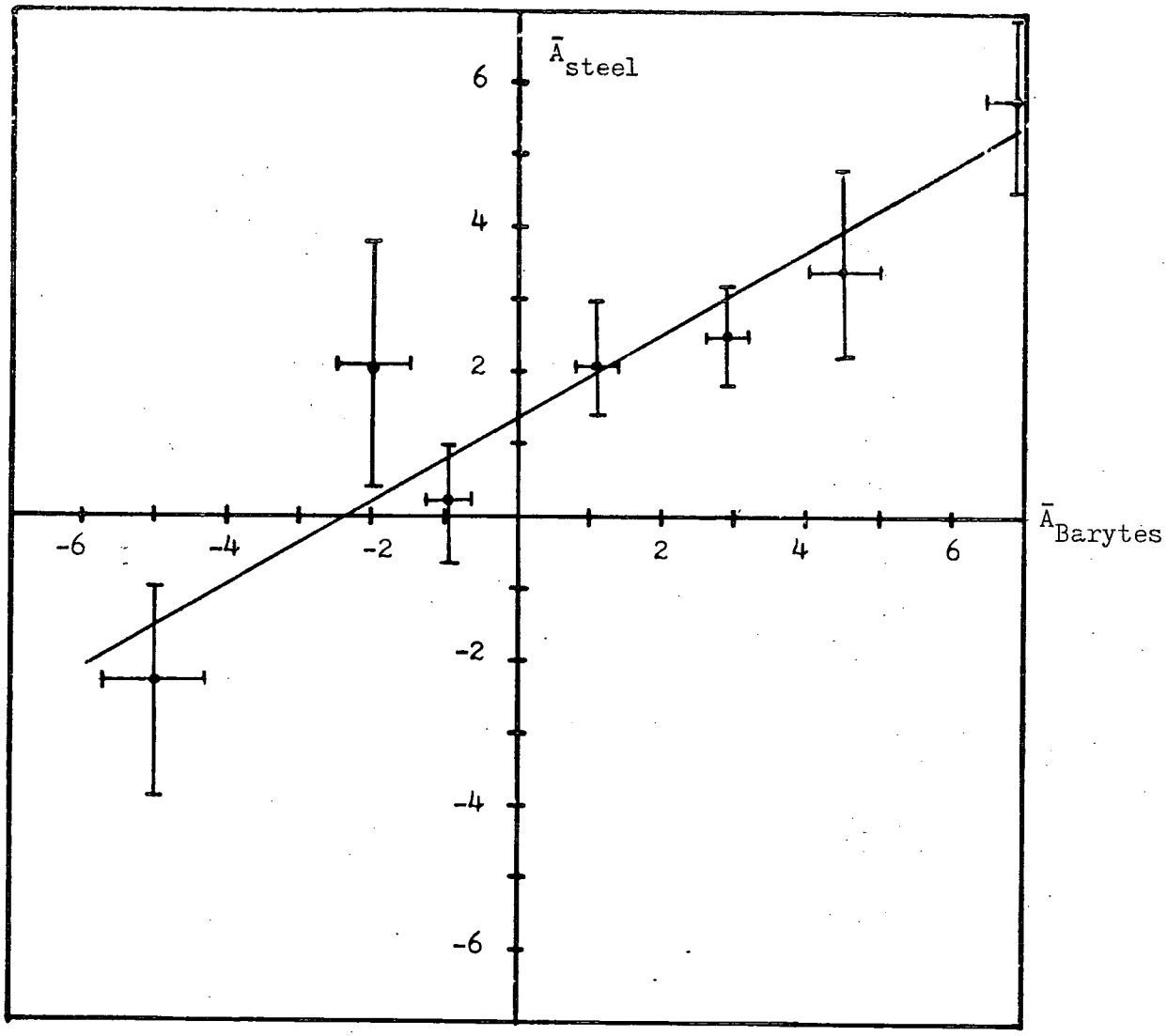
$\bar{A}_{steel}$
$\bar{A}_{Barytes}$
6
4
2
-2
-4
-6
-6
-4
-2
2
4
6

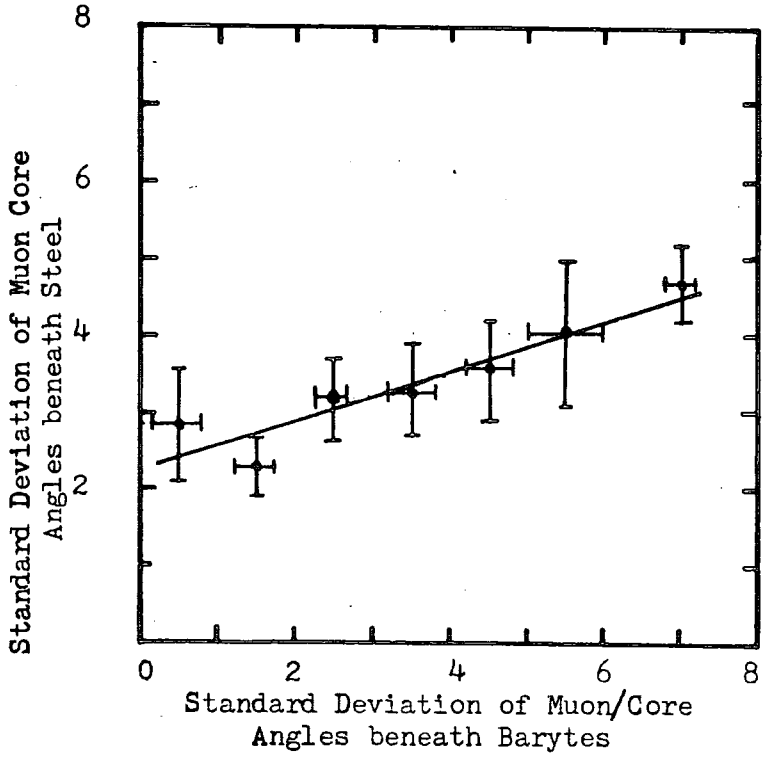
Standard Deviation of Muon Core
Angles beneath Steel
Standard Deviation of Muon/Core
Angles beneath Barytes
0
2
4
6
8

direction are the most important and these have been investigated by Hollows (1969) and were expressed as

$$\delta\theta = 2{\cdot}5\sec\theta \qquad 0^{\circ} < \theta < 75^{\circ}$$

In studying the angle data from the present experiment it was confirmed that a greater degree of uncertainty existed in zenith angle when one of the 500m detectors recorded a very small particle density (hence was very uncertain in its timing measurements). Accordingly, great care was exercised in the analysis of events of this nature with no hesitation over rejecting those having doubtful directions.

## 4-8 The Angles made by Muons to the Shower Core.

As the central detector offers data with differing energy thresholds (due to its barytes and iron shielding), it is as well in the first instance to consider the two sets of data separately. This will avoid systematic errors arising from e.g. different amounts of scattering in the shielding of the detector. Experimental results show that the measurements in the two sections of the detector show a strong relationship to each other in both average angle to the core and standard deviation measurements (figure 4-11), the effects of the differing thresholds being clearly seen. The 'barytes muons', because of their proven electron contamination and the greater local scattering, will tend to give long tails to the angle distribution and affect the mean angle. The tail can be eliminated by using the quantity $A_{25}^{75}$ but, as figure 4-12 shows, it then falls between $\bar{A}$ (barytes) and $\bar{A}$ (steel). Unfortunately it is not possible to make this measurement with all events simply due to the small number of muons recorded in some cases.

For the events considered in this treatment a very strong

Figure 4-12 The dependence of $\bar{A}_{Barytes}$, $A_{25}^{75}$ and $\bar{A}_{Steel}$ on core distance for $\theta < 35^{o}$, $Pd_{(500)} > 0.5$

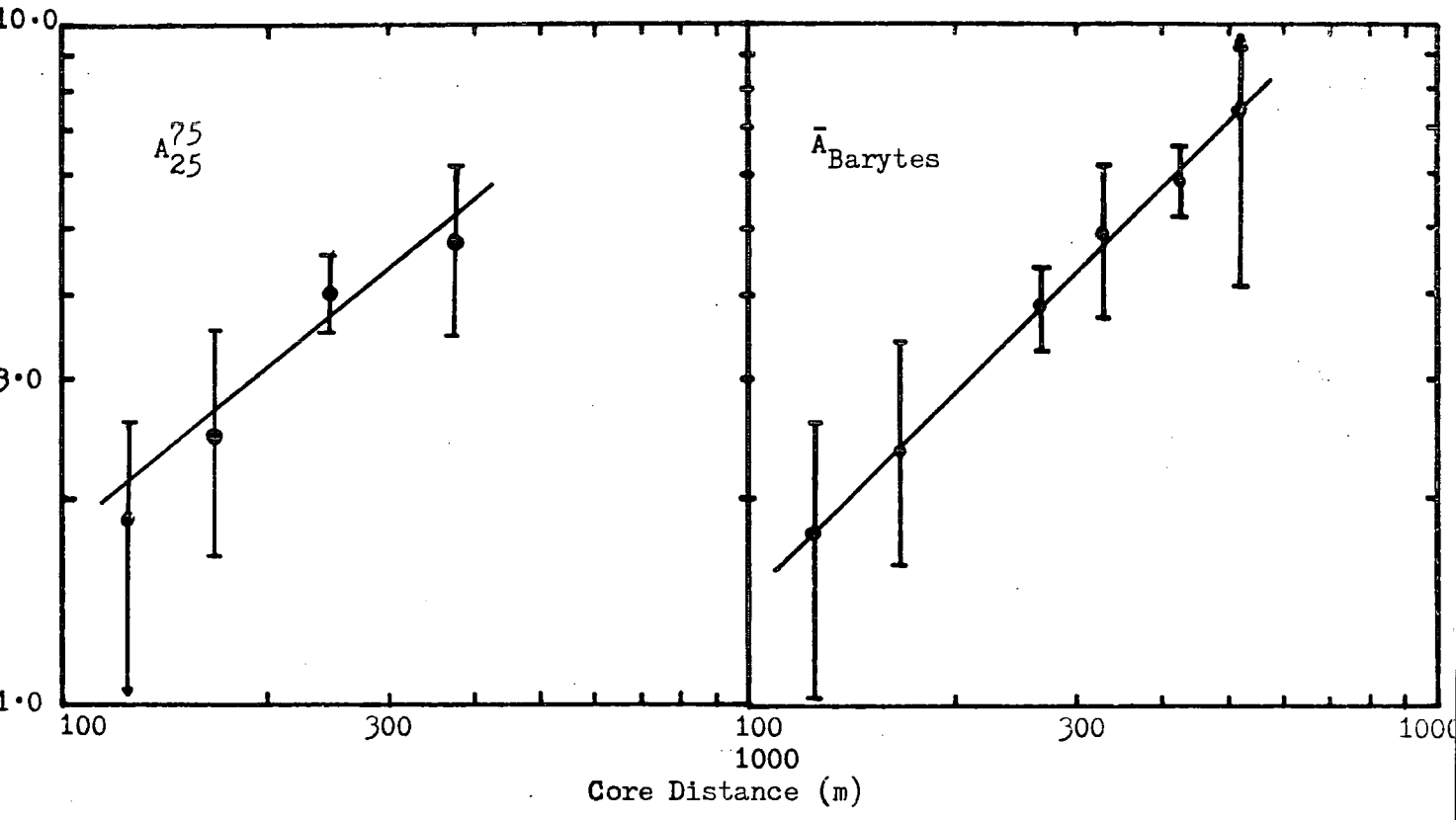
10·0
3·0
1·0
$A_{25}^{75}$
$\bar{A}_{Barytes}$
100
300
100
300
1000
1000
Core Distance (m)

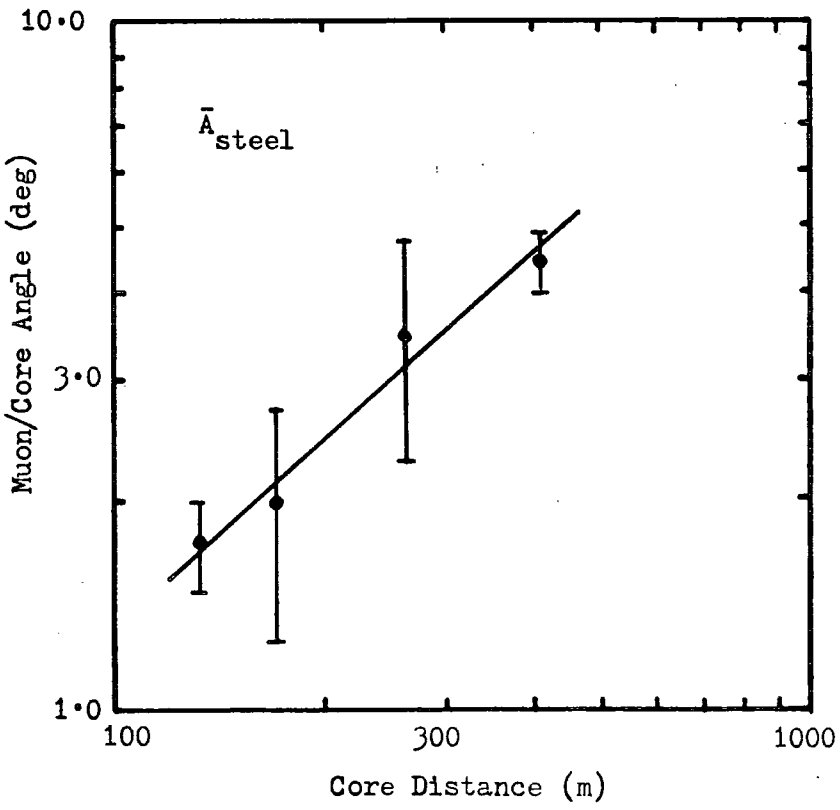
10·0
3·0
1·0
$\bar{A}_{steel}$
Muon/Core Angle (deg)
100
300
1000
Core Distance (m)

correlation between $\bar{A}$ and core distances is seen (it was originally predicted in the early simulations) and is shown in figure 4-12 for near vertical showers. A sensitivity of approximately one degree per hundred metres is seen for the barytes muons and slightly less than this for measurements made beneath steel.

Results of simulations have indicated that the median muon/core angle is possibly a better measure than $\bar{A}$. To be effective it is really necessary to have a large area detector ($30m^2+$) to give a sufficiently large signal. With the present experiment only the largest of the showers or those falling close to the detector permit such measurements to be made. At the time of writing only a few such showers exist and so it is not worthwhile to consider this factor here but it may yield valuable information when the full data set is available.

## 4-9 The Standard Deviation of the Spatial Angles of Muons in the Detector.

The standard deviation of the muon angles is readily available and is a useful measure to obtain from this experiment. Its main advantage is the independance of errors and fluctuations in the analysis of the shower arrival direction by the main array. By contrast the measurement of the mean muon angle was much affected by systematic errors in arrival direction measured by the main array.

As was described earlier the standard deviation of all the muon angles under barytes proved disappointing and it was not until the measure was refined to $S_{25}^{75}$ that the data were well behaved and a better correlation was made with core distance (figure 4-13). When these 'refined' results are compared with a pure standard deviation

Figure 4-13 The standard deviation of mean muon/core angles as a function of core distance for near vertical showers ($\theta \leqslant 35^{o}$), $Pd_{(500)} \geqslant 0{\cdot}5\ m^{-2}$.

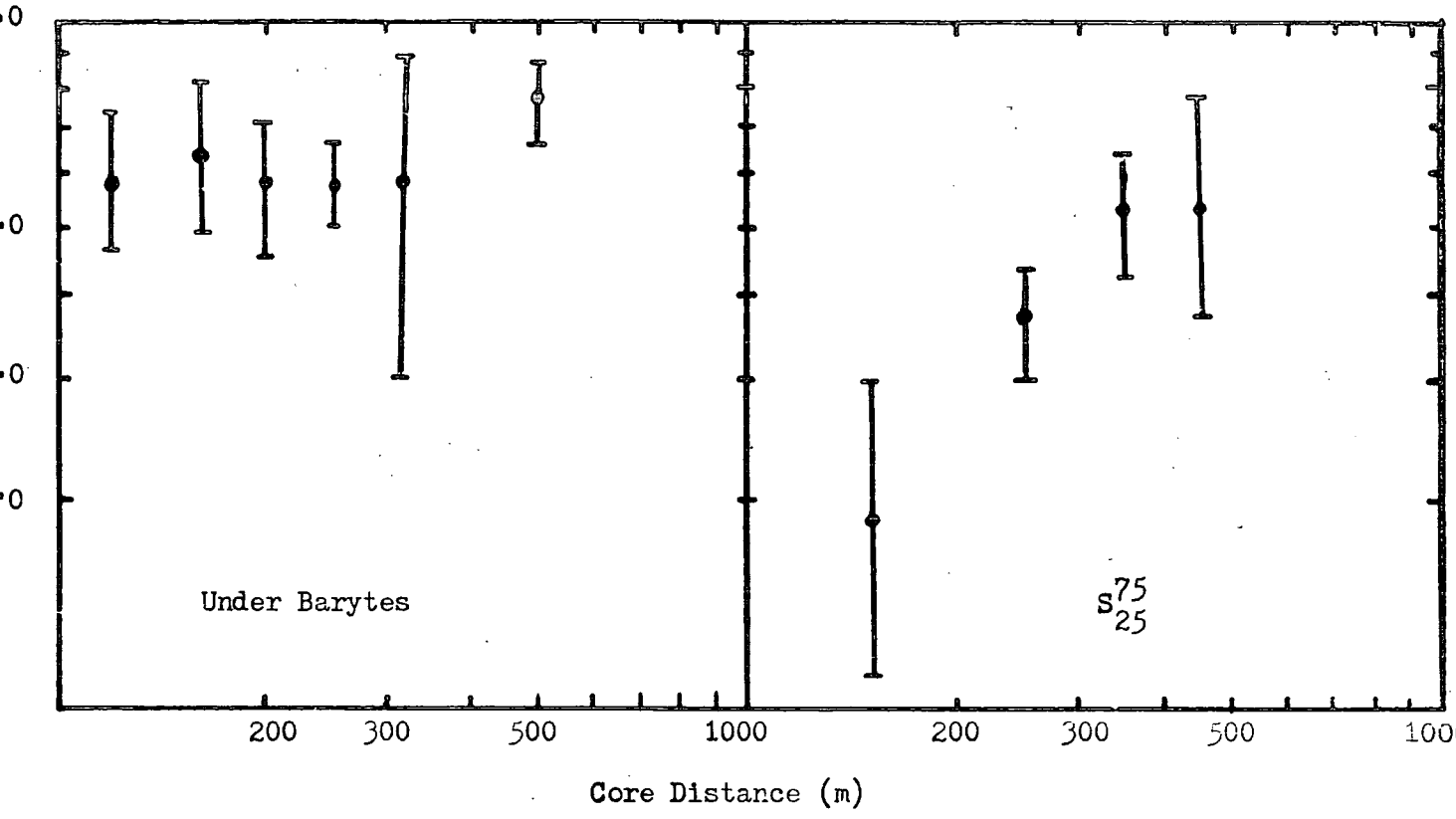
Under Barytes
$S_{25}^{75}$
200
300
500
1000
200
300
500
1000
Core Distance (m)

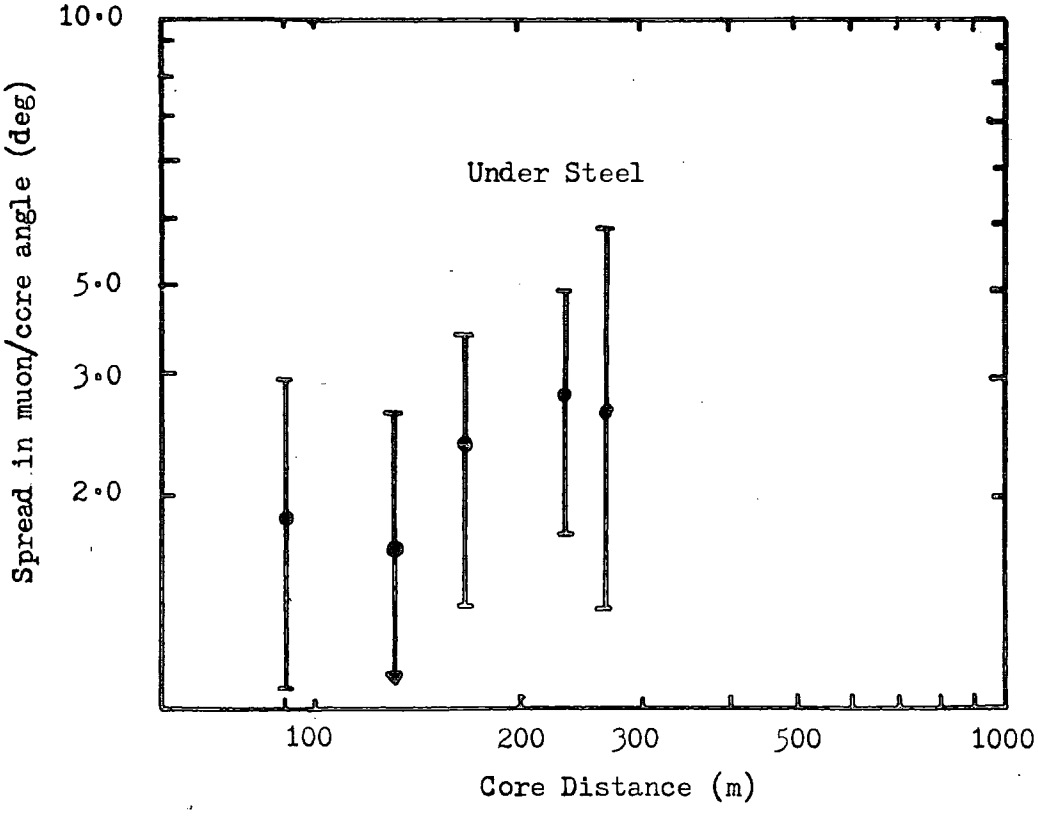
10·0
Under Steel
5·0
3·0
2·0
Spread in muon/core angle (deg)
100
200
300
500
1000
Core Distance (m)

measured beneath the steel shielding in figure 4-13 reasonable agreement is seen. This can be understood as the result of the elimination of the very low energy, highly scattered (in the atmosphere and Barytes) muon-electron component which does not penetrate the steel. However, as with $A_{25}^{75}$ the number of events to which this could be applied are limited and therefore its value is not great. It should be emphasised that this low energy contamination of the signal does not reduce the value of the angle data as the increased scattering of the particles only broadens the muon pulse and does not significantly affect the value of the mean angle.

## 4-10 Summary.

In this chapter the experimental data have been explored and a valuable insight into the performance of the equipment obtained. On the whole it is seen that the desired experimental parameters have been measured and it is now possible to understand the basic data and their implications. Knowing now the operational parameters and having a pool of data on which to draw, attention may now be turned to the physical interpretation with respect to known and postulated air shower phenomena. But first it is necessary to study the results of more rigorous and lifelike (in the context of this chapter) computer simulations of the muon component.

# Chapter Five

## Computer Simulations

### 5-1 Introduction.

The study of extensive air showers and their direct and immediate understanding is far from easy. The nuclear interactions producing the observed particles have occurred under far from ideal and controlled conditions in an unfavourable location. This is compounded by the very high energies involved (many orders of magnitude greater than available even now in the laboratory) and thus it can only be assumed that intelligent extrapolations of the known laws of nuclear physics apply in these interactions.

A possible solution to understanding the observed data lies in comprehensive modelling of air showers. By these means hypotheses of the interactions and the myriad independent and inter-dependent variables can be investigated until simulation results can be brought into agreement with available data and hopefully a fuller comprehension of the air shower cascade obtained. The magnitude of the simulation task has long been realised but only comparatively recently (with the advent of very powerful computer facilities) in the history of cosmic ray studies has it been possible to approach the situation confidently and in detail.

It is now possible to construct air shower models using Monte-Carlo simulation techniques which agree reasonably well with many aspects of the observed data. The situation is by no means complete and is still surrounded by controversy, particularly over the choice of hypothesis for the nucleon cascade (which governs the exact nature of the shower as seen at ground level), see for example

Gaisser et al (1978).

The controversies mentioned above are really outside the scope of this thesis and the role of simulations in understanding observable parameters is of more interest. Simulations are very important in the interpretation of this experiment due to the many varied and different parameters involved. This chapter therefore considers simulations of the muon component with particular application to understanding and interpreting the experimental work described in the preceeding chapter.

## 5-2 Simulation Techniques.

Given a model or hypothesis for the nuclear reactions occurring in an air shower (of necessity based on known and extrapolated work from accelerators) the modelling falls into several discrete sections. The full procedure has been lucidly described by Gaisser et al (1978) and Protheroe (1977) and only a summary will be given here.

The first part of a shower to be considered is the hadron cascade which generates different spectra of pions at varying depths in the atmosphere. As the various interactions in the atmosphere are of a random nature, a Monte-Carlo technique coupled with various analytic methods (to economise on computer time where possible) is the most appropriate. All nucleons and pions of the highest energy are followed throughout the shower's development using Monte-Carlo techniques, the energies of the leading nucleons and pions being sampled from appropriate distributions. The lower energy particles are treated by numerical integration techniques based on the diffusion equations. The neutral pions invariably decay before interacting and therefore only affect the electromagnetic component. Other particles

produced in the hadron cascade are, for simplicity, not considered individually but their effects are included in with the nucleons and pions. This approximation is assumed to have little effect on the overall cascade but may affect specific components of the shower; for example separate treatment of kaons may increase the muon flux but have little effect on the angle distribution.

An important aim of simulations is to assist in the identification of the mass of the initiating particle in real showers and therefore a range of primaries from protons to very heavy nuclei have to be considered. The simplest approach is to assume that the shower produced by a heavy nucleus of mass A and energy E is equivalent to the sum of A nucleon initiated showers each of primary energy E/A. This so called superposition model has been shown by Dixon and Turver (1974) to underestimate fluctuations in cascade development. A more realistic treatment can be had by using the fragmentation data of Freier and Waddington (1975).

It has been assumed that in the first interaction the heavy primary shatters into individual nucleons, $\alpha$ particles and larger fragments plus some pions from interactions between a proportion of the nucleons and the first air nucleus. Tomaszewski and Wdowczyk (1975) suggested that the percentage of nucleons interacting in this way would be $\approx$50% for heavy nuclei increasing to some 75% for lighter nuclei. The actual depth of the first interaction is usually sampled from a mean free path distribution specified by Cleghorn et al (1968).

To simulate average shower characteristics the superposition model is usually sufficient; however, for more detailed studies of fluctuations the choice of fragmentation model (and that of cascade model) are vitally important.

Once the main hadronic cascade has been set up attention can be turned to those parts of a shower actually seen and recorded at ground level. As the propagation of these components (muons particularly) have a direct relevance to the experimental data presented elsewhere in this thesis, a slightly more specific description of the simulation techniques employed will be given.

For the muon component the development of the cascade in space and time arising from pion decay is followed to the recording level, again using Monte-Carlo techniques. In the first case the transverse momentum of the parent pion is sampled from a distribution with the form:-

$$F(P_t)dP_t = 25{\cdot}0P_t \exp(-5{\cdot}0P_t)dP_t \qquad \ldots\ldots 5.1$$

and all or some of this is transmitted to the daughter muon with variations arising from the exact circumstances of decay. Additional factors affecting the transverse momentum of the muons arise from Coulomb scattering in the atmosphere and interactions with the geomagnetic field.

For muons which reach ground level, the muon parameters - core distance, spatial angle, time of arrival, energy etc., are written on to magnetic tape. The data bank thus created can then later be scanned and binned for parameters of interest; this procedure saves a considerable amount of machine time. At the same time other important effects, for example a specific detector response, can be folded in and varied at will.

Other effects of possible relevance have been considered - mention has already been made of kaon decay. Of recent interest has been the effect on the muon flux of photoproduced pions described by McComb et al (1979). This channel gives rise to additional very

low energy muons. The effect is energy dependant and could become important at primary energies $\gtrsim 10^{18}$eV at the largest core distances. Even then, large area detectors would be necessary to make feasible experimentally the testing of the hypothesis and they are a little outside the scope of the present experiment.

The electromagnetic cascade is considered using Rossi and Griesen's (1941) Approximation A (for energies >75GeV) and a Monte-Carlo cascade (for energies <75GeV) with methods developed from those of Butcher and Messel (1960). The lateral distribution of this component is generated mainly from geomagnetic effects and Coulomb scattering. Integral with the e-$\gamma$ cascade is the treatment of the Čerenkov light emission, see Protheroe (1977) and McComb and Turver (1981a).

## 5-3 Models of the Nucleon Cascade.

The simulations performed in parallel with the experimental work of the previous chapters have been based on Scaling and Landau-type models, in accordance with past and present work at Durham. The disparities between these and other long established models are well documented. Although direct comparison between other 'standard' models and this muon angle work will not be made, it would not be impossible knowing the way in which scaling compares with other experimental work. To a large extent the precise model(s) used are not particularly relevant in the context of this thesis - what is required are predictions from plausible models to aid in the interpretation of the experimental results. However, to place the results in context with other work and simulations, a summary of the nucleon cascade models used is in order.

The fundamental tenet of Feynman Scaling [Feynman (1969)] was that the production cross-sections scale with primary energy. This enables one to start at the highest accelerator energies and scale to the energies found in air showers. The distributions for the nucleon/charged pion cross sections are derived from Fishbane et al (1974) and Gaisser (1974). In accelerator work many workers [e.g. Amaldi et al (1973. 1977)] have observed the proton-proton cross-section to increase beyond 2000GeV with an assumed corresponding increase in $\sigma_{p\text{-air}}$. It is possible to extend the data in various ways to air shower energies with consequent effects on interaction lengths of the constituents in the nucleon cascade.

The Landau Model [ Landau (1953)] is characterised by an energy dependent pion number such that $< n > \alpha E^{\frac{1}{4}}$, in comparison with $< n > \alpha$ Ln E in Feynman Scaling. The model approximates to Scaling in the fragmentation region [Carruthers and Minh (1973)] and good agreement with data at accelerator energies is noted [Andersson et al (1976)]. The model improves on Scaling in many aspects but still is an unacceptable representation of many EAS phenomena if we assume proton primaries. For iron primaries, however, things are better, the muon component is increased and its energy dependance on shower size is in better agreement with the experimental data. Changing the pion multiplicity to increase still faster with energy ($\alpha E^{\frac{1}{3}}$) improves agreement with experimental data still further. To summarize, all factors of large showers which agree with Scaling also agree well with the Landau model.

## 5-4 Simulations of the Muon Component of EAS.

On the basis of the design study simulations for this

experiment, Turver (1975) showed that the spatial and temporal characteristics of muons in EAS are directly related. Accordingly there will be some reference to muon arrival times as a complement to the muon angles contained in this section.

The simulations have been refined and updated from those made by Turver and adjusted to closely resemble the experiment in terms of shielding and detector response. To illustrate the effects of shielding on the muon angle signal many of the figures relating to this section show predictions for the two different absorbers in the equipment (barytes and steel).

The first parameter to consider is the lateral distribution; it is a known and understood measurement and thus sets the scale for any simulations. Shown in figure 5-1 are the results of $10^{17}$eV simulations for both iron and proton primaries using Landau $E^{\frac{1}{4}}$ and scaling models respectively (representing a muon rich and a muon poor simulation as described in the previous section, thus covering the typical muon content of all current models). All results are the average over many showers to remove the effects of fluctuations on the calculations. The data are compared with experimentally derived results of Strutt (1976) and good agreement is seen, particularly for the simulation for heavy primaries. In many of the results from the new experiment a strong dependence on zenith angle is seen. Initially simulations of inclined showers did not exist; however for the final analysis of all the data such work will be necessary.

The ratio of the densities under steel and barytes ($\Delta S/\Delta B$) arises as a direct consequence of the muon lateral distributions as does the muon/deep water signal ratio (figures 5-2 and 5-3). The measurements of the latter quantity are compared with the results of

Figure 5-1 The simulated muon lateral distribution for $10^{17}$ eV showers with proton and iron primaries. Also shown are the experimental results of Strutt (1976), (from McComb, private communication).

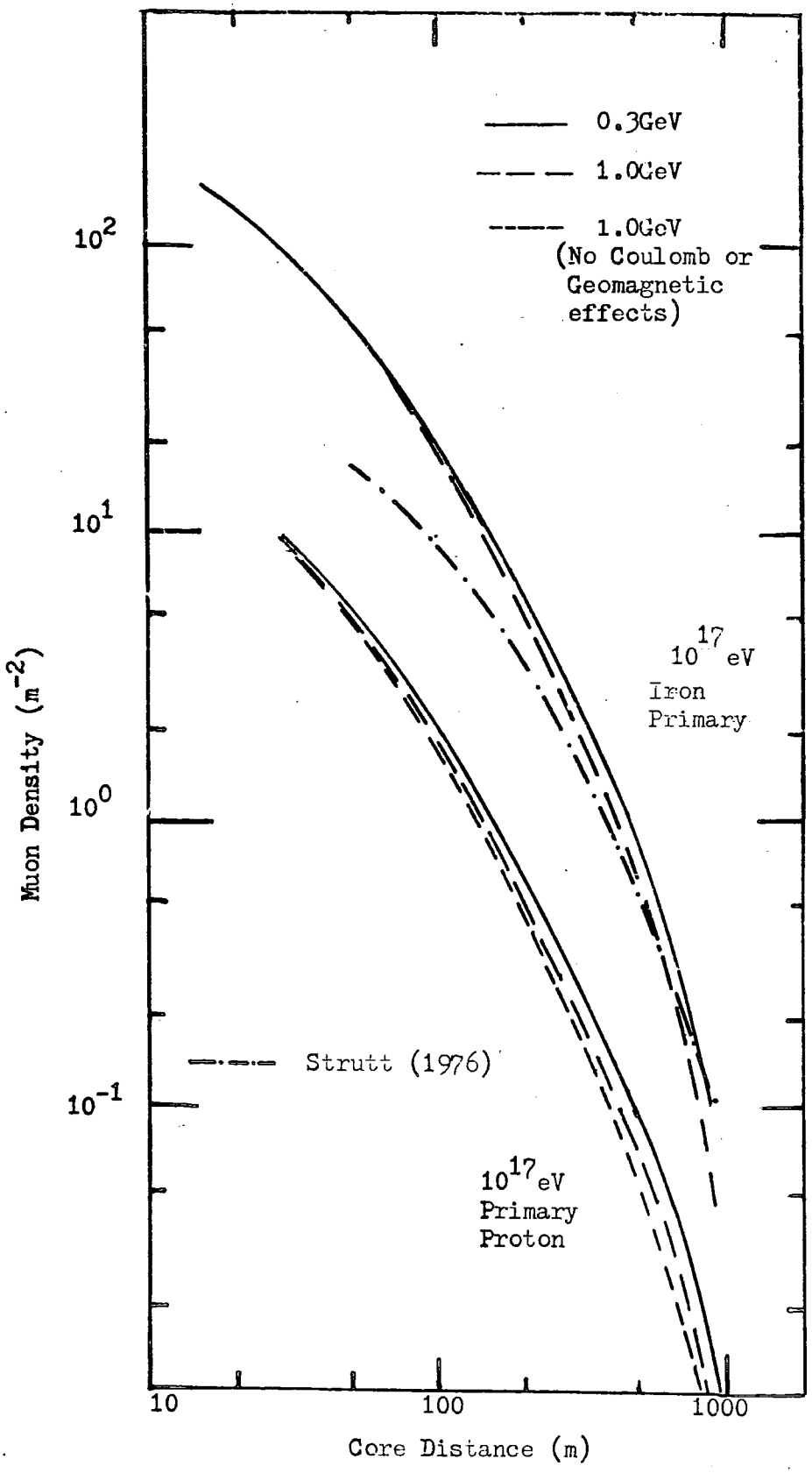
0.3GeV
1.0GeV
1.0GeV
(No Coulomb or Geomagnetic effects)
$10^{17}$ eV
Iron
Primary
Strutt (1976)
$10^{17}$eV
Primary
Proton
$10^2$
$10^1$
$10^0$
$10^{-1}$
Muon Density ($m^{-2}$)
10
100
1000
Core Distance (m)

Figure 5-2 The Steel to Barytes ratio ($\Delta S/\Delta B$) as a function of core distance for two different primaries.

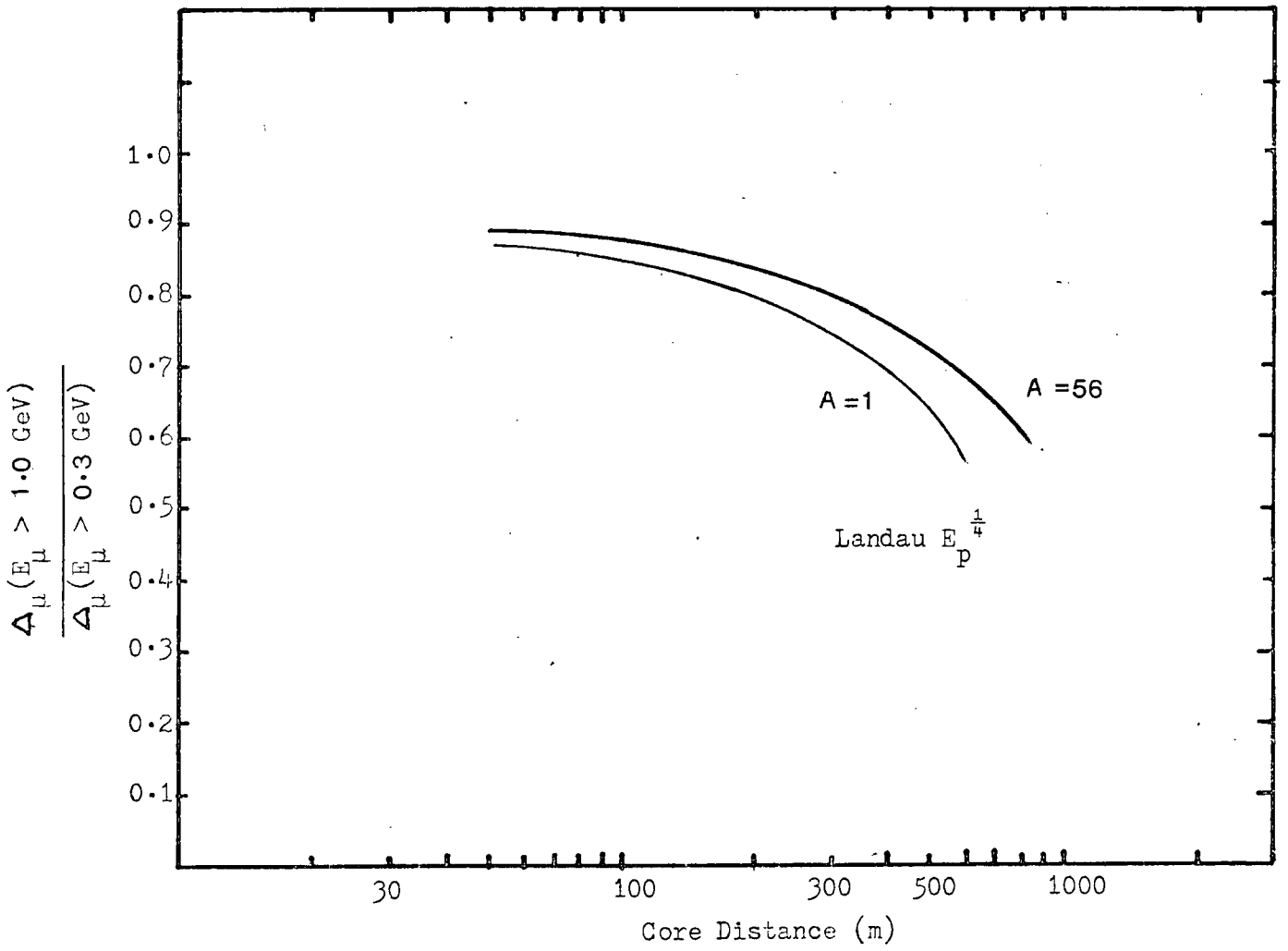
$\frac{\Delta_\mu(E_\mu > 1.0\ \text{GeV})}{\Delta_\mu(E_\mu > 0.3\ \text{GeV})}$
1·0
0·9
0·8
0·7
0·6
0·5
0·4
0·3
0·2
0·1
A =1
A =56
Landau $E_p^{\frac{1}{4}}$
30
100
300
500
1000
Core Distance (m)

Figure 5-3 The muon/deep water signal according to the results of Strutt (1976) compared to simulations of showers with three depths of cascade maximum.

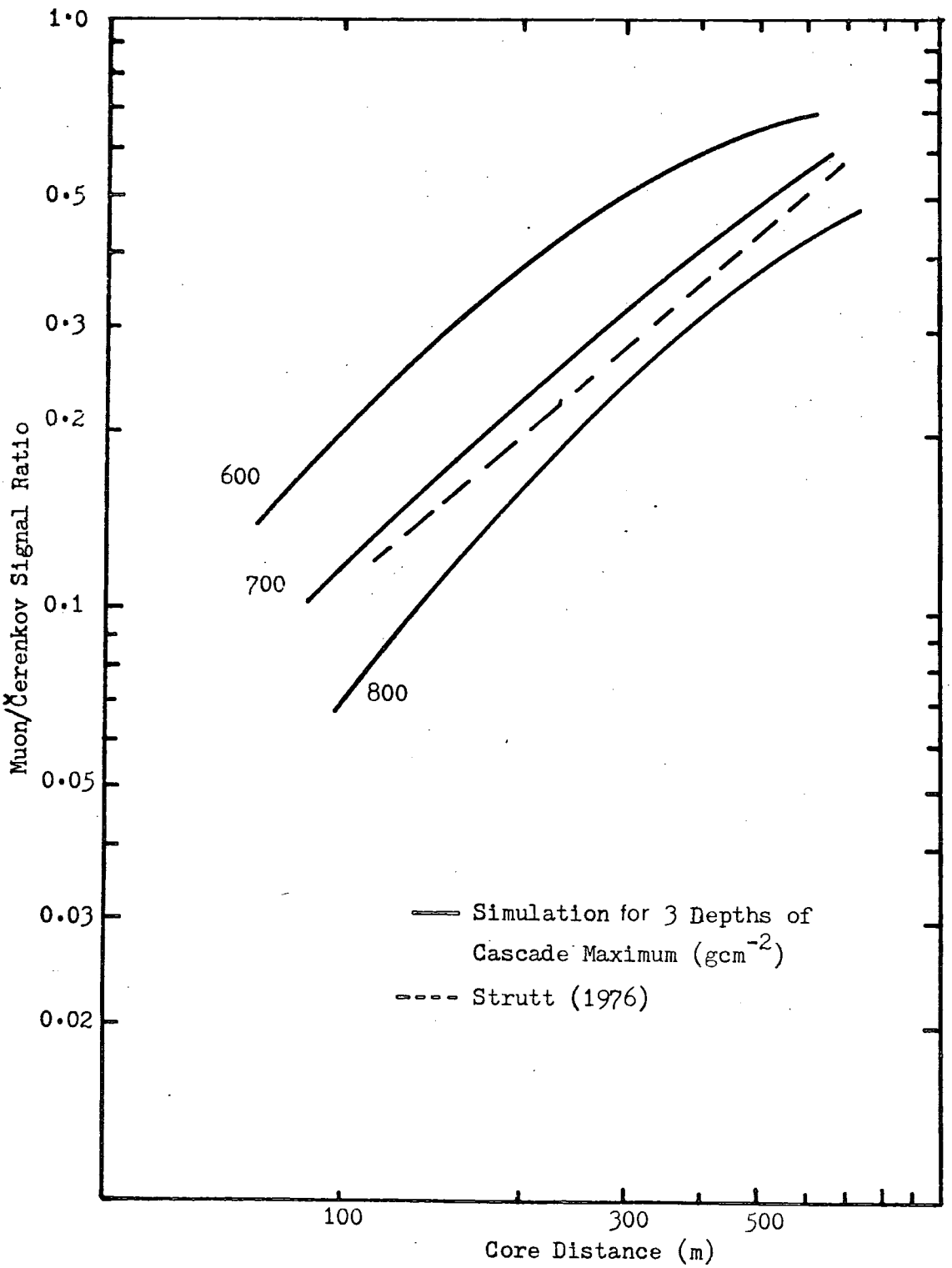
1·0
0·5
0·3
0·2
0·1
0·05
0·03
0·02
Muon/Cerenkov Signal Ratio
600
700
800
Simulation for 3 Depths of Cascade Maximum (gcm$^{-2}$)
Strutt (1976)
100
300
500
Core Distance (m)

Figure 5-4 Simulated muon 'angle profiles' at different core distances showing the distribution about the mean angle (McComb, private communication).

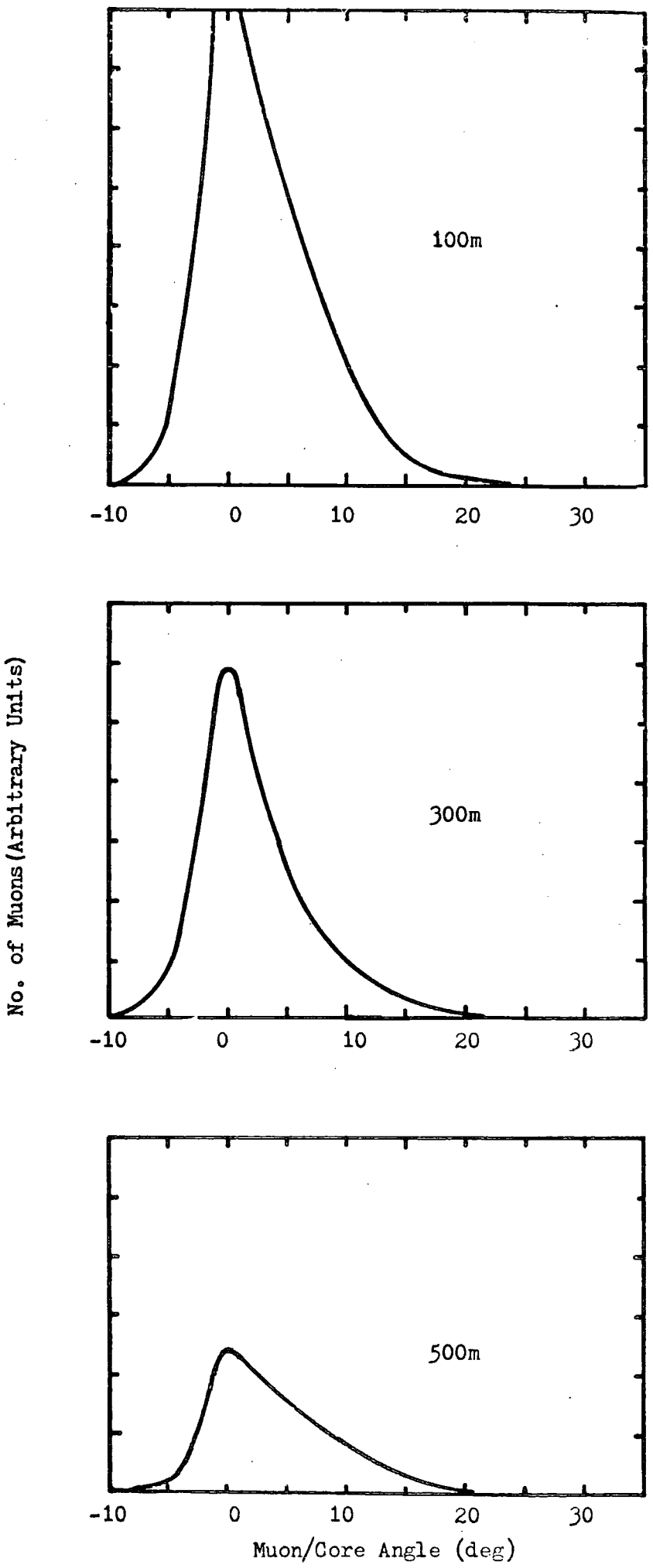
100m
300m
500m
-10
0
10
20
30
No. of Muons (Arbitrary Units)
Muon/Core Angle (deg)

Figure 5-5 Simulated time pulses for the same core distances as figure 5-4 in a $10^{17}$eV iron primary shower, (McComb, (Private Communication)).

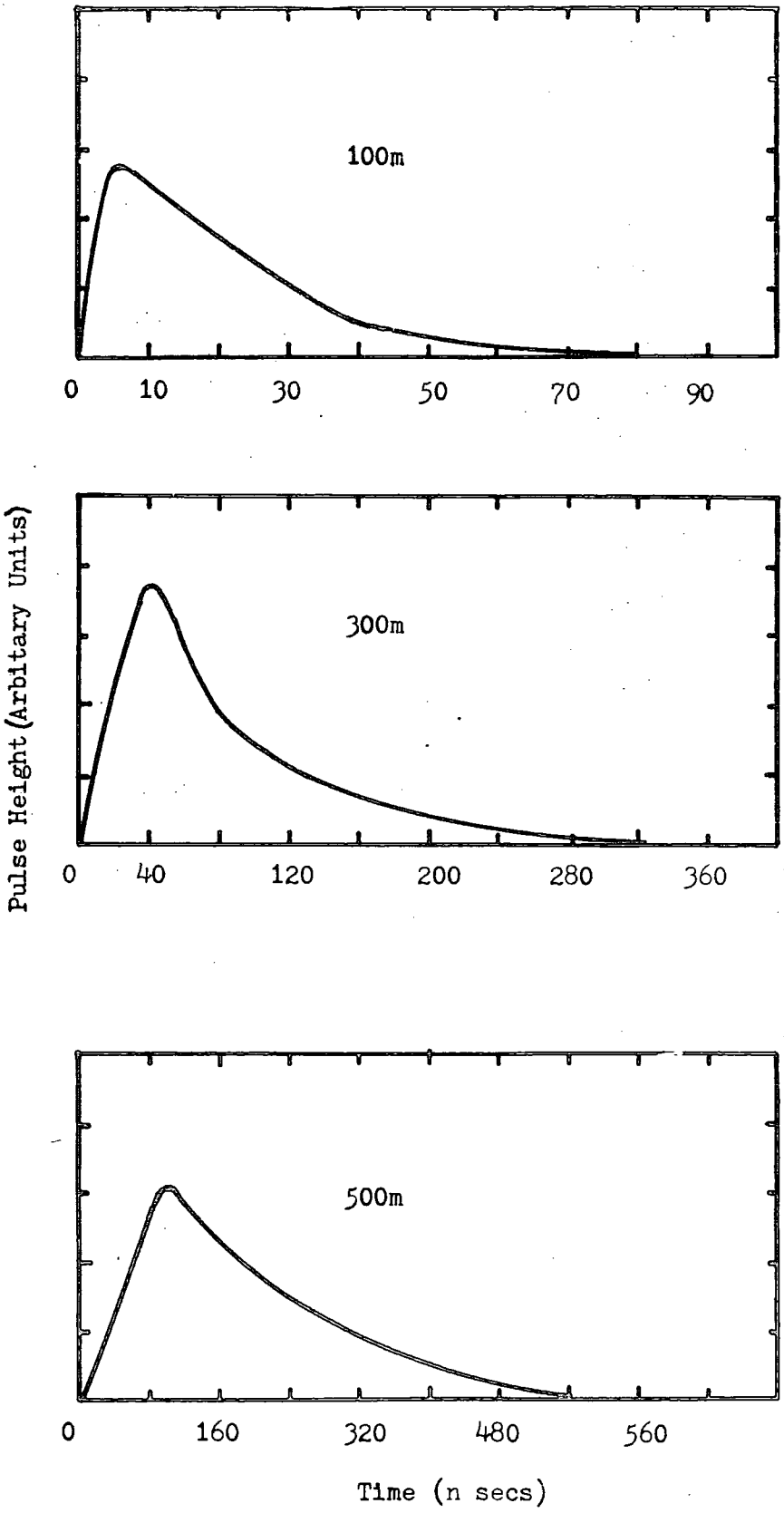
100m
0
10
30
50
70
90
300m
0
40
120
200
280
360
500m
0
160
320
480
560
Pulse Height (Arbitary Units)
Time (n secs)

Figure 5-6 The muon/core angle ($\overline{A}$) with different shielding as a function of the core distance. $10^{17}$eV, A = 56. (McComb, private communication).

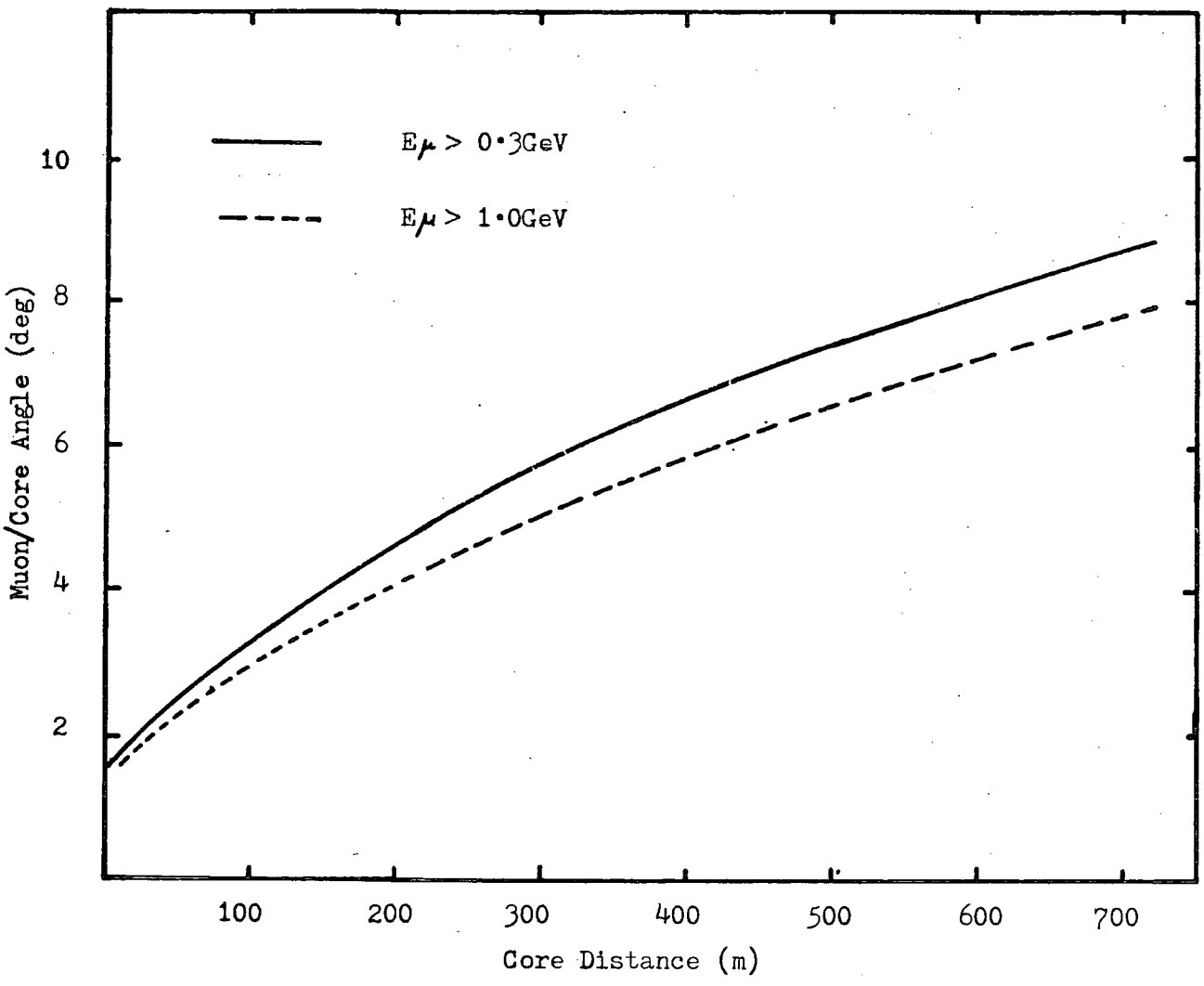
Eμ > 0·3GeV
Eμ > 1·0GeV
Muon/Core Angle (deg)
2
4
6
8
10
100
200
300
400
500
600
700
Core Distance (m)

Strutt (1976). It should be noted that the experimental results shown in figure 5-3 may include effects of the detector and shielding not included in the simulations.

Having established the trustworthyness of the simulations through comparison with recently measured known quantities, their predictions for the spatial properties can now be approached with confidence. Looking first at the muon/core angle for varying core distances, these are best displayed as a pulse profile in angle (cf. figures 4-3 and 4-4). With the simulations a much larger muon sample can be considered than is available from the experiment and a much clearer signal is therefore obtained. Figure 5-4 compares the predicted angle profiles for the two shielding levels in the central detector. The similarity between angle and time pulses (figure 5-5) is clear and this likeness led to the investigation of $S_{25}^{75}$ (cf. Chapter 4) as a useable parameter. The scattering of the lowest energy muons has been shown (Chapter 4) to disrupt the standard deviations as measured by the experiment and its origins are now clearly seen.

Figure 5-6 shows the effect of greater shielding on the mean core angle as a function of core distance, this can be seen to increase slightly with core distance; the muon-core angle increases, due to the muons passing through an increasing amount of shielding, suffering more scattering and absorption en route as the total path length increases. A similar effect is visible for the standard deviation (figure 5-7).

Comparing figures 5-7 and 5-8 enables $S_{25}^{75}$ to be better appreciated whilst differences still exist between the true signal and the observed it is a little more sensitive to core distance albeit with a smaller signal. As was shown in chapter 4 the measure

Figure 5-7 The variation of the standard deviation of the muon/core angle ($\sigma$) with increasing shielding and core distance; $10^{17}$eV, A = 56 (McComb, private communication).

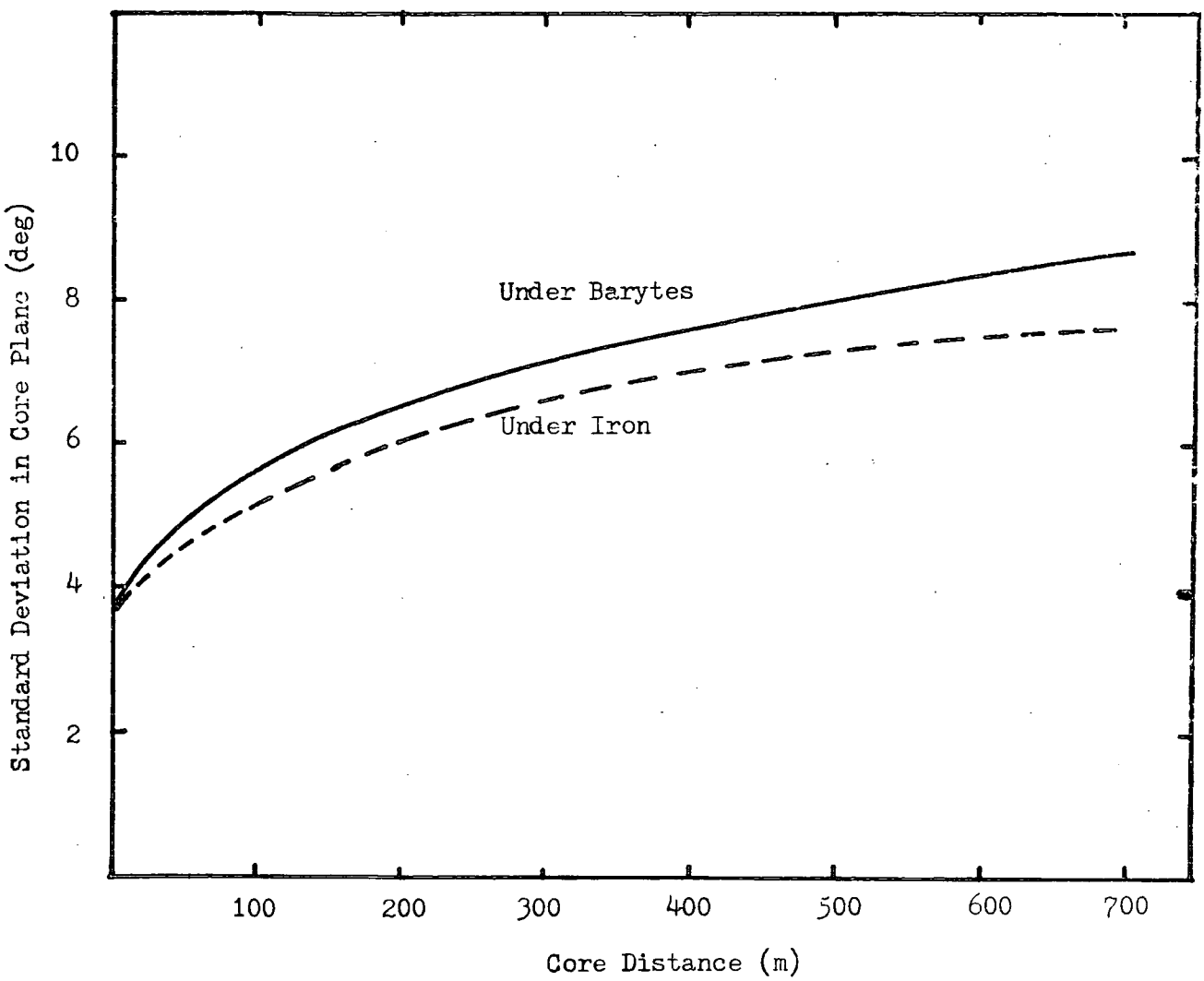
Standard Deviation in Core Plane (deg)
10
8
6
4
2
Under Barytes
Under Iron
100
200
300
400
500
600
700
Core Distance (m)

Figure 5-8 $S_{25}^{75}$ as a function of core distance and shielding thicknesses.

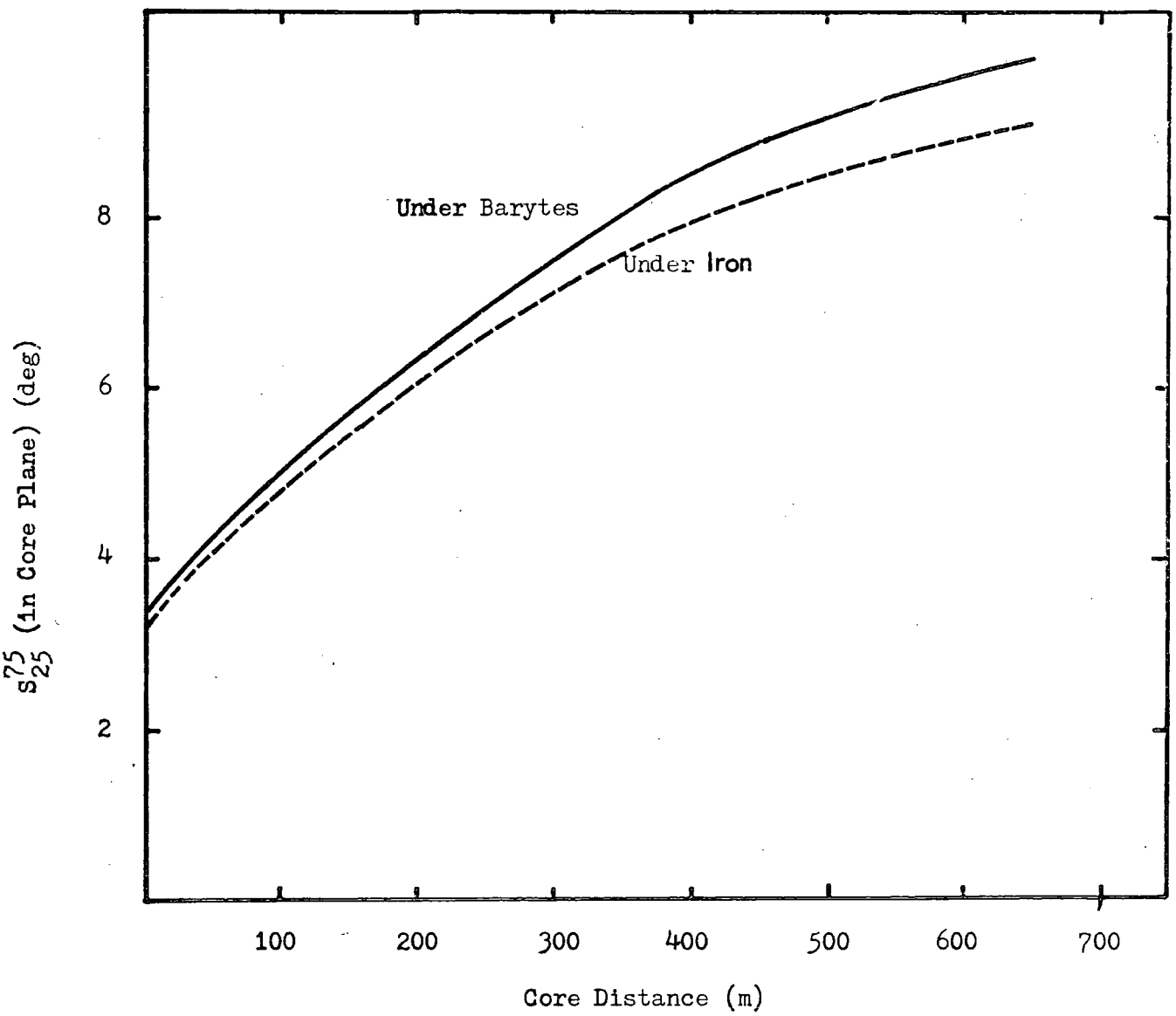
Under Barytes
Under Iron
8
6
4
2
100
200
300
400
500
600
700
$s_{25}^{75}$ (in Core Plane) (deg)
Core Distance (m)

Figure 5-9 Time of muon pulse peak as function of core distance; $10^{17}$eV, A = 56. (McComb, private communication).

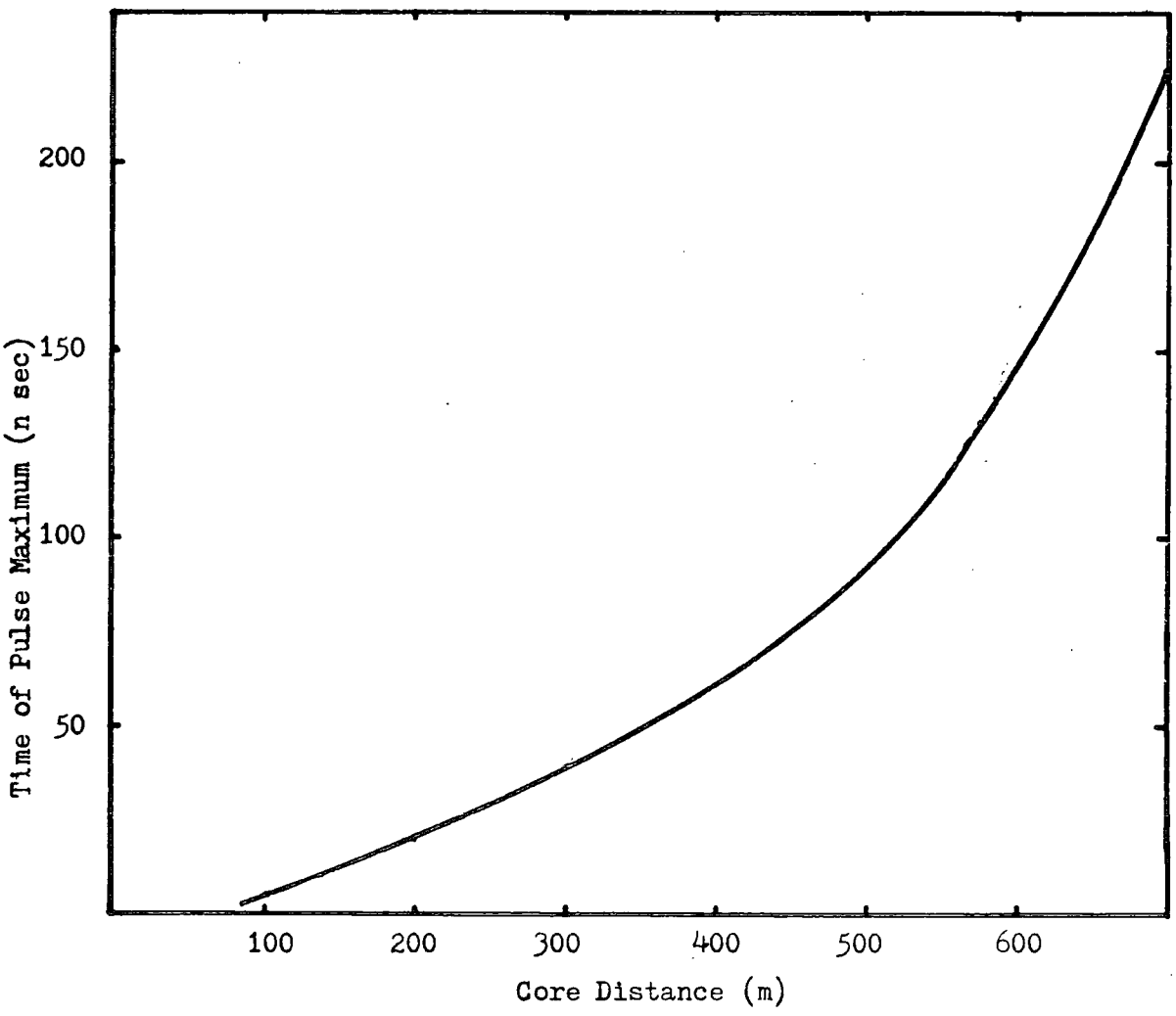
200
150
100
50
Time of Pulse Maximum (n sec)
100
200
300
400
500
600
Core Distance (m)

Figure 5-10 Full width half maximum of muon pulse as seen by a 'perfect' detector; $10^{17}$eV, A = 56 . (McComb, private communication).

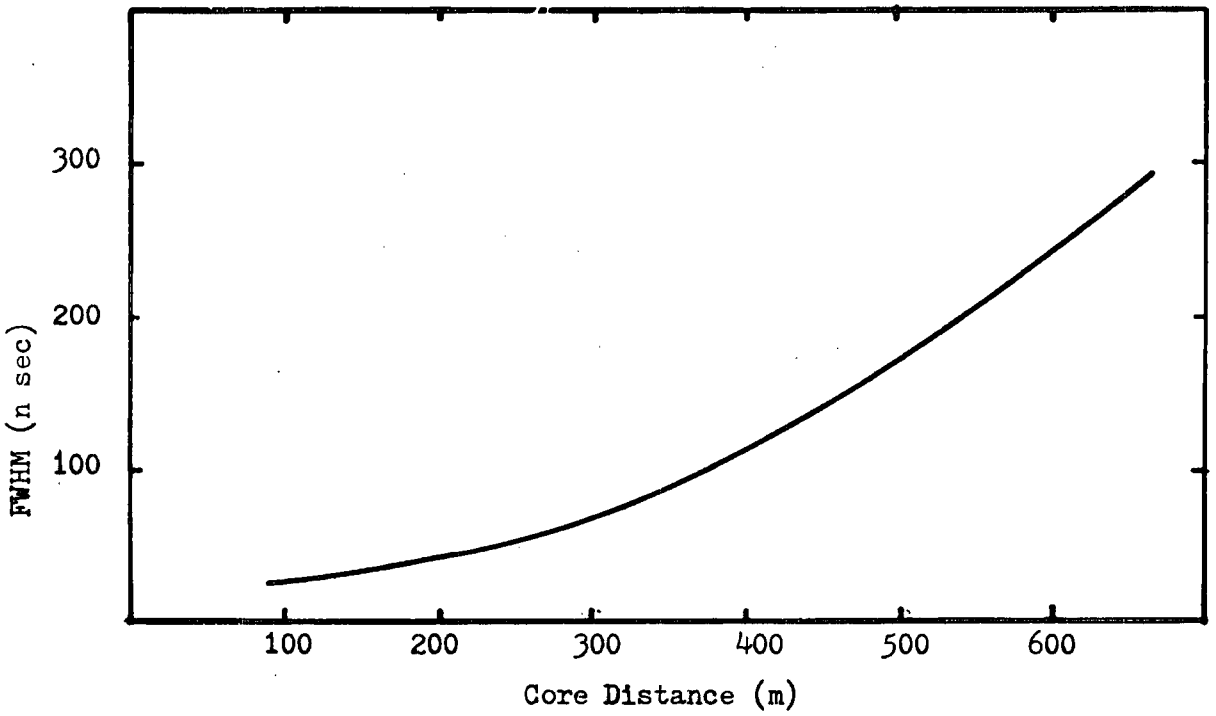
300
200
100
FWHM (n sec)
100
200
300
400
500
600
Core Distance (m)

becomes more useful with a smaller detector when, with a much smaller sample (typically 10 - 15 muons as against 150+ with these simulations) one or two muons in the extremes of the signal tail can have a more dramatic broadening effect on the signal. This could be negated with a larger data set.

It is worthwhile comparing these simulations with predicted muon arrival times for the same showers. Looking at both the time of pulse maximum and full width half maximum (figures 5-9 and 5-10 respectively) it will be seen that both time parameters increase rapidly with core distance as the distances flown increases. It should be noted that this timing data is raw, i.e. no allowance has been made for shielding or detector and recording system losses in band-width.

If the data are binned by core distance a clear sensitivity to depth of cascade maximum is indicated with both $\bar{A}$ and standard deviation (figures 5-11 and 5-12). Given a large enough data sample it is to be hoped that this effect will be seen in the experimental data and if so, would perhaps be the most valuable overall contribution of the experiment.

## 5-5 Summary.

Having now examined the simulation predictions in the light of Chapter 4 several interesting and encouraging points can be noted. Firstly, the primary aim of the experiment to study spatial angles may be achieved and the data so obtained should show average values and fluctuations of relevance to estimates of the development of air showers. By taking the examples of muon poor and muon rich showers differences between models are apparent. Secondly, the simple two threshold energy measuring capability of the central detector can perhaps yield useful

Figure 5-11 The sensitivity of muon/core angle $\bar{A}$ to depth of maximum. (McComb, private communication).

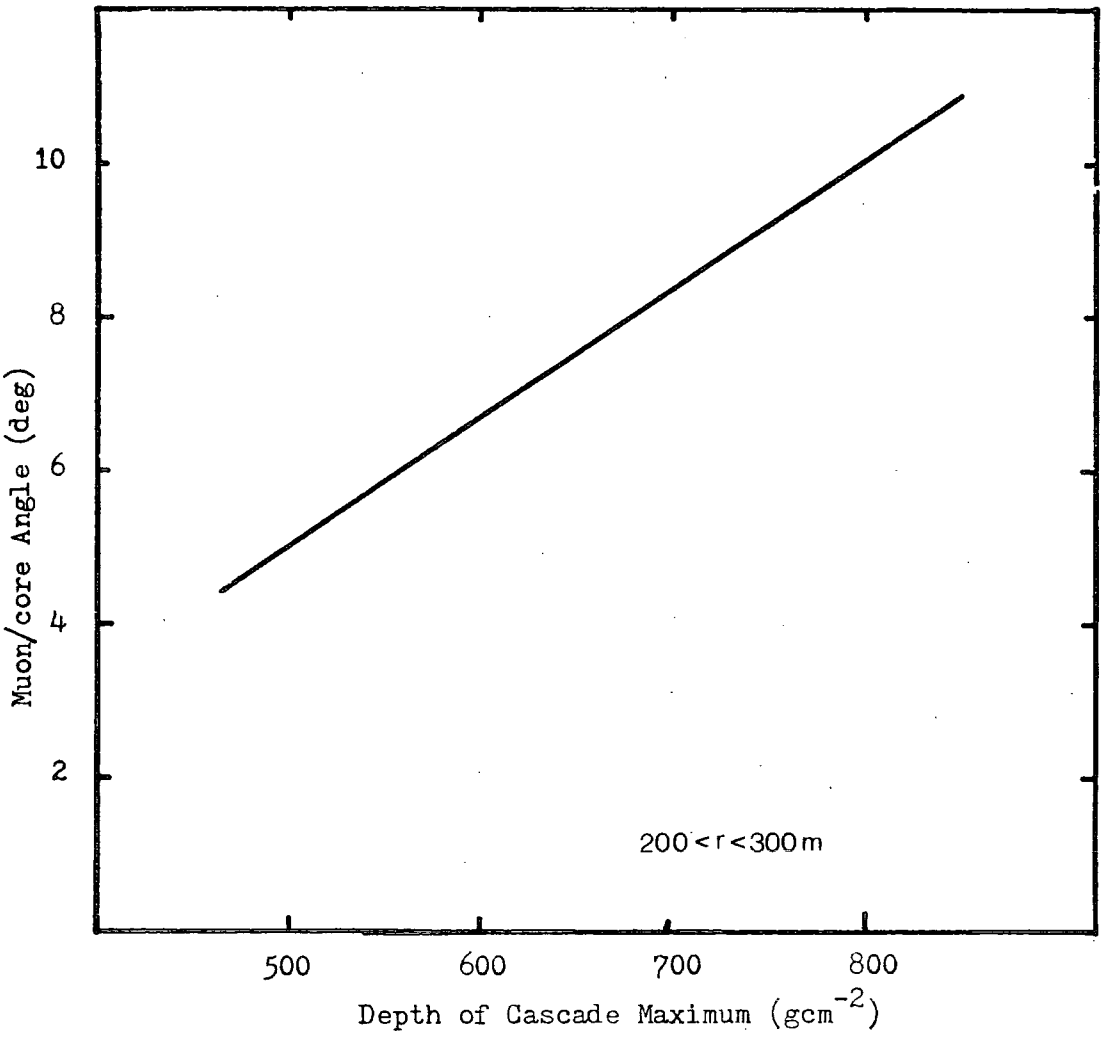
10
8
6
4
2
Muon/core Angle (deg)
200 < r < 300 m
500
600
700
800
Depth of Cascade Maximum (gcm$^{-2}$)

Figure 5-12 The sensitivity of the spread in muon/core angles to depth of maximum. (McComb, private communication)

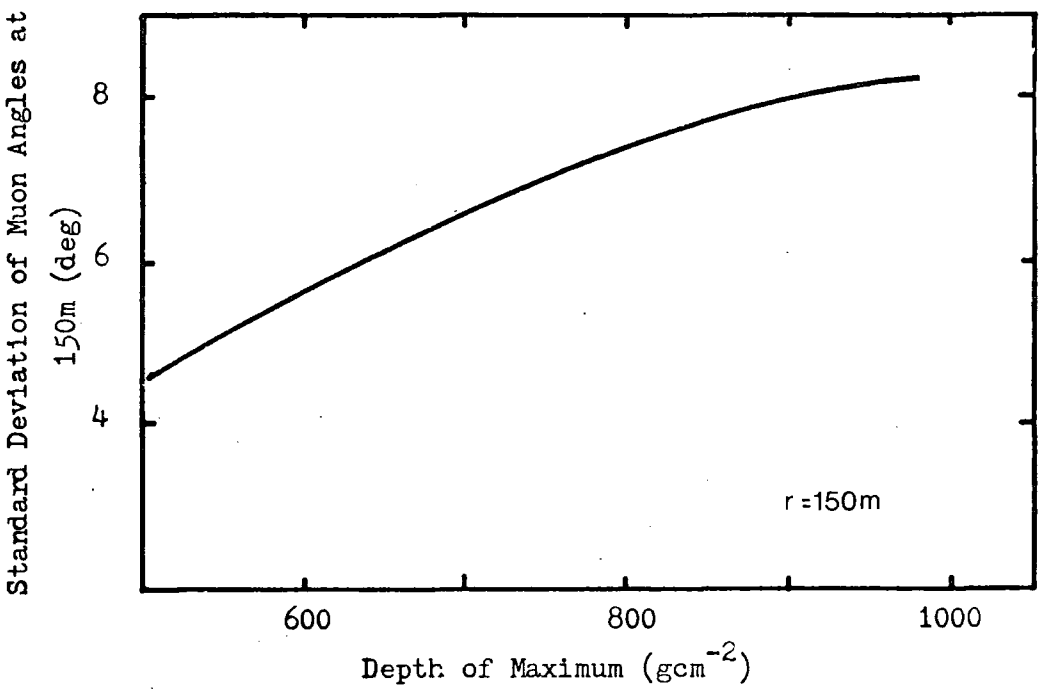
Standard Deviation of Muon Angles at 150m (deg)
8
6
4
r =150m
600
800
1000
Depth of Maximum (gcm$^{-2}$)

information of a form which can be compared directly with other workers' simulations. Finally, there exists the possibility of easily measured parameters relating directly to the cascade development.

# Chapter Six

## An Interpretation of the Spatial Angle Data

### 6-1 Introduction

The interpretation of data from any air shower experiment is never straightforward. There are a great many correlated variables and to eliminate these and isolate the underlying physics is a major task in itself and only then can some reason be attributed to the observed phenomena. Thus, (as was demonstrated in Chapter 4) it is relatively easy to understand the 'behaviour' of an experimental system which conceals many effects, but a totally different matter to interpret the data.

In this chapter the various aspects of the muon spatial angles measured by the equipment are considered and attempts are made to relate them to air shower development and other experimental data by means of customized simulations. The original aims of the experiment are pursued, not too successfully but a good estimate of the mean depth of electron maximum is obtained.

### 6-2 The Muon Angle Measurements

Chapter Four showed that the muon-core angle signal measured by the equipment was reasonably well behaved beneath both barytes and steel shielding. In the former case the attempted refinement of the signal by trimming the leading and trailing edges of the angle distribution does not alter the signal significantly when used with a larger data sample; in any case the number of events to which this measure could be applied is limited. Using now an expanded data set ($\approx$ 700 events) than Chapter 4 the bin widths can be reduced and more data points obtained.

Figure 6-1 The relation between mean muon/core angle ($\bar{A}$) (at an energy threshold of 0·3 GeV) and core distance for near vertical showers and a mean primary energy of $\sim 3 \times 10^{17}$ eV compared with simulation results.

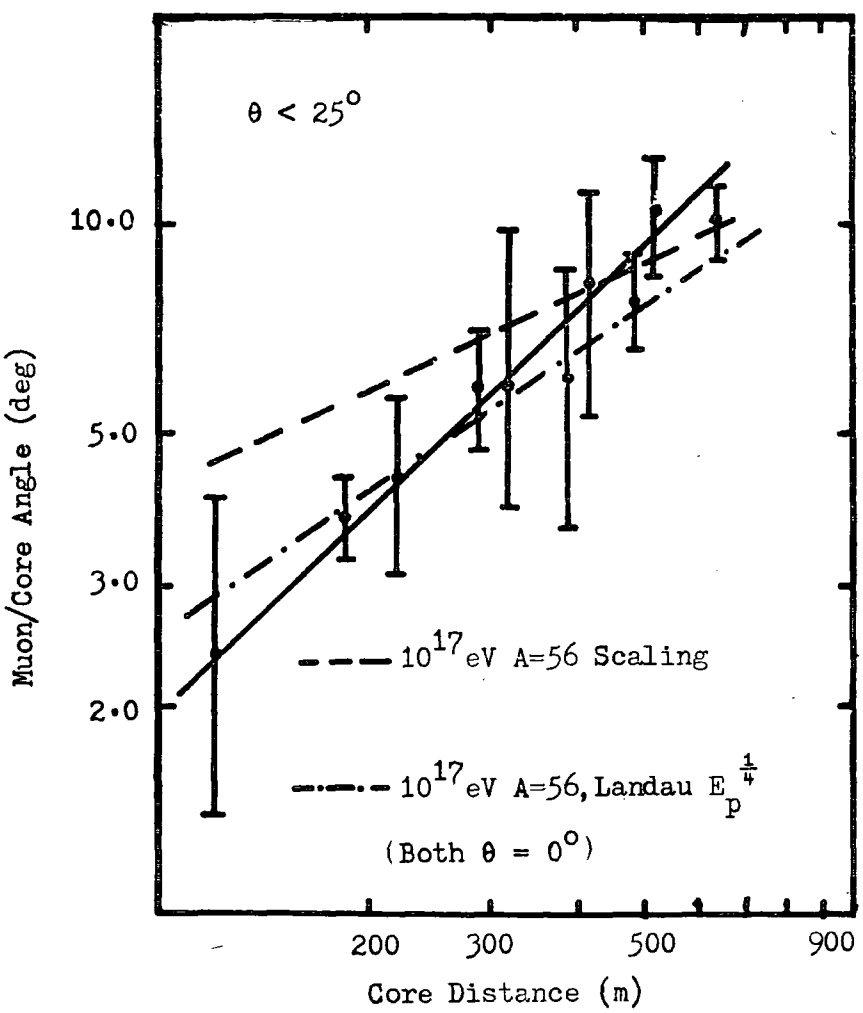
θ < 25°
10·0
5·0
3·0
2·0
Muon/Core Angle (deg)
$10^{17}$eV A=56 Scaling
$10^{17}$eV A=56, Landau $E_p^{\frac{1}{4}}$
(Both θ = 0°)
200
300
500
900
Core Distance (m)

Figure 6-2 As for the previous diagram, but for higher energy muons (> 0.8 GeV).

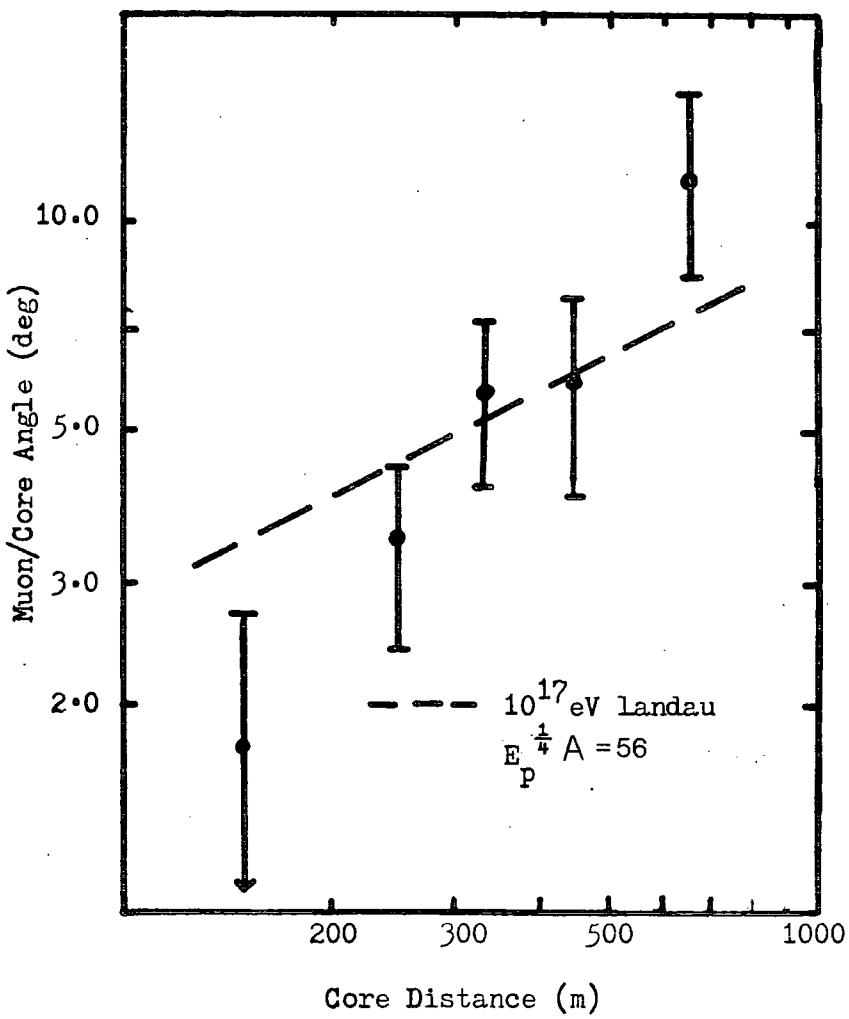
10.0
5.0
3.0
2.0
Muon/Core Angle (deg)
200
300
500
1000
Core Distance (m)
$10^{17}$eV Landau
$E_p^{\frac{1}{4}} A = 56$

The muon-core angle under barytes and steel as a function of core distance are shown in figures 6-1 and 6-2 respectively. In each case data from a $10^{17}$eV Landau $E_p^{\frac{1}{4}}$ A=56 simulation is also shown. It should be noted that the simulation data are for vertical showers, whilst the data extend to a zenith angle of $25^{\circ}$, some differences are thus inevitable and this is clearly shown in the diagrams.

A search for some sensitivity to zenith angle and hence longitudinal development of the cascade was made by comparing the muon/core angle in various core distance bins and, overall, proved disappointing with the most significant results appearing in the 200 to 300 metre band. These are shown for both barytes and steel results in figures 6-3 and 6-4 together with a $10^{17}$eV Landau A=56 simulation. It is clearly obvious that the higher energy data resemble prediction more closely but in neither case can the agreement be said to be good or in the case of lower energies particularly convincing. It could be and most probably is the case that the extra atmospheric depth traversed with increasing zenith angle is becoming more manifestly apparent in the form of increased scattering of the low energy component.

A similar search through the data was made for an energy dependence and, as is shown in figure 6-5, there is only a very weak dependence evident for near vertical showers in the core distance band 200 to 300 metres. For comparison a simulation curve is also shown.

As the simulations described in chapter five were specifically tailored to the experiment it is possible to relate the data to some of the more important cascade parameters, in particular the depth of the electron cascade maximum ($t_{max}$). The simulations in general show a unique relationship between the observable muon parameters and $t_{max}$.

Figure 6-3 The muon/core angle ($\bar{A}_B$) ($E_\mu \geqslant 0.3$ GeV) as a function of zenith angle (Sec $\theta$) for a core distance range of $200 < r < 300$m. Also shown is a $10^{17}$eV Landau $Ep^{\frac{1}{4}}$ simulation ($A \simeq 56$).

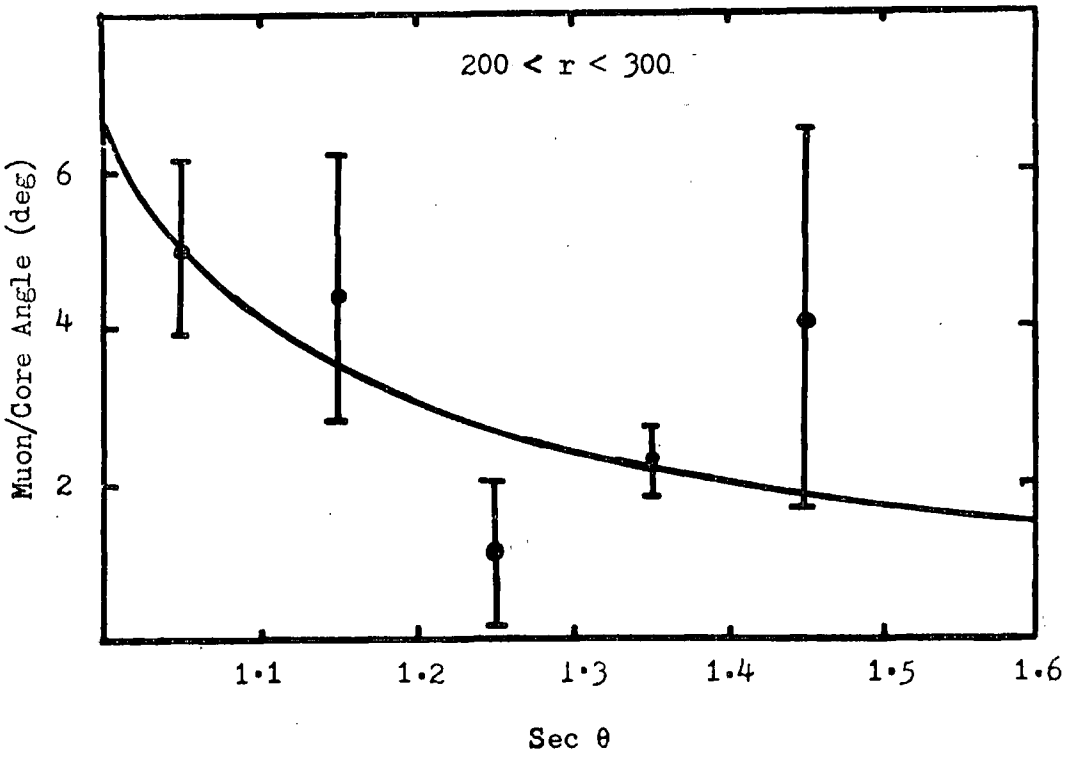
200 < r < 300
Muon/Core Angle (deg)
6
4
2
1·1
1·2
1·3
1·4
1·5
1·6
Sec θ

Figure 6-4 The muon-core angle ($\bar{A}_s$) ($E_\mu \geqslant 0{\cdot}8$ GeV) as a function of zenith angle (Sec $\theta$) for a core distance of $200 < r < 300$m. Also shown is a $10^{17}$eV Landau $Ep^{\frac{1}{4}}$ (A = 56) simulation.

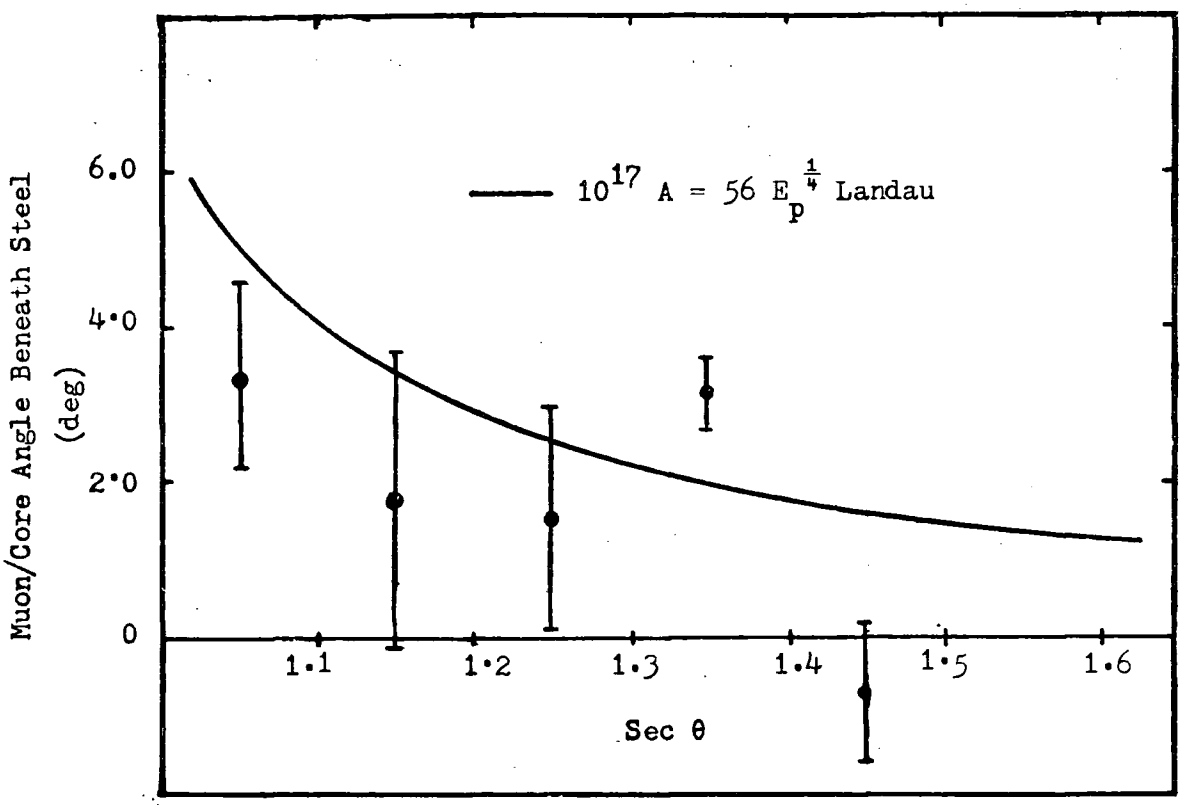
Muon/Core Angle Beneath Steel (deg)
6.0
4·0
2·0
0
$10^{17}$ A = 56 $E_p^{\frac{1}{4}}$ Landau
1·1
1·2
1·3
1·4
1·5
1·6
Sec θ

However, the derived values are very dependent on the choice of model and therefore the values of $t_{max}$ quoted in this chapter could be biassed by the scaling based Durham models used for its derivation.

Accordingly the value of $t_{max}$ at the average energy of the data available ($3 \times 10^{17}$eV) of $717 \pm 40 gcm^{-2}$ has been derived for muons with $E_\mu > 0{\cdot}3$ GeV and $672 \pm 49 gm\ cm^{-2}$ for muons beneath the iron shielding. These figures are obviously consistent with other experimental work in this energy region.

The weak energy dependence of the spatial characteristics at present precludes the making of any convincing estimate of an elongation rate. This situation might be improved upon by a much larger data sample but is probably unlikely with the current trends indicated by the data.

## 6-3 Measurement of the Spread in Muon/Core Angles

As was shown earlier the spread in muon/core angles is a parallel measure to the angle determinations. Unfortunately it does not appear to be as sensitive as simulations have predicted and this is clearly demonstrated in figures 6-6 and 6-7 for low and higher energy muons respectively and is particularly evident at greater core distances (>200m). A reduced sensitivity is also seen in the higher energy component (but not illustrated here). The improved measurement of standard deviation $S_{25}^{75}$ described in chapter 4 does not seem to offer any substantial improvement with an increased data set. The inherent fluctuations eliminated by it earlier are themselves smoothed out with the better statistics associated with a larger data set.

No evidence of any strong correlation was found with primary energy or zenith angle, an example of the latter being shown in figure 6-8.

Figure 6-5 The energy dependence of $\bar{A}_B$ ($E_\mu \geqslant 0.3$ GeV) in near vertical showers in the core distance band $200 < r < 300$m.

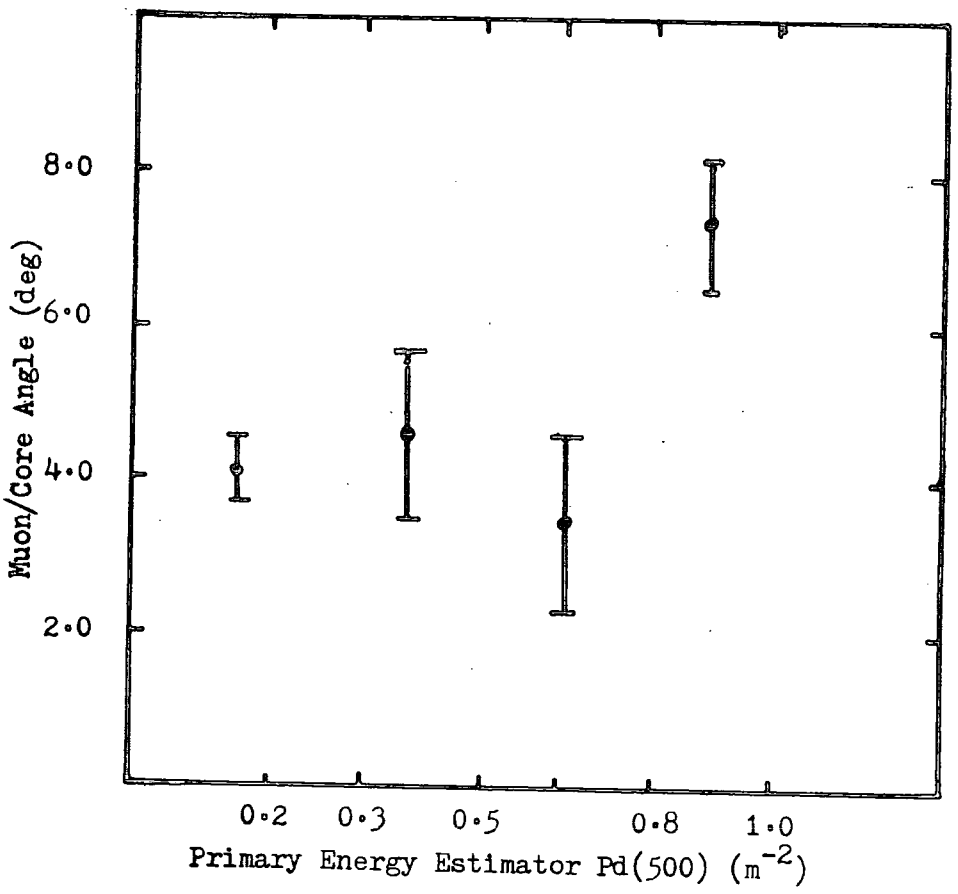
8·0
6·0
4·0
2·0
Muon/Core Angle (deg)
0·2
0·3
0·5
0·8
1·0
Primary Energy Estimator Pd(500) (m$^{-2}$)

Figure 6-6 The spread in muon/core angles ($E_\mu \geqslant 0{\cdot}3$ GeV) as a function of core distance together with a $10^{17}$ eV, Landau $E^{\frac{1}{4}}$, A = 56 simulation.

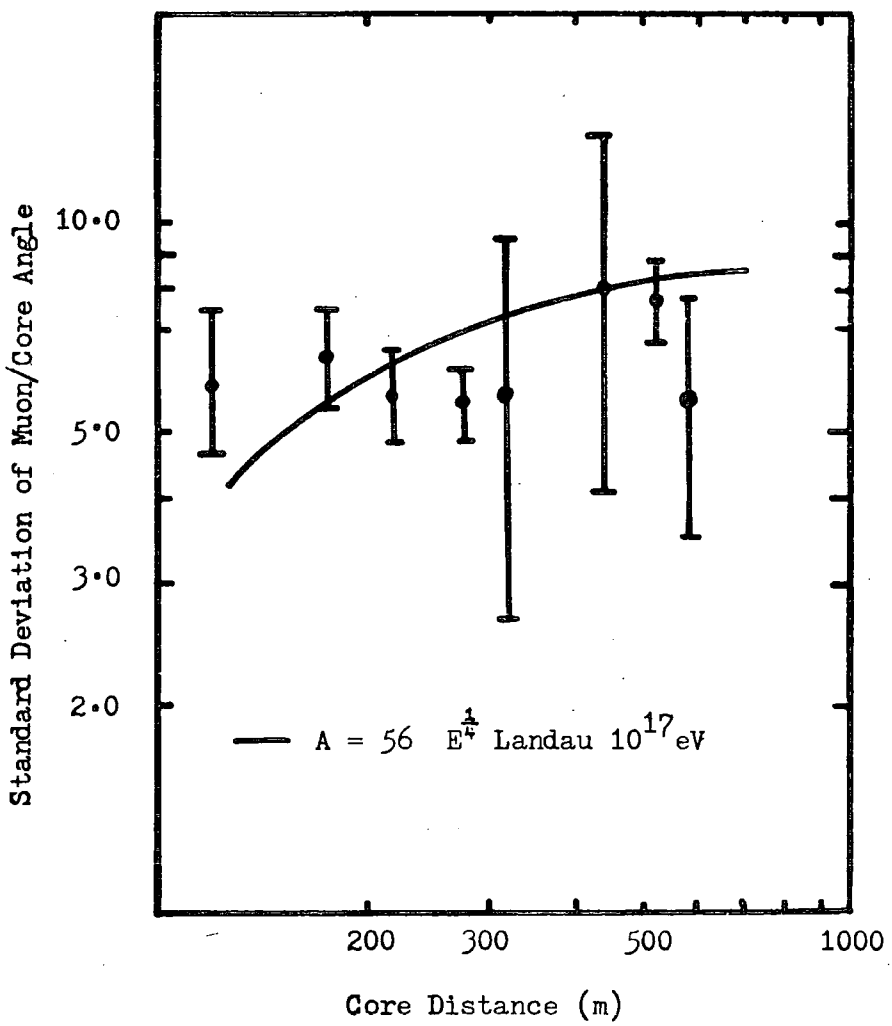
Standard Deviation of Muon/Core Angle
10·0
5·0
3·0
2·0
A = 56 E^1/4 Landau 10^17 eV
200
300
500
1000
Core Distance (m)

Figure 6-7 The spread of muon/core angles ($E_\mu \geqslant 0.8$ GeV) as a function of core distance with a $10^{17}$ eV, Landau $E^{\frac{1}{4}}$, A = 56 simulation.

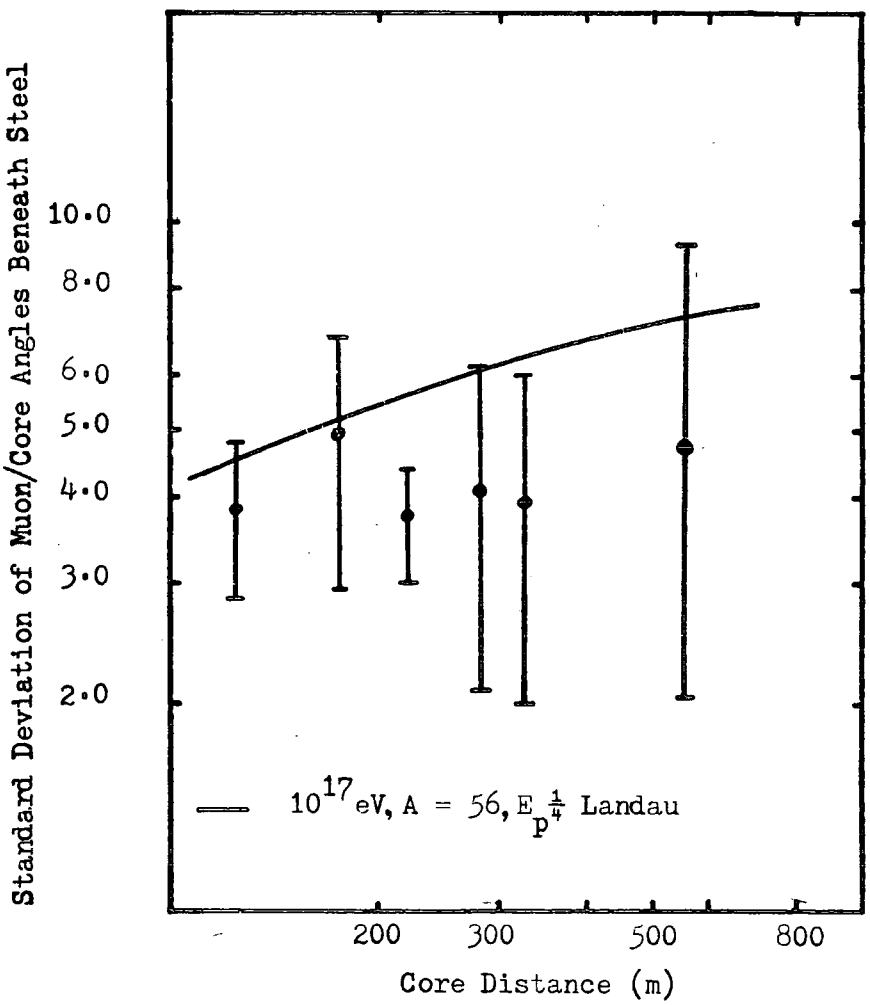
Standard Deviation of Muon/Core Angles Beneath Steel
10·0
8·0
6·0
5·0
4·0
3·0
2·0
200
300
500
800
Core Distance (m)
$10^{17}$eV, A = 56, $E_p^{-\frac{1}{4}}$ Landau

Figure 6-8 The spread in muon-core angles ($E_\mu > 0.3$ GeV) as a function of zenith angle (Sec $\theta$). The lack of sensitivity to zenith angle is clearly seen.

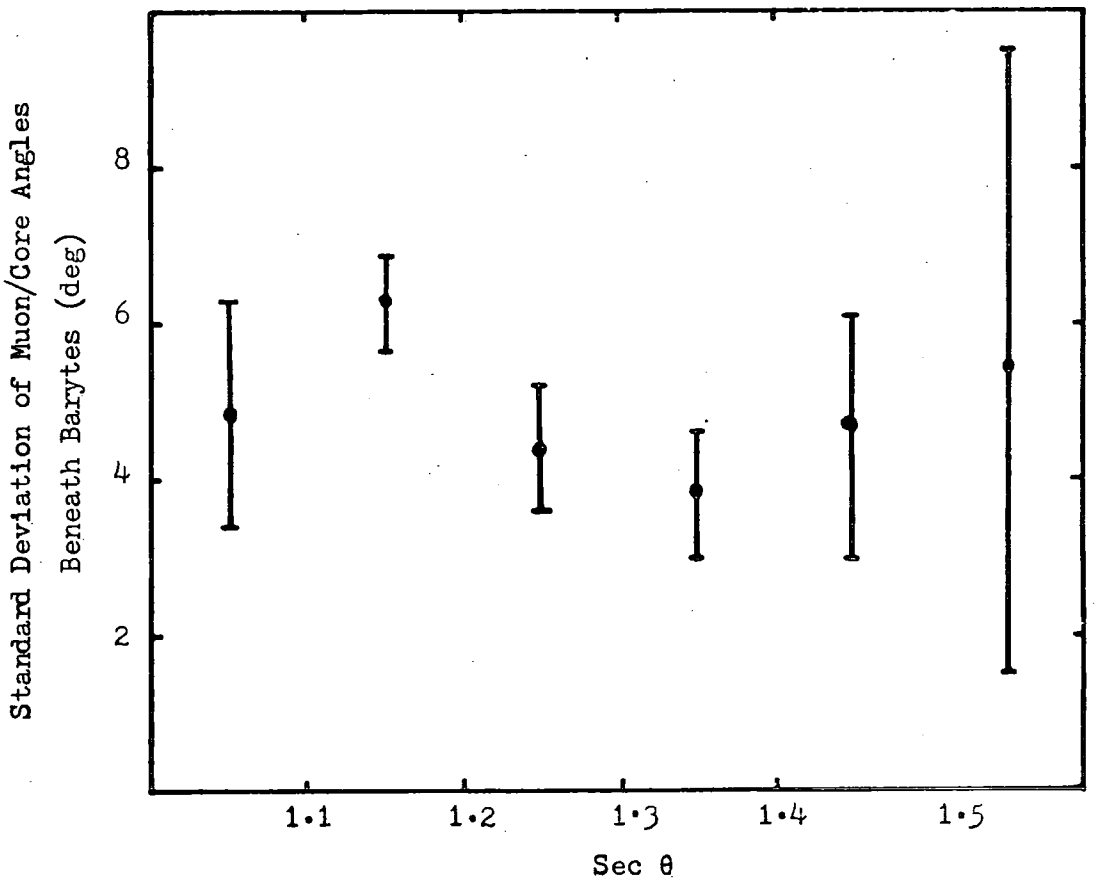
Standard Deviation of Muon/Core Angles
Beneath Barytes (deg)
8
6
4
2
1·1
1·2
1·3
1·4
1·5
Sec θ

It was suggested by McComb (private communication) that the standard deviation of muon/core angles is independent of the shower impact point or azimuthal angle and thus the size of the data sample could be increased. When an enlarged data set is created by using this technique no significant improvement in sensitivity is obtained as is shown in figure 6-9 for the higher energy muon sample. It must therefore be concluded that the shape of the muon angle signal is independent of zenith angle effects.

Relating the standard deviation data to simulations in a similar way to the angle data, values of $745 \pm 60 gm\ cm^{-2}$ and $580 \pm 57 gm\ cm^{-2}$ for the depth of the electron cascade maximum are obtained for the low and high energy component respectively. The lack of sensitivity to core distance of the high energy component is probably the cause of the large difference between this better result and the other values.

## 6-4 Results from Contemporaneous Muon Experiments at Haverah Park for Comparison with the Muon Angle Data

The density measurements possible with the experiment described in this thesis were comprehensively described in Chapter 4 and are there subject to some basic analysis. They were shown to be in agreement with other work using other measurement techniques. Refinement of the simulations to resemble the experimental conditions leads to good agreement (figures 4-6 and 6-10).

Two other experiments at Haverah Park have been running concurrently with the Durham Spatial Angle Experiment (The 'Infilling Experiment' operated jointly by the Universities of Durham and Leeds and the University of Nottingham muon timing experiment) and results of both of them are of great interest for comparison with the present

Figure 6-9 The spread in muon-core angles with an enlarged dataset (following the suggestion of McComb - private communication); $E_\mu > 0{\cdot}8$ GeV.

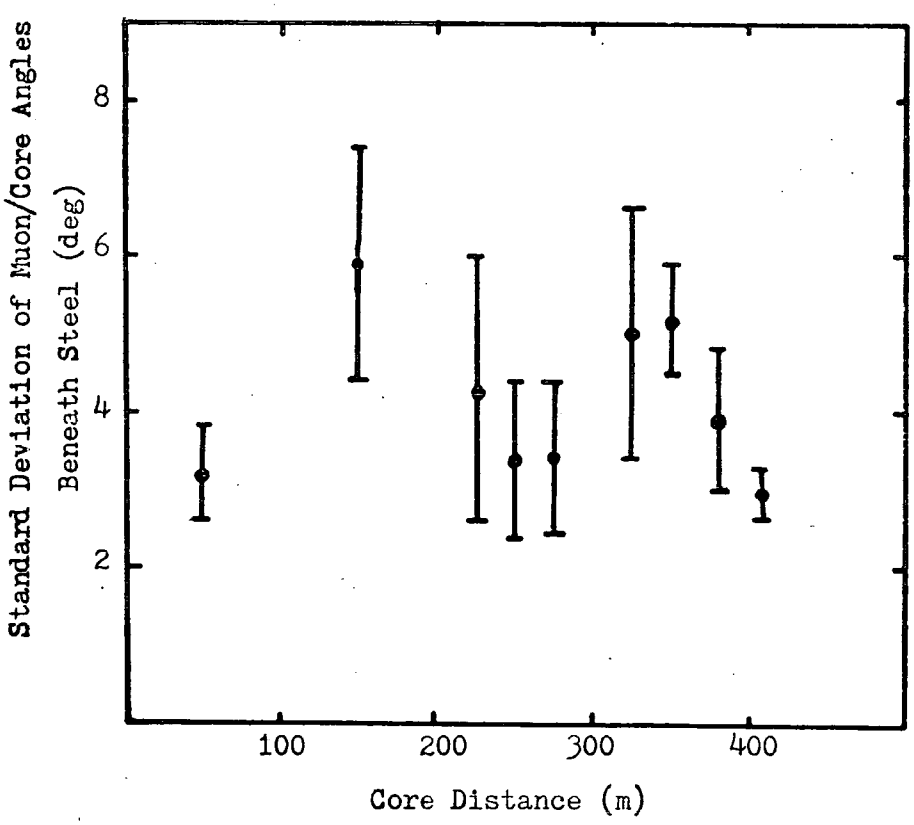
Standard Deviation of Muon/Core Angles
Beneath Steel (deg)
2
4
6
8
100
200
300
400
Core Distance (m)

experiment.

The Infilling Experiment comprises 30 small deep water detectors (area $\approx 1m^2$) on a closely spaced array with an aim of measuring the lateral distribution of shower particles in the range 50 - 500m with great precision. The Array and its characteristics have been described by Edge et al (1977) and an analysis of the results has been published by Craig et al (1979). The data has subsequently been subject to further analysis by McComb and Turver (1981a) and an elongation rate of $75 \pm 15 gcm^{-2}$ decade$^{-1}$ over the energy range $3 \times 10^{17}$ - $10^{18}$eV is quoted.

The University of Nottingham experiment has been described by Blake et al (1979) and uses three widely spaced liquid scintillator detectors beneath different thicknesses of shielding (giving muon energy thresholds of 426MeV, 481MeV and 306MeV). The equipment was designed to investigate the muon pulse shape and measures the integrated rise time of the muon signal with a delta function response of 32·5ns. Mann (1980) quotes results for the integrated signal rise time between the 10% and 70% levels ($t_{10}^{70}$) and these are shown for the two extremes of the energy sensitivity in figures 6-11 and 6-12 (It should be noted that the results have been corrected to the vertical). McComb and Turver (1981b) have expanded their muon simulations to include the response characteristics and shielding of the Nottingham experiment and these results are also shown on the diagrams. Agreement between the data and the simulations is seen at the lower energy threshold but it is obvious that, like the muon angle work, further simulation data is needed to fully understand the high end of the spectrum. It is very encouraging however that the Nottingham muon timing data and the muon spatial angle data both on the whole agree with simulations (at lower

Figure 6-10 The lateral distribution of muons beneath the barytes ($E_\mu > 0{\cdot}3$ GeV) and steel ($E_\mu > 0{\cdot}8$ GeV) absorbers compared with a $10^{17}$ eV Landau simulation.

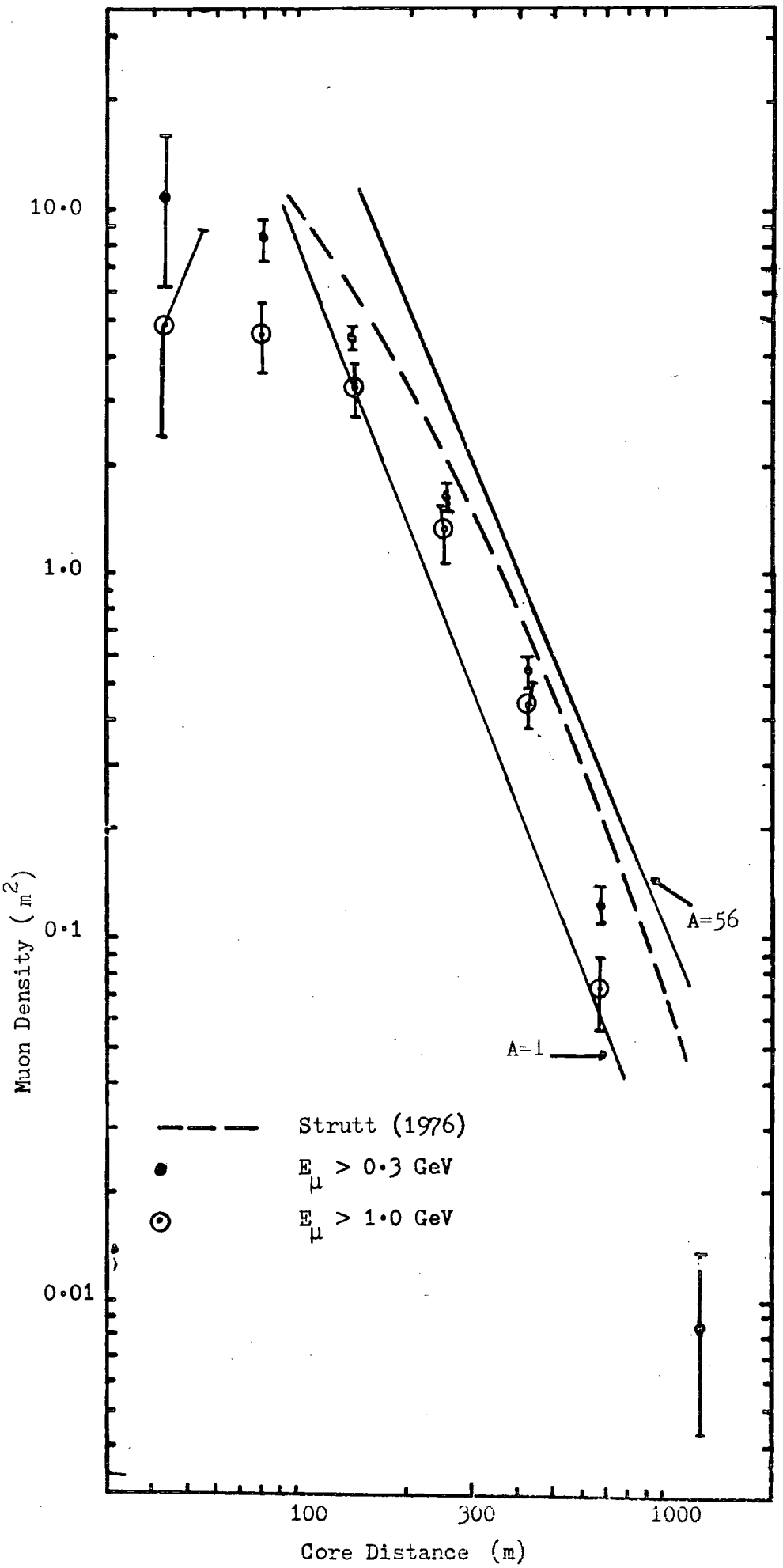
10·0
1·0
0·1
0·01
Muon Density ( m$^{-2}$)
100
300
1000
Core Distance (m)
A=56
A=1
Strutt (1976)
$E_\mu$ > 0·3 GeV
$E_\mu$ > 1·0 GeV

**Figure 6-11** The rise time ($t_{10}^{70}$) of the lowest energy muon pulses recorded by Mann (1980) compared with the simulations of McComb and Turver (1981).

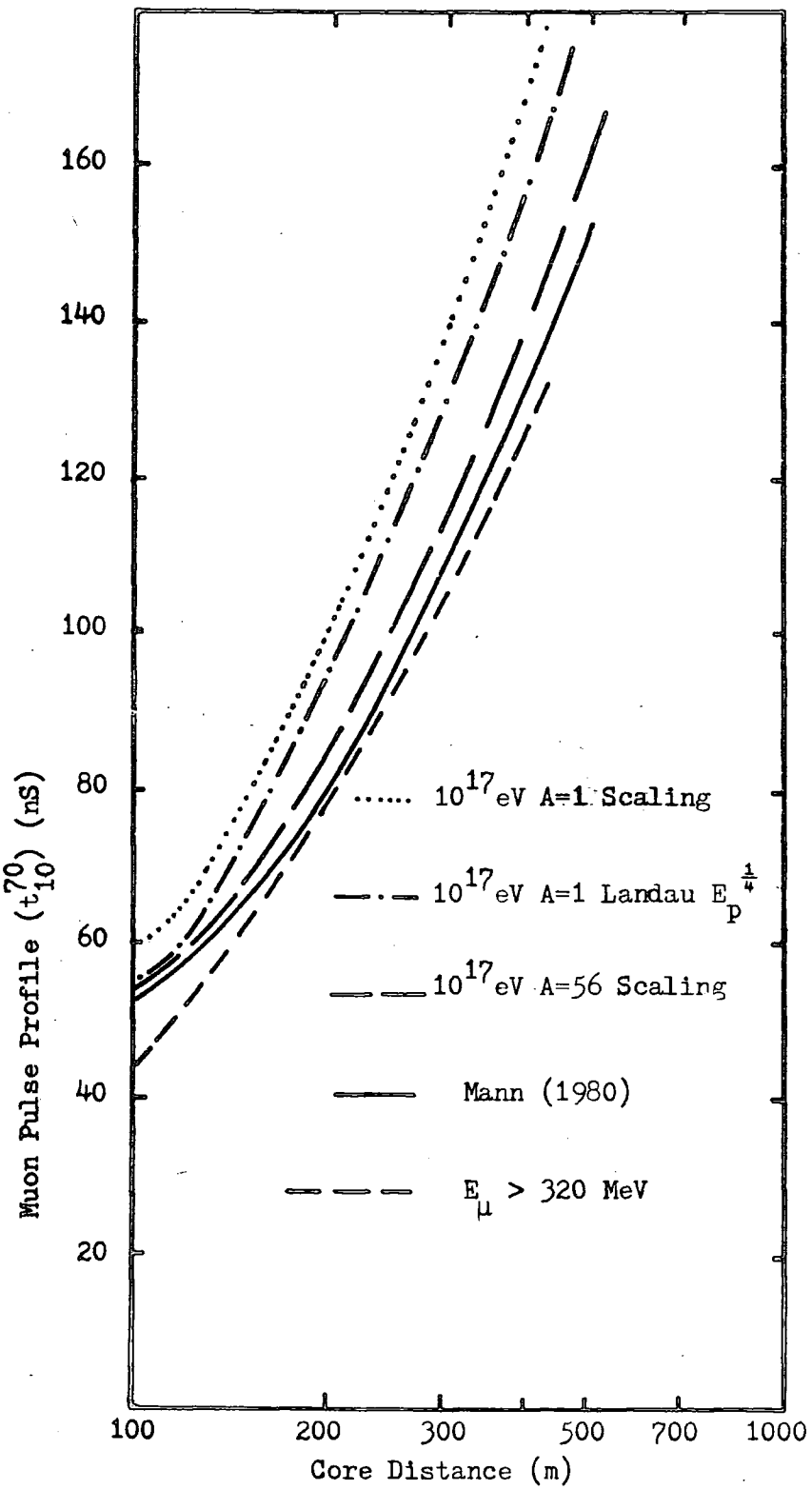
160
140
120
100
80
60
40
20
Muon Pulse Profile ($t_{10}^{70}$) (nS)
$10^{17}$eV A=1 Scaling
$10^{17}$eV A=1 Landau $E_p^{\frac{1}{4}}$
$10^{17}$eV A=56 Scaling
Mann (1980)
$E_\mu$ > 320 MeV
100
200
300
500
700
1000
Core Distance (m)

Figure 6-12 The risetime ($t_{10}^{70}$) of the highest energy muon pulses recorded by Mann (1980) compared with the simulations of McComb and Turver (1981b).

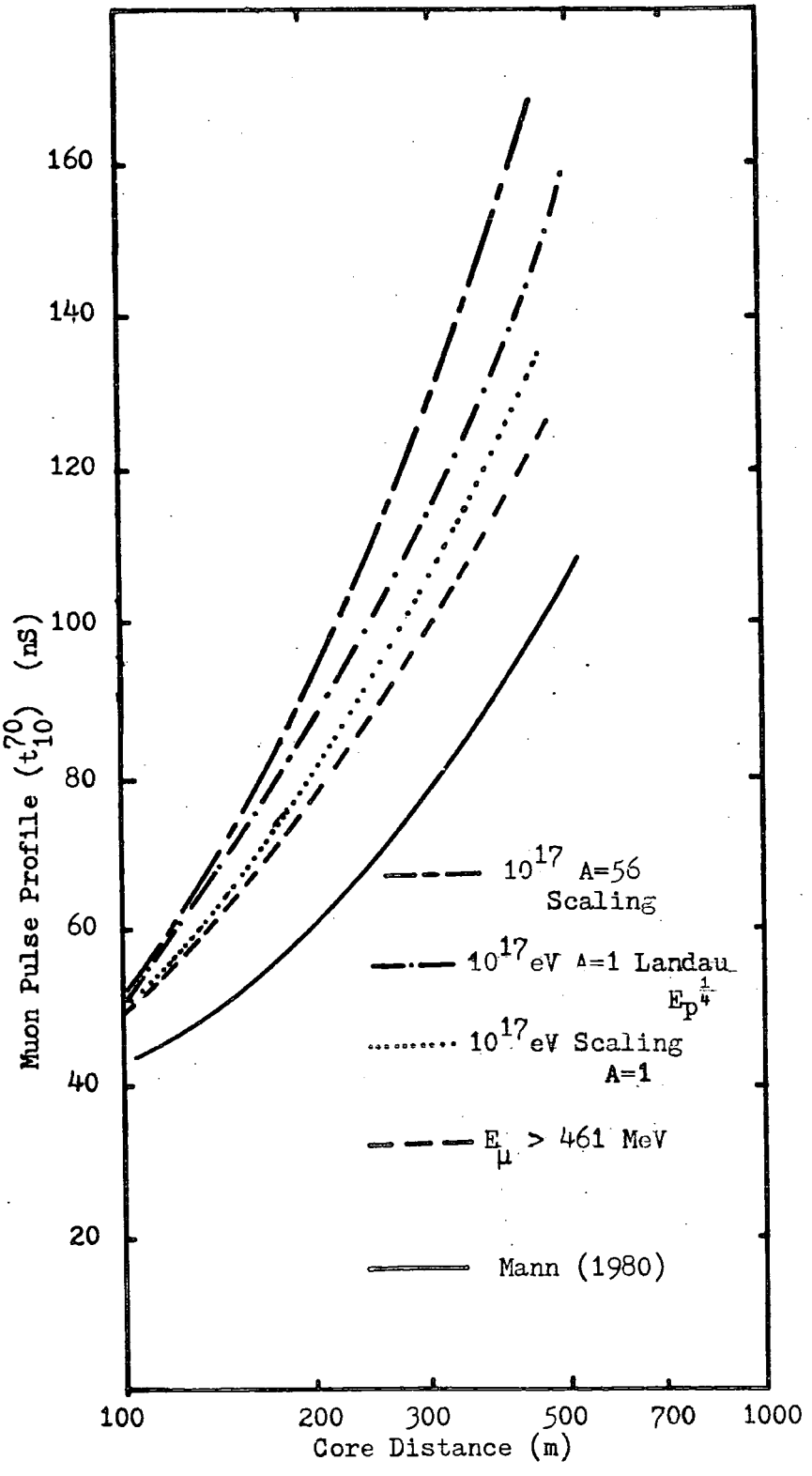
160
140
120
100
80
60
40
20
Muon Pulse Profile ($t_{10}^{70}$) (nS)
100
200
300
500
700
1000
Core Distance (m)
$10^{17}$ A=56 Scaling
$10^{17}$eV A=1 Landau $E_p^{\frac{1}{4}}$
$10^{17}$eV Scaling A=1
$E_\mu$ > 461 MeV
Mann (1980)

energies) and are therefore reasonably consistent with each other.

Other work in recent times has also been consistent, when interlinked through simulations. A useful linking measure is the elongation rates measured by various experiments. Protheroe and Turver (1978) deduce a value of $85 \pm 37 gcm^{-2}$ decade$^{-1}$ from the Night Sky Čerenkov data of Hammond et al (1978). From an analysis of rise time measurements in the Haverah Park deep water detectors Linsley and Watson (1981) are at some variance with the accepted values by obtaining a value of 50 g $cm^{-2}$ decade$^{-1}$ at the highest energies. The simulations of McComb and Turver (1981b) used for the analysis of the muon angle data predict values of $80 - 100 gcm^{-2}$ decade$^{-1}$ for the Scaling and Landau type models employed. This general agreement with other work adds encouraging strength to the analysis of the Durham data.

## 6-5 Fluctuation Measurements

One of the original aims of the experiment was to establish the mean parameters of muon spatial angles so that fluctuation studies between individual showers could be undertaken with the hope of throwing some light on the primary mass spectrum.

McComb and Turver (1981a) propose that a shower observable P could be represented by a relation of the form

$$P = a_o + a_1(\mathrm{Sec}\theta - 1) + a_2 \log_{10} E_p + \sigma$$

where $E_p$ = Primary Energy

$\theta$ = Zenith Angle

$\sigma$ = Total effects of fluctuations plus measurement effects.

Thus, provided realistic estimates of measurement errors can be achieved

and the energy and zenith angle terms are genuinely independent, real changes in the longitudinal cascade should manifest themselves as residual fluctuations. Simulations of the muon cascade in the atmosphere for inclined showers were performed by the authors to investigate the independence of the primary energy and zenith angle terms and the overall effects of fluctuations on the muon signal. They have clearly demonstrated for the two principal experimental measures for the experiment a relatively straightforward connection with primary energy but a very complex relation with zenith angle.

The predicted fluctuation values are small, typically $1{\cdot}3^{o}$ and $2{\cdot}5^{o}$ in muon angle and standard deviation respectively per decade in energy and $1{\cdot}3^{o}$ and $1{\cdot}5^{o}$ per $100 gcm^{-2}$ change in depth of cascade maximum. The consequences of these figures for the experimental results of this thesis are not good. A perusal of the muon/core angle and muon core angle standard deviation diagrams elsewhere in this chapter shows, in all cases, a high level of noise mixed in with the signal and any genuine fluctuations of this magnitude would be lost completely.

Unless a different approach to fluctuation measurements is discovered and supported by simulations which show at least a factor of two increase in the size of expected fluctuations it would probably not be worth processing the currently available angle data to search for meaningful fluctuations. Whether or not it would be worthwhile to consider an improved experiment for fluctuation studies is a different matter and hinges very much on the cleanliness and resolution of the data recorded. An important fact to be borne in mind is that an angle experiment of this nature has inevitably a noisy signal simply due to interactions with the atmosphere and shielding material before any quirks of the equipment are included. Thus, to be sure of success,

Figure 6-13 Fluctuations in mean muon-core angle recorded in the two halves of the central detector.

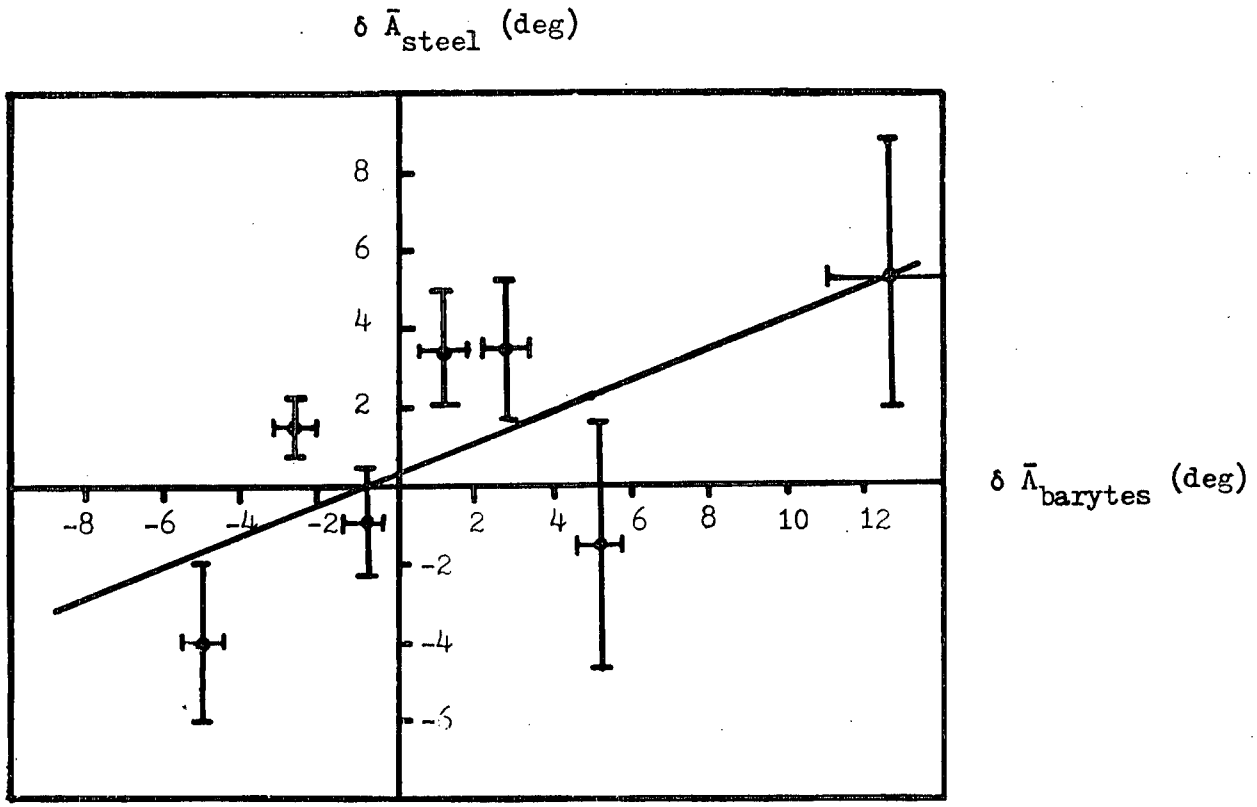
δ Ā steel (deg)
δ Ā barytes (deg)
8
6
4
2
-2
-4
-6
-8
-6
-4
-2
2
4
6
8
10
12

the expected fluctuations should be shown to be much larger than those introduced by the atmosphere, shielding and equipment. Even then, unless the experimental equipment had a much larger sensitive area than at present any fluctuation signal would still only be marginal.

Nevertheless, and despite the previous section a search was made through the available data seeking any correlation between fluctuations in individual showers. Some slight effect is noted when fluctuations between muon/core angles at the two energy thresholds are considered - figure 6-13. It was originally hoped to correlate data on fluctuations from the present experiment with other experiments at Haverah Park. This, however, even if there were a strong signal present, would be a very long term task if the extremely selective nature (of air shower events) of the equipment were to be overcome and reasonable statistics accrued.

## 6-6 Conclusions

The spatial angle data investigated so far has shown itself to be analysable when allied with dedicated simulations although it is not as sensitive to changes in the air shower cascade as was originally hoped. The hoped for fluctuation measurements are not readily apparent, being lost in the noise total of the experiment and the shower's development. To advance on the present situation would require an improvement of at least a factor of two in the resolution and a corresponding increase in the statistics.

A useful estimate of the depth of electron cascade maximum is however obtained from the muon spatial angles themselves and their spread for two muon energy cuts, the overall average value of 684 ± 30 $gcm^{-2}$ being in good agreement with other work in the same energy

range. Unfortunately an estimate of the elongation rate is not yet possible (and may not be) due to a lack of energy sensitivity in the experimental data. It is a pity, as there are now many measurements and estimates of this parameter and it would add extra weight to the angle measurements if a value agreeing with contemporary work were to be obtained.

Overall, the current Durham simulations are in broad general agreement with the muon spatial and temporal characteristic data currently available. However, at higher muon energies, there is some residual discrepancy between the observed and predicted values. This agrees with the findings of Suga et al (1979) that Scaling models cannot account for all the observed characteristics of muons in air showers. In particular, there is a consistent underestimation of the total number of muons for any given shower primary energy.

# Chapter Seven

# Conclusion

## 7-1 Introduction

The experiment and its data have now been thoroughly investigated and it is fully understood both within itself and in the context of other experiments. Practically all aspects of the data have been explored with varying measures of success and with the data presently available there is probably not a great deal more that can be obtained.

In view of the knowledge gained from this experiment suggestions for the next generation are made in this chapter as there is clearly a lot of information on the muon cascade still to be had and if the suggested improvements in sensitivity can be achieved a big step forward could be made.

## 7-2 The Relation to Other Work

There are many other sources of work world wide available for comparison with the present data set, all of which paint a similar picture. The average characteristics are now well understood and well measured. Much attention is now being turned to investigating fluctuations from the mean and other sensitivities to primary mass are now also being sought with vigour. However, these would still appear to be some way off.

Many comparisons with other data, both experimental and theoretical have been made in previous chapters and only a summary will be given here. Many interpretations of experimental data now exist which are in broad agreement and a convincing picture of the depth of electron cascade maximum is beginning to emerge. To this data can now

be added the interpretation of the University of Nottingham muon/Čerenkov ratio data [Blake et al (1979)] by McComb and Turver [Private Communication (1981)]. Their work shows values for $t_{max}$ ranging from 720 $gcm^{-2}$ to 850 $gcm^{-2}$ over the primary energy range $10^{17}$ - $10^{19}$eV. No errors on the measurements are quoted by Blake et al, so an estimate of some 10% was made and this leads to an error in $t_{max}$ of $\pm$ 30 $gcm^{-2}$. An elongation rate is also derived and is 65 $\pm$ 30 $gcm^{-2}$ $decade^{-1}$. When all the $t_{max}$ data is considered together (Figure 7-1) over the primary energy range of $10^{15}$ - $10^{20}$eV good agreement is seen right across the range including the Durham results from the spatial angle experiment. It is noticeable however that the depths from the Nottingham data are a little high. There is also broad agreement with the much earlier data of Gaisser et al (1978) reported in chapter 2 which gave mean heights of origin of muons as between 2.5 and 4 Km with showers in the $10^{17}$ - $10^{18}$eV range.

The majority of the available experimental data agree with the simulations, the only discrepancies occurring in the muon timing data, although the latter is consistent within itself (between Chacaltya and Haverah Park), there are consistent differences with the simulations. Although this is possibly an experimental effect arising from the relatively new nature of the data (unlikely if both experiments are consistent) it is more likely to be a defect in the modelling. Either some secondary effect is being overlooked or the current generation of models is wrong in its fundamental assumptions and this is only now becoming apparent in the muon timing data.

## 7-3 The Achievements of the Experiment in Relation to the Original Aims.

Figure 7-1 The depth of electron cascade maximum from various experiments compared as a function of primary energy. From McComb and Turver (1981c)

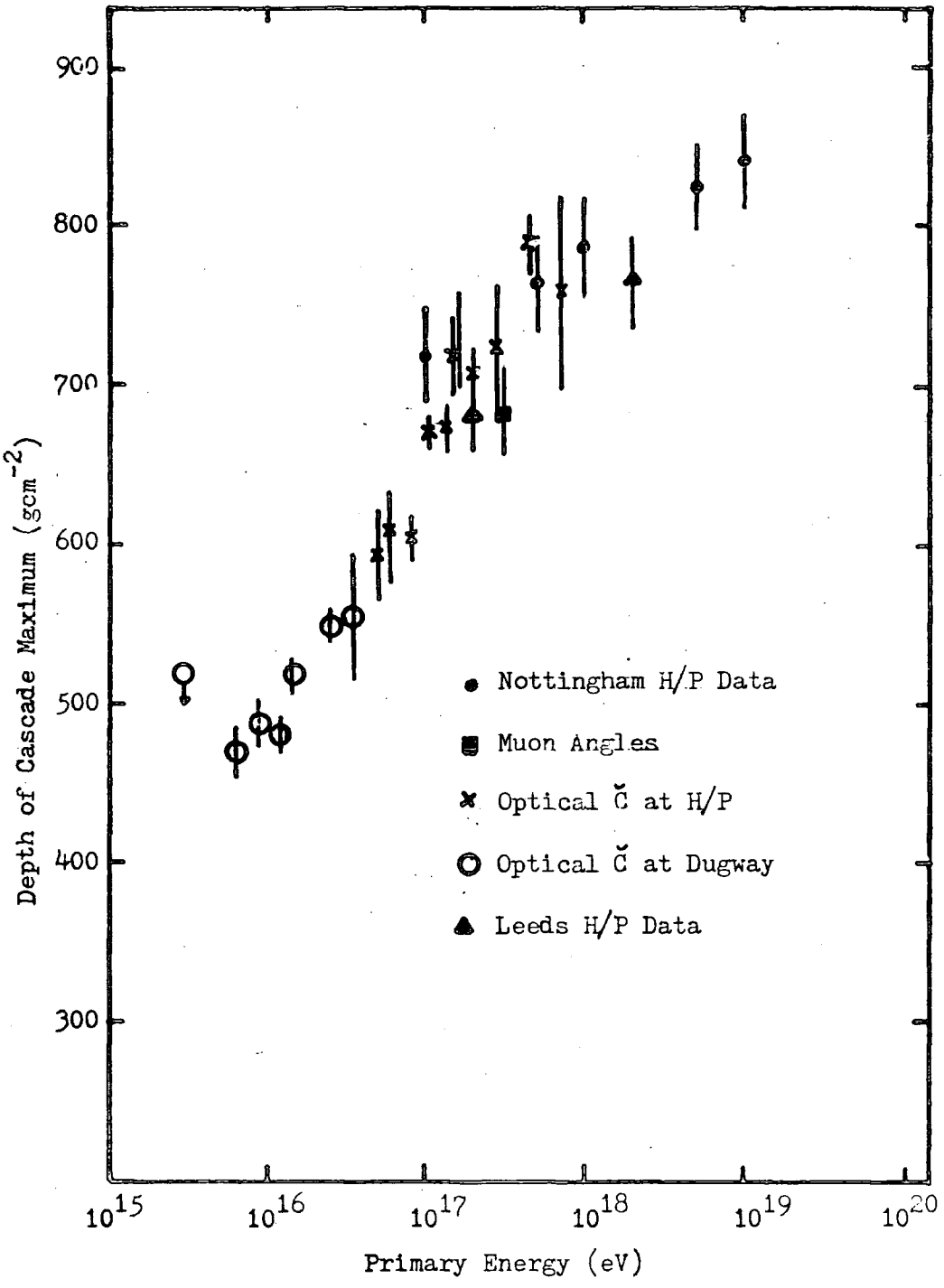
900
800
700
600
500
400
300
Depth of Cascade Maximum (gcm$^{-2}$)
$10^{15}$
$10^{16}$
$10^{17}$
$10^{18}$
$10^{19}$
$10^{20}$
Primary Energy (eV)
Nottingham H/P Data
Muon Angles
Optical Č at H/P
Optical Č at Dugway
Leeds H/P Data

The original aim of the Durham Muon Experiment of producing large area detectors (on a limited budget) to properly investigate phenomena originally studied on a very small scale has overall, been met. The equipment has been shown in Chapter Four to perform to the design specifications and produce measurements to the degree of accuracy originally intended. The only area where it fell short was in the rate of data capture particularly with the higher energy events.

The validity of the observations has been confirmed by comparison with well understood and measured parameters at the same time giving a thorough understanding of the workings of the experimental equipment. The ultimate aim of the experiment, to investigate fluctuations in the shower cascade has not been met, but average characteristics have been determined which are always an essential pre-requisite of any such study. These are also in good agreement with earlier work. In addition, and unexpectedly, a surprisingly good value for the depth of electron cascade maximum is obtained.

The flash tubes and their orientation with respect to the main E.A.S. array (governed by the geometry of the enclosing hut) are responsible for giving a much poorer data rate than was originally hoped. It is also unfortunate that the location of the infilling array in practice prevents any interlinking of the data. Any future experiment should pay greater attention to details of this nature if any significant advance is to be made over the present data.

## 7-4 The Way Ahead

At some time during the life of an experiment it becomes necessary to review its performance and consider improvements to the next generation of equipment. The results from this muon experiment show

many areas for improvement. The data sample recorded in a detector is small and hence very prone to non physical statistical fluctuations arising both externally and in the detector itself. An increase in the resolution (the original design figure was $\pm 0{\cdot}5^{o}$) would also be an advantage as refined dedicated simulations have shown the hoped for shower dependent fluctuations to be much smaller than previously estimated and hence probably out of reach of the present experiment.

As well as a large increase in the sensitive area and resolution of the detectors the other major improvement to be made would be to remove the constraint (imposed by the flash tubes) of only being able to use a very small percentage of the total data recorded by the main array. Such a large area omnidirectional detector probably could not use flash tubes and some of the more esoteric techniques practised at accelerators would probably have to be used. In any case the measurement of the raw data has, with the present equipment, shown itself to be very labour intensive and so any future experiment should preferably be on line to a mass data storage system. Even so, the data is still very dependent (perhaps more so than any other cosmic ray experiment yet attempted) on the precision with which the parent air shower array can measure the shower parameters, particularly zenith and azimuthal angles. It may be that the only way to achieve such accuracy is with the shower imaging technique described by Orford and Turver (1976) for night sky Čerenkov light but this of course brings with it a dramatic reduction in the data rate and the necessity to operate in regions of good seeing.

Simulations have shown that as much information on the muon cascade could be available from fast timing experiments (capable of a few nanoseconds time resolution). McComb and Turver (1979) have

suggested that, given a large enough detector system, it would be possible to image the muon cascade in a similar way to that described by Orford and Turver. Such a large area detector ($>30m^2$) would not be as prone to intrinsic fluctuations and because it would be omni-directional should be capable of acquiring data from the majority of events. Furthermore, such an experiment would be easy to operate on line and thus yield usable data quickly which would also be easier to analyse.

The way ahead is fairly clear, the 'basic air shower' is well understood but many aspects still need clarification. First and foremost, simulations, without which a full understanding will never be reached. The present inconclusive scenario needs much more work, particularly to the development of refined models which can encompass more of the observed phenomena together. The next steps as to ultra high energy interactions will no doubt be indicated by the results from the next generation of accelerators. Once this is achieved the long term aim of identifying the primary mass spectrum would follow more easily.

## 7-5 Conclusion

The original aim at the start of the work covered by this thesis has been modified with hindsight and practical discoveries. The validity of the technique has been amply confirmed and an unambiguous measurement of a single air shower phenomenon obtained. The fact that the equipment has recorded a single facet of the muon component is probably why there is such good agreement with simulation.

The straightforward determination of $t_{max}$ albeit the only measurement of direct relevance to air shower physics is both timely

and useful. The originally hoped for fluctuations have been shown by simulations to be beyond the reach of the equipment as it stands and it is up to the next generation of experiments to develop the accuracy necessary to measure them. The ultimate question of the origin of the highest energy primary particles is still very elusive and is likely to remain so for some considerable time yet.

## Appendix I

## The Heights of Origin of Muons in EAS from a Simple Trigonometric Approach

The height of origin of a muon can be derived from elementary dynamics and is represented in figure (A1). An energetic muon of momentum P (and transverse momentum $P_t$) originating from a height H landing a distance r from the shower core must obey:-

$$\frac{P_t}{P} = \frac{r}{H} \qquad (1)$$

Scattering effects (Coulomb and Geomagnetic) on particles below a momentum of 10GeV/c cause deviation from this relation, but it is still broadly correct.

The experimental work is constrained by the geometry of the recording instrument, in case of the present experiment recording is essentially restricted to one plane. Thus, as the muons' angles of incidence in this plane are known, all other measurements need to be transferred to this plane. The angle to the zenith made by the shower core in the instrument measuring plane ($\Psi_p$) is given by:-

$$\tan(\Psi_p) = \tan(\theta) . \cos(\phi+E) \qquad (2)$$

where:- $\theta$, $\phi$ are zenith and azimuthal angles respectively measured by the main array and E arises from orientation of the instrument recording plane wrt the main array.

From the rotation of the axes the core distance $r_\perp$ from the

Figure A1 (a) The relation between muon momentum, core distance, height of origin and transverse momentum.

(b) The relation used to determine the height of origin of a muon after projecting the shower arrival direction into the spectrograph measuring plane.

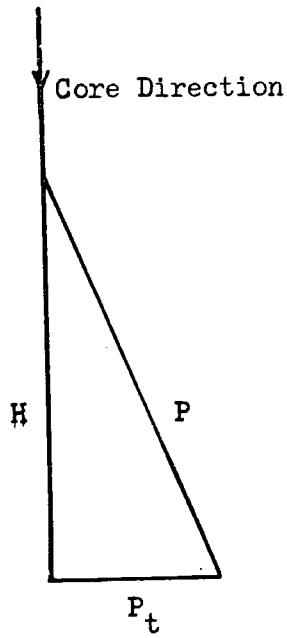
Core Direction
H
P
$P_t$

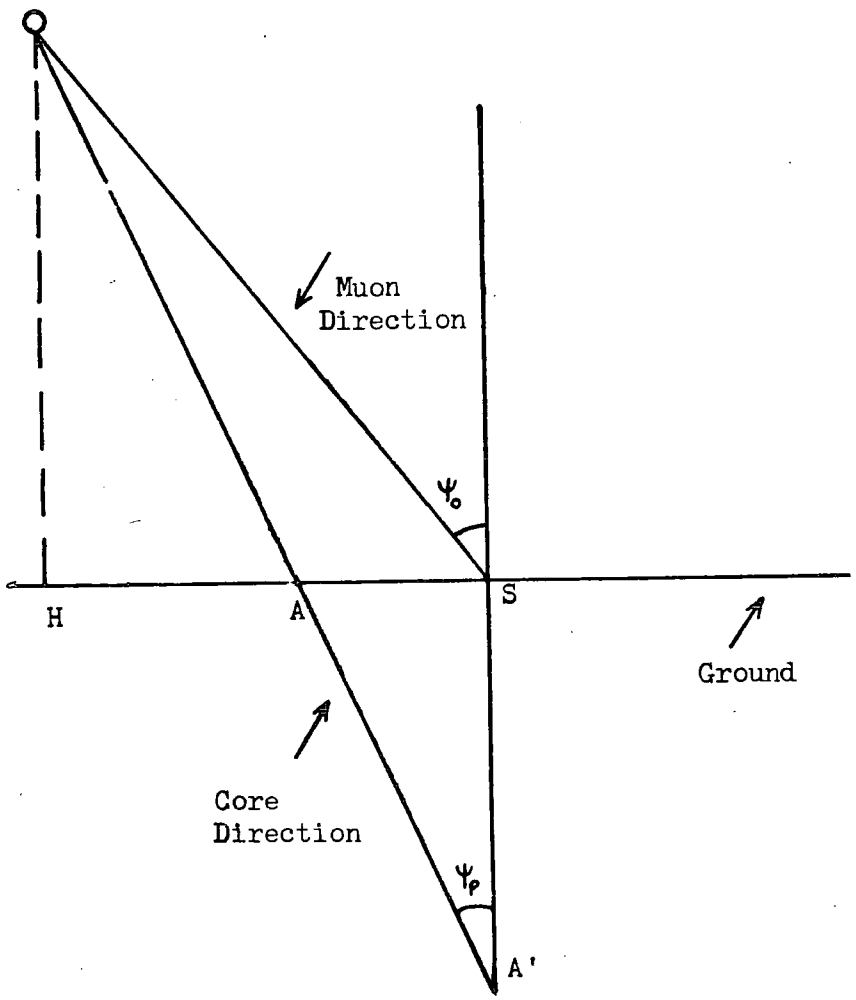
Muon
Direction
$\Psi_o$
H
A
S
Ground
Core
Direction
$\Psi_p$
A'

instrument is given by:-

$$r_{\perp} = Y\cos(E) - X\sin(E) \qquad (3)$$

where:- X,Y are core coordinates.

Study of figure A1b enables the following relationship to be derived:-

$$H = \frac{r_{\perp}\cos(\psi_p)\cos(\psi_o)}{\sin(\psi_p - \psi_o)} \qquad (4)$$

or

$$\frac{r_{\perp}}{H} = \tan(\psi_p) - \tan(\psi_o) \qquad (5)$$

Simulations and experimentally obtained data have shown that the angle between the muon and core directions $(\psi_p - \psi_o)$ is usually small ($10^{\circ}$ or less), thus errors in heights of origin are mainly dependant on errors in $(\psi_p - \psi_o)$.

## References

Note: The abbreviation PICCR represents the Proceedings of the International Conference on Cosmic Rays.


Amaldi U., Biancastelli R., Bosio C., Matthiae G., Allaby J.V., Bartel W., Cocconi G., Diddens A.N., Dobinson R.W., and Wetherell A.M. (1973) Phys. Lett. B 44, 112.

Amaldi U., Cocconi G., Diddens A.N., Dobinson R.W., Dorenbosch J., Dunker W., Gustavson D., Meyer J., Potter K., Wetherell A.M., Baroncelli A., and Bosio C., (1977), Phys. Lett. B 66, 390.

Andersson B., Jarlskog G., and Damgaard G., (1976) Nucl. Phys. B 112, 413.

Andrews D. (1970) Ph.D. Thesis University of Leeds.

Armitage M.L. (1973) Ph.D. Thesis University of Nottingham.

Barratt P., Cocconi G., Eisenberg Y. and Greisen K. (1952) Rev. Mod. Phys. 24 113.

Barratt M.L. (1976) Ph.D. Thesis University of Leeds.

Baxter A.J. (1967) J. Phys. A 2, 50.

Blake P.R., Fergusson H., Nash W.F., (1971) PICCR Hobart.

Blake P.R., Connor P.J., Nash W.F., Mann D.M. and O'Connell B. (1979) PICCR Kyoto.

Bull R.M., Coates D.W., Nash W.F., and Rastin B.C. (1962) Nuovo Cimento 8 628.

Burger J., Bohm E., and Suling M., (1975) PICCR Munich 2 2784.

Butcher J.C. and Messel H. (1960) Nucl. Phys. 20, 15.

Carruthers P. and Minh Duong- Van (1973) Phys. Rev. D 8, 859.

Cleghorn J.F., Freier P.S. and Waddington C.J. (1968) Can. J. Phys. 46, S572.

Conversi M. and Gozzini A. (1955) Nuovo Cimento 2 189 - 91.

Craig M.A.B., McComb T.J.L. and Turver K.E. (1979) PICCR Kyoto.

de Beer J.F., Crawshaw T.E. and Parham A.G. (1962) Phil. Mag. 7 499 - 514.

Dennis B.R. (1964) Ph.D. Thesis University of Leeds.

Dixon H.E. et al (1974) Proc. Roy. Soc. 339 133-55.

Dixon H.E. and Turver K.E. (1974) Proc. Roy. Soc. 339 171-95.

Earnshaw J.C., Machin A.C., Pickersgill D.R. and Turver K.E. (1973) J. Phys. A. 6 1244-61.

Edge D.M., Pollock A.M.T., Reid R.J.O., Watson A.A. and Wilson J.G. (1977) PICCR Plovdiv. 9 137-142.

Evans A.C. (1971) Ph.D. Thesis University of Leeds.

Feynman R.P. (1969) Phys. Rev. Lett. 23, 1415.

Fishbane P.M., Gaisser T.K., Maurer R.H. and Trefil J.S. (1974) Phys. Rev. D 9, 3083.

Freier P.S. and Waddington C.J. (1975) Astrophys. Space Sci. 38, 419.

Gaisser T.K. (1974) Nature (Lond.) 248, 122.

Gaisser T.K., Protheroe R.J., Turver K.E. and McComb T.J.L. (1978) Rev. Mod. Phys. 50.

Galbraith W. and Jelley J.V. (1953) Nature (Lond.) 171, 349.

Gibson A.I. (1976) M.Sc. Thesis University of Durham.

Greisen K. (1966) Phys. Rev. Lett. 16 748.

Hammond R.T., Orford K.J., Protheroe R.J., Shearer J.A.L., Turver K.E., Waddoup W.D. and Wellby D.W. (1978) Nuovo Cimento 4 315.

Hassegawa et al (1975) PICCR Munich. 7 2393.

Hillas A.M. (1969) PICCR Budapest. 3 355

Hillas A.M. (1971) Acta Physica Hung. 29, 3. 355.

Hillas A.M., Marsden D.J., Hollows J.D. and Hunter H.W. (1971) PICCR Hobart. 3 1001

Hess V.F. (1912) Physics 2 13 1084.

Hollows J.F. (1969) Ph.D. Thesis University of Leeds.

Landau L.D. (1953) Izu Akad Nauk SSSR 17, 51.

Lapikens J. (1977) Private Comm.

Linsley J. and Scarsi L. (1962) Phys. Rev. Lett. 9 123-5.

Linsley J. and Watson A.A. (1981) Phys. Rev. Lett. 46 459.

Machin A.C. (1973) Ph.D. Thesis University of Durham.

Mann D. (1980) Ph.D. Thesis University of Nottingham.

McComb T.J.L. and Turver K.E. (1979) PICCR Kyoto. 9 126

McComb T.J.L., Protheroe R.J. and Turver K.E. (1979) J. Phys. G. 5, 1613.

McComb T.J.L. and Turver K.E. (1981 a & b). To be published.

McComb T.J.L. and Turver K.E. (1981c) PICCR Paris 6 234

Orford K.J. and Turver K.E. (1976) Nature 264 722.

Pickersgill D.R. (1973) Ph.D. Thesis University of Durham.

Protheroe R.J. (1977) Ph.D. Thesis University of Durham.

Protheroe R.J. and Turver K.E. (1979) Il Nuovo Cimento 1c 315

Rossi B. and Greisen K. (1941) Rev. Mod. Phys. 13 240.

Sreekantan B.V. (1972) Space Science Reviews 14 103.

Strutt R.B. (1976) Ph.D. Thesis University of Nottingham.

Suga K., Kakimoto F., Mizumoto Y., Inone N., Kawai M., Yuguchi T., Tachi K., Isu N., Kamouchi Y., Kaneko T., Yoshii H., Murakami K., Toyoda Y., MacKeown P.K., Nishi K., Yamada Y., Tajima N., Nakatini H., Gotoh E., Aquirre C., Anda R. and Trepp A. (1979) PICCR Kyoto 13, 142.

Suri A.N. (1966) Ph.D. Thesis University of Leeds.

Tennent R.M. (1967) Proc. Phys. Soc. 92.

Tomazewski A. and Wdowcyzk J. (1975) PICCR Munich. 8 2899-2904.

Turver K.E. (1963) Ph.D. Thesis University of Leeds.

Turver K.E. (1975) PICCR Munich. 8 2851-57.

Wellby D.W. (1977) Ph.D. Thesis University of Durham.

Acknowledgements.

I am indebted to Professor A.W. Wolfendale and Dr. K.E. Turver for making this study possible. Dr. K.E. Turver is also thanked for his continual encouragement, advice and guidance. Mr. T.J.L. McComb is thanked for his help with computer simulations and data analysis on many occasions.

I am also very grateful to those many members of the technical staff of the Physics Department of the University of Durham for their invaluable advice and assistance on countless occasions. Particularly Mr. W. Leslie, Mr. P. Cottle and Mr. H. Davison for their help in construction work. The Science Research Council is thanked for financial assistance in the construction of the new experiment and for the provision of a research studentship.

Finally for their encouragement and assistance in preparing and typing this thesis, my parents are sincerely thanked.